

Optimizing Portfolio Management of Hybrid Power Plants under Uncertainty

L.B. de Jager

Master of Science Thesis

Optimizing Portfolio Management of Hybrid Power Plants under Uncertainty

MASTER OF SCIENCE THESIS

For the degree of Master of Science in Systems and Control at Delft
University of Technology

L.B. de Jager

January 9, 2025

Faculty of Mechanical, Maritime and Materials Engineering (3mE) · Delft University of
Technology

The logo for TNO, consisting of the letters 'TNO' in a bold, black, sans-serif font.

The work in this thesis was supported by TNO. Their cooperation is hereby gratefully acknowledged.

The logo for TU Delft, featuring a stylized flame icon above the text 'TU Delft' in a bold, blue, sans-serif font. To the right of 'TU Delft', the words 'Delft University of Technology' are written in a smaller, black, sans-serif font, stacked vertically.

Copyright ©
All rights reserved.

The logo for DCSC, consisting of the letters 'DCSC' in a bold, blue, sans-serif font with a slight 3D effect.

Abstract

The rapid integration of renewable energy sources, such as wind and solar power, into modern electricity systems has introduced challenges in balancing supply and demand, managing grid congestion, and ensuring efficient energy market participation. This thesis develops a framework for optimizing the portfolio management of hybrid power plants (HPPs) under uncertainty. HPPs combine renewable generation, energy storage (batteries), and flexible demand (electrolyzers) to improve grid efficiency and market participation.

This thesis develops a framework for optimizing HPP portfolio management under uncertainty, specifically targeting participation in the day-ahead market, the Dutch aFRR market, and the strategic use of passive imbalance. Two complementary optimization methods were developed and compared. Stochastic programming (SP) manages uncertainties in wind generation, activations, and day-ahead market prices using scenario-based approaches. Adaptive robust optimization (ARO) employs worst-case scenarios defined by budgeted polyhedral uncertainty sets for wind generation and activations, while using scenarios for day-ahead market price uncertainty. The ARO framework leverages duality theory and a column-and-constraint generation algorithm (CCGA) to iteratively refine robust solutions. Both methods were implemented within a shrinking horizon framework, which allowed for iterative decision-making at each time-step and tested the robustness of the first-stage decisions.

A case study using real-world Dutch market data demonstrated that both methods achieved zero violations by leveraging passive imbalance. ARO consistently delivered more robust first-stage decisions and higher revenue by effectively utilizing activation capacity. Additionally, a parameter study revealed the trade-offs between robustness and revenue, offering valuable insights into the flexibility and effectiveness of each method under varying conditions. This work highlights the potential of hybrid power plants to improve operational reliability and profitability in modern electricity systems.

Table of Contents

Acknowledgments	vii
1 Introduction	1
1-1 Scope and contributions	2
2 General modeling of hybrid power plant and multi-market optimization	5
2-1 Electrolyzer modeling	5
2-2 Battery modeling	7
2-3 Wind power and day-ahead market offering	7
2-4 AFRR explanation and modeling	8
2-4-1 Capacity bidding explanation	8
2-4-2 AFRR model definitions	10
2-5 Passive imbalance	14
2-5-1 combined monetary	15
2-6 Order of market clearance and optimization	15
2-7 Deterministic optimization model	16
2-8 Uncertainty in a two-stage model	18
2-8-1 Types of uncertainty	18
2-8-2 Definition of two-stage models	20
2-8-3 Adapting the two-stage model for HPP optimization	20
2-8-4 First-stage decision model	21
2-8-5 Second stage decision model	22
2-8-6 Forecasting and uncertainty management	23
2-9 Iterative second-stage optimization through a shrinking horizon approach	23
2-9-1 Additional Constraints	24
2-10 Chapter summary: general modeling	25

3	Approach 1: stochastic programming	27
3-1	Stochastic Model Framework	27
3-2	Two-Stage Stochastic Programming Model	29
3-2-1	Scenario programming definitions	29
3-2-2	Second-stage stochastic programming model	30
3-3	Scenario generation	31
3-4	Challenges with reserve energy activation uncertainty	32
3-5	Chapter summary: stochastic programming framework	33
4	Approach 2: adaptive robust optimization	35
4-1	ARO framework	35
4-2	Formulation for adaptive robust optimization model	38
4-2-1	Uncertainty set	38
4-2-2	ARO model formulation HPP	40
4-3	Column-constraint generation algorithm	41
4-3-1	Master problem model	42
4-3-2	Subproblem	44
4-4	Solving the subproblem	45
4-5	Shrinking horizon adaptation ARO	48
4-6	Chapter summary: ARO Framework	49
5	Case study	51
5-1	set-up	51
5-1-1	Power plant set-up and assumptions	51
5-2	Data gathering and preparation	53
5-2-1	Market prices and DA price forecasts	53
5-2-2	Wind data gathering and analysis	54
5-2-3	Real-time aFRR activations	54
5-2-4	Scenario generation available wind power	56
5-2-5	Robust bounds for available wind power	57
5-3	Metrics	59
5-3-1	Benchmarks: Deterministic Forecasting (DF) and Perfect Information (PI)	59
5-4	Case study A: monthly analysis	60
5-4-1	Results base case	60
5-4-2	Monthly Results Excluding Passive Imbalance	64
5-5	Case study B: weekly runs for parameter sensitivity analysis	66
5-5-1	benchmarks results	67
5-5-2	Stochastic programming parameter analysis	67
5-5-3	ARO parameter analysis	70
5-5-4	Computational times	72

5-6	Discussion of case study results and model limitations	73
5-6-1	Start-up costs	73
5-6-2	Performance CCGA	73
5-6-3	Passive imbalance impact and price uncertainty	75
5-6-4	Impact of aFRR activation energy	75
5-6-5	Limited impact of DA price uncertainty	76
5-6-6	Risk neutral stochastic programming	76
5-6-7	Case study limitations	76
5-7	Chapter summary: case study	77
5-7-1	Methods	77
5-7-2	Results and insights	77
6	Conclusions and future work	79
6-1	Conclusions	79
6-2	Future work	81
A	Appendix: asset parameters used	83
B	Appendix: old models	85
B-1	old model with a higher fidelity	85
B-1-1	electrolyzer old constraints for allowing storage	86
B-1-2	old electrolyzer segmentation	86
C	Appendix: robust optimization	87
C-1	Full reformulation	87
D	Appendix: results	89
D-1	Observation wind data	89
D-2	SP weekly case study results	89
D-2-1	SP week results: DA prices	91
D-2-2	SP week results: wind scenarios	92
D-2-3	SP week results: random draws	94
D-3	Robust optimization weekly results	97
D-3-1	Different budgets with passive imbalance option	97
D-3-2	Different budgets No passive imbalance	100
E	Appendix: Frameworks enlarged	103
F	Appendix: stochastic full model	107
	Bibliography	111
	Glossary	115
	List of Acronyms	115
	List of Symbols	115

Acknowledgements

First of all, I would like to thank to my TU Delft supervisor Sergio Grammatico, for his guidance and support throughout the process of writing this thesis. Your feedback and expertise have had a positive impact on the thesis, and I have learned a great deal under your supervision.

I am also grateful to my TNO supervisor Raja for dedicating many hours to listening to my ideas and providing thoughtful perspectives. Your encouragement and insights have been a source of motivation.

I would also like to express my gratitude to TNO for providing me with the opportunity to conduct my thesis research within their organization. Being involved in the internal project on multi-market optimization has been an enriching and valuable experience.

Lastly, I would like to thank my friends, girlfriend and family for their support and understanding throughout this journey. Your encouragement has been very welcome during the days of tinkering. And finally, I would like to apologize to my roommates for the constant humming of a laptop running simulations—thank you for your patience and understanding.

Delft, University of Technology
January 9, 2025

L.B. de Jager

Chapter 1

Introduction

The increasing penetration of renewable energy sources is transforming modern electricity systems. Wind turbines and solar photovoltaic installations are now major contributors to energy supply, accelerating the transition toward a sustainable future. However, this growth introduces several challenges. One prominent issue is the mismatch between renewable generation and demand, leading to energy oversupply. When generation exceeds consumption, electricity prices can become negative, resulting in economic inefficiencies and curtailment of renewable energy. Recent years have witnessed record numbers of negative price hours in the Netherlands, highlighting the urgency of addressing this imbalance [1].

In addition to energy oversupply, the Dutch electricity grid faces significant congestion issues. The grid infrastructure struggles to accommodate the increasing volume of renewable energy, limiting the ability to connect new projects. These constraints hinder the efficient distribution of electricity and slow down progress toward decarbonization goals. To alleviate grid congestion and manage the variability of renewable energy, innovative solutions are needed.

A promising approach to tackle these challenges is the development of the hybrid power plant (HPP). An HPP integrates renewable generation, energy storage, and flexible demand assets into a single, grid-connected system. This co-location of assets allows for optimized energy flows, improving efficiency and reducing grid congestion by consolidating multiple energy streams into a single connection point. Unlike the virtual power plant (VPP), where assets are geographically dispersed, HPPs benefit from the physical proximity of their components, enhancing coordination and operational flexibility.

Among the various components of a HPP, electrolyzers are emerging as an increasingly valuable addition. Electrolyzers convert surplus electricity into green hydrogen through water electrolysis, offering a promising way to store excess renewable energy. This hydrogen can be stored, transported, or used in industrial applications, providing additional flexibility to manage renewable variability. While the use of electrolyzers in HPPs is still relatively new, interest in their potential is growing rapidly due to their ability to alleviate grid congestion and maximize renewable energy utilization. Recent projects, such as large-scale hydrogen initiatives in the Netherlands, demonstrate the feasibility and benefits of coupling wind farms

with electrolyzers [2]. These initiatives aim to convert excess wind power into green hydrogen, which can be integrated into industrial processes or energy systems. Research has shown that incorporating electrolyzers into HPPs can help balance supply and demand more effectively, particularly during periods of excess renewable generation [3]. Furthermore, electrolyzers can reduce renewable curtailment and provide ancillary services to the grid, enhancing overall system flexibility and resilience [4].

However, optimizing an HPP portfolio is complicated by multiple sources of uncertainty. Renewable generation from wind and solar is inherently unpredictable, making it difficult to forecast exact output. Market prices in the day-ahead and balancing reserves fluctuate, further complicating decision-making. Additionally, participation in the Dutch automatic Frequency Restoration Reserve (aFRR) market introduces another layer of uncertainty due to the unpredictable nature of reserve activation. In the Netherlands, aFRR capacity is bid on a daily basis, imposing strict constraints on energy availability throughout the day.

Current research has made significant strides in addressing these uncertainties. Uncertainty in energy decision-making typically leads to two-stage or multi-stage optimization frameworks, reflecting the sequential nature of decisions and uncertainty realizations. Three main methods are commonly used for such problems, as summarized by Roald [5]. These methods include scenario-based programming, which uses generated scenarios to capture uncertainties in parameters [6]; robust optimization, which focuses on worst-case uncertainty realizations within predefined uncertainty sets [7]; and distributionally robust optimization, which optimizes across a family of potential distributions [8].

These methods have been applied to HPPs in various ways. For example, in [9], a data-driven chance-constrained programming scheme optimizes daily HPP operations, including an electrolyzer. However, this study focuses solely on day-ahead market decisions and excludes ancillary services and real-time market participation. Robust optimization has also been deployed in VPPs to optimize for ancillary services under uncertain activation [10] [11]. While effective, this approach focuses primarily on pre-scheduling and does not capture the sequential flow of uncertainty realization or real-time decision adjustments.

While many existing studies focus primarily on day-ahead market participation, the real-time dynamics associated with balancing and reserve activation are often given less attention. Furthermore, few approaches address the specific constraints of the Dutch balancing market, such as daily aFRR capacity bidding. These limitations highlight the need for a comprehensive optimization framework that can manage uncertainties across multiple markets, integrate key assets like electrolyzers effectively, and account for the rolling nature of uncertainty realizations.

1-1 Scope and contributions

This thesis aims to address these challenges by developing a tractable, data-driven optimization approach for managing the portfolio of a hybrid power plant. The proposed framework integrates wind turbines, batteries, and electrolyzers, optimizing participation in both the day-ahead market and the Dutch balancing market. The focus is on handling the uncertainties inherent in renewable generation, market prices, and reserve activation, while ensuring practical applicability within the constraints of the Dutch electricity market.

The central research question guiding this work is:

How can we effectively manage the portfolio of a hybrid power plant, including wind turbines, photovoltaic cells, batteries, and electrolyzers, for participation in the day-ahead market and the Dutch balancing market, using a tractable data-driven optimization approach?

To answer this question, the thesis is divided into two main objectives. The first objective is to develop a model of the assets within a hybrid power plant, including their interactions and market participation mechanisms. This involves modeling of electrolyzers, batteries, and power balance constraints, as well as the mechanisms of aFRR capacity bidding and activation. And develop a method of testing the validity of the solutions found using a shrinking horizon approach. The research will look into asset specific aFRR capacity, allowing for better control over the level of viable aFRR capacity bidding.

The second objective is to design methods for navigating the various sources of uncertainty using real-world Dutch market data. The thesis explores two optimization approaches: **stochastic programming** and **adaptive robust optimization**. The stochastic programming approach addresses uncertainties by generating scenarios for renewable generation and market prices, while the robust optimization approach uses polyhedral uncertainty sets and a column-constraint generation algorithm to account for worst-case scenarios.

Thesis outline

The remainder of this thesis is structured as follows. Chapter 2 provides a detailed overview of hybrid power plant modeling and multi-market optimization, including electrolyzer and battery modeling, power balance, and aFRR mechanisms. Chapter 3 introduces the stochastic programming approach, covering model formulation, scenario generation, and challenges related to reserve activation. Chapter 4 presents the adaptive robust optimization optimization framework, detailing the problem formulation, uncertainty sets, and solution algorithms. Chapter 5 discusses case studies, including data preparation, experimental setup, and results. Chapter 6 offers a discussion on the findings, limitations, and implications of the work, and Chapter 7 concludes with key insights and recommendations for future research.

By addressing the challenges of renewable variability, market uncertainty, and grid congestion, this thesis aims to support the development of efficient, resilient, and sustainable energy systems.

General modeling of hybrid power plant and multi-market optimization

This chapter presents the general modeling of the various components of the hybrid power plant through the use of mathematical formulations and constraints. First, the models for the electrolyzer and battery are detailed, with a particular focus on their operational dynamics and constraints. Subsequently, the Dutch aFRR market is introduced, with particular emphasis on its integration into the hybrid power plant model. This is followed by the introduction of the passive imbalance system, which represents the final component of the Dutch balancing market structure.

The chapter concludes by combining these elements into a deterministic model that summarizes the behavior of the system when all parameters are assumed to be known. To account for uncertainties, the deterministic model is extended into a two-stage framework, in which uncertain parameters such as wind power and market prices are considered. Finally, the second stage is adapted into a multi-stage shrinking horizon approach, which simulates the progressive realization of uncertainties and evaluates the robustness of the first-stage solutions.

2-1 Electrolyzer modeling

The modeling of the electrolyzer is based on the three-state model [3]. These states are represented by binary variables: z_t^{on} (on), z_t^{sb} (standby), and z_t^{su} (startup). The following constraint ensures that the electrolyzer can only be in one state at any given time:

$$z_t^{\text{on}} + z_t^{\text{sb}} + z_t^{\text{off}} = 1, \quad \forall t \in \mathcal{T}. \quad (2-1)$$

The transition dynamics for the electrolyzer are defined to prevent bypassing startup costs. The following constraints capture these dynamics:

$$z_t^{\text{su}} = 0, \quad \text{if } t = 1, \quad (2-2)$$

$$z_t^{\text{su}} \geq z_t^{\text{on}} - z_{t-1}^{\text{on}} - z_{t-1}^{\text{sb}}, \quad \forall t \in \mathcal{T} \setminus \{1\}, \quad (2-3)$$

$$z_{t-1}^{\text{off}} + z_t^{\text{sb}} \leq 1, \quad \forall t \in \mathcal{T} \setminus \{1\}. \quad (2-4)$$

$$z_t^{\text{on}}, z_t^{\text{sb}}, z_t^{\text{off}}, z_t^{\text{su}} \in \{0, 1\}, \quad \forall t \in \mathcal{T}. \quad (2-5)$$

Equation 2-4 ensures that the state switch from off is always to on, this ensure the the start-up constraints is not skipped.

The power consumption of the electrolyzer is constrained by its operational state. The maximum power consumption is given by its maximum power consumption \bar{P}^{H2} or power use in $P^{H2_{\text{sb}}}$:

$$P_t^{H2} \leq \bar{P}^{H2} z_t^{\text{on}} + P^{H2_{\text{sb}}} z_t^{\text{sb}}, \quad \forall t \in \mathcal{T}, \quad (2-6)$$

and the minimum power consumption is given by its minimum power consumption (\underline{P}^{H2}) or power use in standby $P^{H2_{\text{sb}}}$:

$$P_t^{H2} \geq \underline{P}^{H2} z_t^{\text{on}} + P^{H2_{\text{sb}}} z_t^{\text{sb}}, \quad \forall t \in \mathcal{T}. \quad (2-7)$$

These constraints ensure that the electrolyzer's power consumption stays within its designed limits, depending on whether it is in operational or standby mode.

The amount of kg hydrogen produced (Q_t^{H2}) is modeled as:

$$Q_t^{H2} = (A^{H2} \hat{P}_t^{H2} + B^{H2} z_t^{\text{on}}) \Delta T, \quad \forall t \in \mathcal{T}. \quad (2-8)$$

With A^{H2} , being the slope of the linearized production curve in [kg/MW] and B^{H2} the intercept in [kg]. Here \hat{P}_t^{H2} is used to define power that is used in the electrolyzer to create hydrogen. As in standby mode the electrolyzer does not actually produce any hydrogen. This model is completely linearised while the true working of an electrolyzer is not, more on that can be found in Appendix B. The power bounds for hydrogen production are defined as:

$$\underline{P}^{H2} z_t^{\text{on}} \leq \hat{P}_t^{H2} \leq \bar{P}^{H2} z_t^{\text{on}}, \quad \forall t \in \mathcal{T}, \quad (2-9)$$

effectively only giving power to production when it is in operational mode and not in standby. Lastly the power consumption by the electrolyzer (P_t^{H2}) is given by:

$$P_t^{H2} = \hat{P}_t^{H2} + P^{\text{sb}} z_t^{\text{sb}}, \quad \forall t \in \mathcal{T}. \quad (2-10)$$

2-2 Battery modeling

The modeling of the battery is based on a state-of-charge (SOC) model, a dynamic model where the next state is a function of the last SOC and the amount of power relative to the total battery capacity. This is a simplified model where we assume no losses due to efficiency. If we do account for losses, the battery should be split into outgoing and incoming power, as efficiency is handled differently for both cases. The old model, based on [12], included these considerations but was abandoned to exclude the extra binary constraint needed for the mutual exclusivity of the power flows.

The state of charge of the battery is defined by adjusting for power inputs and outputs, with consideration for initial SOC and total battery capacity:

$$SOC_t^{\text{bat}} = SOC_0^{\text{bat, init}} - \frac{P_t^{\text{bat}} \Delta T}{P^{\text{bat, cap}}}, \quad t = 1 \quad (2-11)$$

$$SOC_t^{\text{bat}} = SOC_{t-1}^{\text{bat}} - \frac{P_t^{\text{bat}} \Delta T}{P^{\text{bat, cap}}} \quad \forall t \in \mathcal{T} \setminus \{1\} \quad (2-12)$$

A constraint on the final SOC ($SOC^{\text{bat, final}}$) is included to ensure the final state of charge of the battery meets or exceeds a specified level, considering the entire operational period:

$$SOC_0^{\text{bat, init}} + \sum_{t \in \mathcal{T}} \left(\frac{P_t^{\text{bat}} \Delta T}{P^{\text{bat, cap}}} \right) \geq SOC^{\text{bat, final}} \quad (2-13)$$

To ensure safe and reliable operation, the battery must operate within a predefined state-of-charge range. Operating outside this range can lead to significant degradation or failure of the battery. The lower bound (SOC^{min}) ensures the battery is not over-discharged, which could damage the battery cells. Similarly, the upper bound (SOC^{max}) prevents overcharging. These constraints are defined as:

$$SOC^{\text{min}} \leq SOC_t \leq SOC^{\text{max}} \quad \forall t \in \mathcal{T} \quad (2-14)$$

Additionally, the power flow through the battery must remain within its operational charging and discharging limits. The maximum charging power ($P^{\text{bat, ch, max}}$) and maximum discharging power ($P^{\text{bat, dis, max}}$) are specified based on the battery's design and ensure that the battery operates within its thermal and electrical limits:

$$-P^{\text{bat, ch, max}} \leq P_t^{\text{bat}} \leq P^{\text{bat, dis, max}} \quad \forall t \in \mathcal{T} \quad (2-15)$$

2-3 Wind power and day-ahead market offering

Instead of directly modeling the wind-to-power conversion process, this thesis focuses on the available wind power, denoted as $P_t^{W,A}$. The available wind power depends on the installed capacity of the wind turbine and the forecasted wind power. It is assumed that a reliable forecasting system is already in place, and hence, the forecasted available power $P_t^{W,A}$ serves as an parameter to the optimization model.

The available wind power imposes an upper bound on the power that can be generated by the hybrid power plant:

$$0 \leq P_t^W \leq P_t^{W,A}, \quad \forall t \in \mathcal{T}. \quad (2-16)$$

The main energy is sold on the day-ahead market. The power generated by the wind turbine, along with contributions from the battery and electrolyzer, determines the energy committed to the DA market (P_t^{DA}). The power balance equation is formulated as follows:

$$P_t^{\text{wind}} + P_t^{\text{bat}} - P_t^{\text{H2}} = P_t^{\text{DA}}, \quad \forall t \in \mathcal{T}. \quad (2-17)$$

The main energy is sold on the day-ahead (DA) market, which serves as the primary trading platform for electricity. In the DA market, participants submit their bid and offer curves to the market operator, indicating their willingness to buy or sell electricity for each hour of the day. The market operator aggregates all bids and offers, clearing the market at a price where the aggregate demand curve intersects with the aggregate supply curve. This clearing price determines the value received or paid by participants for the traded energy. Since the market operates daily, participants must commit their bids at least 12 hours in advance, making accurate forecasting of renewable generation a critical factor for optimizing their positions.

The amount of energy committed to the DA market is further constrained by the grid connection limits:

$$-\underline{P}^{\text{net}} \leq P_t^{\text{DA}} \leq \overline{P}^{\text{net}}, \quad \forall t \in \mathcal{T}. \quad (2-18)$$

The objective function of the optimization problem is to maximize the daily revenue, which incorporates profits from DA market participation with energy sold at price λ^{DA} and hydrogen sales with hydrogen sold at λ^{H2} , while accounting for startup costs (C^{SU}) of the electrolyzer:

$$\text{Daily Revenue} = \sum_{t \in \mathcal{T}} \left(P_t^{\text{DA}} \Delta T \lambda_t^{\text{DA}} + Q_t^{\text{H2}} \lambda_t^{\text{H2}} - z_t^{\text{SU}} C^{\text{SU}} \right). \quad (2-19)$$

2-4 AFRR explanation and modeling

2-4-1 Capacity bidding explanation

Automatic Frequency Restoration Reserve (aFRR) capacity is reserved in the system to maintain grid stability. A minimum amount of aFRR is acquired through capacity bidding. Here, TenneT procures a minimum of 300 MW of aFRR capacity to be available throughout the day [13]. These required capacity bids are procured the day before. They are called capacity bids because these bids determine the amount of energy available to balance from the balance service provider (BSP) during the day, and the aim is to meet the minimum required aFRR capacity in the Netherlands.

These capacity bids turn into obligatory energy bids. Energy bids dictate the price at which the power plant is willing to provide aFRR when activated. The period over which the imbalance is settled is referred to as the Imbalance Settlement Period (ISP). Currently, capacity bidding is done for a 24-hour period. For example, if you bid 10 MW of capacity for the next day, you are obliged to submit energy bids for every ISP of the next day for 10 MW. You are responsible for being able to deliver that 10 MW at any moment. Systematically

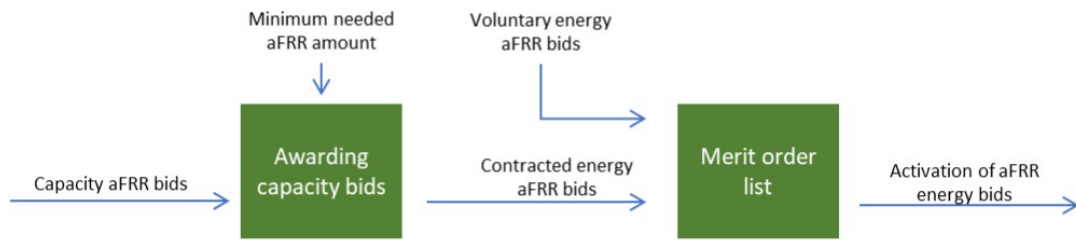


Figure 2-1: Relation between capacity and energy bids [13]

failing to provide this balancing energy will result in exclusion from the market. From an interview personally taken with TenneT, it is expected that the 24-hour bidding period will transition to a 4-hour period in the near future, and later to a 1-hour capacity bidding period. Capacity bids currently must be submitted in multiples of 1 MW.

Energy bids and voluntary bids explanation

In addition to the obligatory bids, other parties that are not obligated to bid can also submit their voluntary bids to TenneT; these are called free bids and are referred to as energy bids. The key difference between capacity bids and energy bids is that the amount to be offered as an energy bid is not predetermined, but is instead decided by the offering party. As a result, energy bids can change throughout the day, reflecting the amount of energy a party has available for balancing.

The energy bids of obligated parties that submitted capacity bids, along with other energy bids, are combined to form the merit order list. The process of forming this merit order list is visualized in Figure 2-1. The merit order list shows the available aFRR energy and the corresponding price. A visualization of the up and down-regulation prices is shown in Figure 2-2.

Participants in the aFRR market may revise their energy bids up to two ISPs prior to the start of a new ISP. The ISP in the Netherlands is 15 minutes. Bids must be in multiples of 1 MW, with a maximum of 999 MW [14].

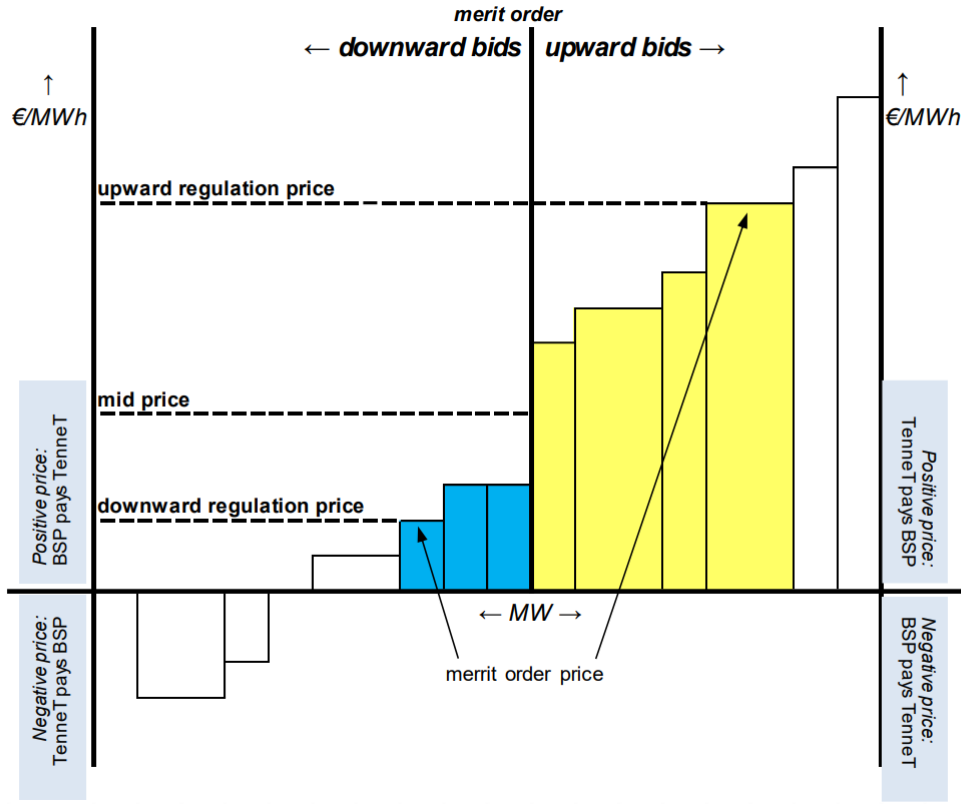


Figure 2-2: Merit order list with up and down-regulation prices [14]

This is achieved in the HPP by reserving energy from both the battery and the electrolyzer, subject to the following constraints.

2-4-2 AFRR model definitions

In some studies, aFRR capacity is not treated as a strict requirement to be available at all times but rather as sufficient to fulfill activation needs when required [10]. Other research, such as [11], links the amount of capacity offered to decisions made during day-ahead bidding. A more pragmatic approach models the available aFRR capacity as asset-dependent while considering the capacity needed for system activations.

The total reserve from the storage system and the electrolyzer is defined as:

$$r_t^\uparrow = r_t^{\uparrow, \text{bat}} + r_t^{\uparrow, \text{H2}} \quad (2-20)$$

$$r_t^\downarrow = r_t^{\downarrow, \text{bat}} + r_t^{\downarrow, \text{H2}} \quad (2-21)$$

$$\text{where } r_t^\uparrow, r_t^{\uparrow, \text{H2}}, r_t^{\uparrow, \text{bat}}, r_t^\downarrow, r_t^{\downarrow, \text{H2}}, r_t^{\downarrow, \text{bat}} \geq 0 \quad \forall t \in \mathcal{T} \quad (2-22)$$

Here, $r_t^{\text{AFRR}\uparrow, \text{H2}}$ and $r_t^{\text{AFRR}\uparrow, \text{bat}}$ represent the upward aFRR provided by the hydrogen storage and battery, respectively. Similarly, $r_t^{\text{AFRR}\downarrow, \text{H2}}$ and $r_t^{\text{AFRR}\downarrow, \text{bat}}$ represent the downward aFRR.

The total aFRR capacity is uniform across all ISPs within a 24-hour period and therefore is not indexed with t . However, the aFRR capacity of individual components, such as the electrolyzer and battery, depends on their current SOC and operational state, which are indexed with t .

The reserve amount is constrained by the grid connection:

$$P_t^{\text{DA}} - r^\downarrow \geq -\underline{P}^{\text{net}} \quad (2-23)$$

$$P_t^{\text{DA}} + r^\uparrow \leq \overline{P}^{\text{net}} \quad (2-24)$$

Market regulations dictate that reserve values must be integer values [13]:

$$r^\uparrow, r^\downarrow \in \mathbb{Z}$$

The activation of reserves is determined by the parameters β_t^\downarrow and β_t^\uparrow , which can take values in the interval $[0,1]$.

Battery-specific aFRR constraints

The following equations define the constraints for reserving aFRR capacity from the battery, based on the work in [15]. While the original model provides a strong foundation, it does not explicitly account for the connection between the final state of charge, aFRR availability, and the battery's power limitations. These constraints have been adapted to address this gap, ensuring consistency and feasibility across the entire time horizon.

The constraints in Equation 2-25 and Equation 2-28 define the SOC limits, ensuring sufficient capacity for either charging or discharging the battery. They guarantee that the battery can provide up-regulating energy and down-regulating energy, while ensuring that the battery SOC remains above the minimum threshold during activation. Notably, the lower bound in the final time-step equals the final SOC requirement. The constraints are defined as follows:

$$\text{SOC}_{t-1}^{\text{bat}} - \frac{(P_t^{\text{bat}} + r_t^{\uparrow, \text{bat}})}{P^{\text{bat, cap}}} \Delta T \geq \underline{\text{SOC}} \quad \forall t \in \mathcal{T} \setminus \{1, T\} \quad (2-25)$$

$$\text{SOC}^{\text{init}} - \frac{(P_{t=1}^{\text{bat}} + r_{t=1}^{\uparrow, \text{bat}})}{P^{\text{bat, cap}}} \Delta T \geq \underline{\text{SOC}} \quad (2-26)$$

$$\text{SOC}_{T-1}^{\text{bat}} - \frac{(P_T^{\text{bat}} + r_T^{\uparrow, \text{bat}})}{P^{\text{bat, cap}}} \Delta T \geq \text{SOC}^{\text{final}1} \quad (2-27)$$

$$\text{SOC}_{t-1}^{\text{bat}} + \frac{(-P_t^{\text{bat}} + r_t^{\downarrow, \text{bat}})}{P^{\text{bat, cap}}} \Delta T \leq \overline{\text{SOC}} \quad \forall t \in \mathcal{T} \setminus \{1\} \quad (2-28)$$

¹Alternatively, the minimal SOC, $\underline{\text{SOC}}$, can be modeled as a time-dependent parameter vector $\mathbf{SOC}^{\text{min}}$, defined as $\mathbf{SOC}^{\text{min}} = \{\underline{\text{SOC}}, \underline{\text{SOC}}, \dots, \underline{\text{SOC}}, \text{SOC}^{\text{final}}\}$, where $\mathbf{SOC}^{\text{min}} \in \mathbb{R}^T$.

$$\text{SOC}^{init} + \frac{(-P_{t=1}^{\text{bat}} + r_{t=1}^{\downarrow, \text{bat}})}{P_{\text{bat}, \text{cap}}} \Delta T \leq \overline{\text{SOC}} \quad (2-29)$$

The amount of upregulating power (Equation 2-30) can be provided by reducing the planned output of the battery or increasing the amount of energy charged into the battery. If the battery is already charging, it can only discharge up to the maximum discharge rate. Down-regulating power (Equation 2-31), on the other hand, is achieved by either reducing the battery's discharge or increasing its charging rate, subject to the maximum charging rate. These constraints are defined as:

$$P_t^{\text{bat}} + r_t^{\uparrow, \text{bat}} \leq \overline{P}^{\text{bat}, \text{dis}} \eta_{\text{bat}} \quad (2-30)$$

$$-P_t^{\text{bat}} + r_t^{\downarrow, \text{bat}} \leq \overline{P}^{\text{bat}, \text{ch}} \eta_{\text{bat}} \quad (2-31)$$

The SOC, accounting for aFRR activation, is only affected when aFRR is activated. This is described by the following constraints:

$$\text{SOC}_t^{\text{bat}} = \text{SOC}_{t-1}^{\text{bat}} + \sum_{t \in T} \left(\frac{P_{t, \omega}^{\text{bat}} - \beta_t^{\uparrow} r_t^{\uparrow, \text{bat}} + \beta_t^{\downarrow} r_t^{\downarrow, \text{bat}}}{P_{\text{bat}, \text{cap}}} \Delta T \right) \quad \forall t \in \mathcal{T} \setminus \{1\} \quad (2-32)$$

$$\text{SOC}^{init} + \sum_{t \in T} \left(\frac{P_{t, \omega}^{\text{bat}} - \beta_t^{\uparrow} r_t^{\uparrow, \text{bat}} + \beta_t^{\downarrow} r_t^{\downarrow, \text{bat}}}{P_{\text{bat}, \text{cap}}} \Delta T \right) \leq \text{SOC}^{final} \quad (2-33)$$

Electrolyzer specific aFRR constraints

The power constraint for the electrolyzer during upward aFRR is described by Equation 2-34 [4]:

$$P_t^{\text{H2}} - r_t^{\uparrow, \text{H2}} \geq \underline{P}^{\text{H2}} z_t^{\text{on}} + P^{\text{sb}} z_t^{\text{sb}} \quad \forall t \in \mathcal{T} \quad (2-34)$$

Similarly, the power constraint for the electrolyzer during downward aFRR is described by Equation 2-35:

$$P_t^{\text{H2}} + r_t^{\downarrow, \text{H2}} \leq \overline{P}^{\text{H2}} z_t^{\text{on}} + P^{\text{sb}} z_t^{\text{sb}} \quad \forall t \in \mathcal{T} \quad (2-35)$$

It is important to note that for both upward and downward aFRR reserves, no aFRR can be delivered if the electrolyzer is in standby mode. This restriction exists due to safety concerns when operating an electrolyzer during the transition between standby and active states [16]. Furthermore, when the electrolyzer is in the off state, both z^{on} and z^{sb} are zero, effectively constraining both Equation 2-34 and Equation 2-35 to zero. Consequently, the equations simplify to the following:

For upward aFRR:

$$\hat{P}_t^{\text{H2}} - r_t^{\uparrow, \text{H2}} \geq \underline{P}^{\text{H2}} z_t^{\text{on}} \quad \forall t \in \mathcal{T} \quad (2-36)$$

For downward aFRR:

$$\hat{P}_t^{\text{H2}} + r_t^{\downarrow, \text{H2}} \leq \overline{P}^{\text{H2}} z_t^{\text{on}} \quad \forall t \in \mathcal{T} \quad (2-37)$$

The hydrogen production dynamics, incorporating the effects of aFRR, are modeled by Equation 2-38:

$$Q_t^{H2} = \left(A \left(\hat{P}_t^{H2} - \beta_t^\uparrow r_t^{\uparrow, H2} + \beta_t^\downarrow r_t^{\downarrow, H2} \right) + Bz^{on} \right) \Delta T \quad \forall t \in \mathcal{T} \quad (2-38)$$

This equation describes how hydrogen production is influenced by aFRR activation. The term \hat{P}_t^{H2} represents the base hydrogen power production, while the aFRR terms, scaled by the activation factors β_t^\uparrow and β_t^\downarrow , adjust the production for upward and downward reserve activation, respectively.

AFRR monetary

The total revenue generated from the aFRR market includes income from capacity reservation in the day-ahead market as well as income from activation during real-time operations. The revenue from day-ahead capacity reservation is given by Equation 2-53:

$$\text{Daily revenue}^{\text{aFRR, DA}} = 96r^\uparrow \lambda^{r^\uparrow} + 96r^\downarrow \lambda^{r^\downarrow} \quad (2-39)$$

This income remains constant for every time step, as it is based on the capacity reserved for the entire operating horizon. λ^r is usually provided as €/ISP and there are 96 IPS across 1 day of operations.

The additional revenue from real-time activation of aFRR is modeled by Equation 2-40:

$$\text{revenue}_t^{\text{aFRR, within day}} = \beta_t^\uparrow r^\uparrow \lambda_t^{r, \text{act}^\uparrow} \Delta T + \beta_t^\downarrow r^\downarrow \lambda_t^{r, \text{act}^\downarrow} \Delta T. \quad (2-40)$$

Here, $\lambda_t^{r, \text{act}^\uparrow}$ and $\lambda_t^{r, \text{act}^\downarrow}$ denote the real-time activation prices for upward and downward aFRR, usually given in [€/MWh].

The total revenue from aFRR is the sum of day-ahead capacity reservation and real-time activation revenues over the entire time horizon.

AFRR activation connection to energy bid strategy

The activation of aFRR is directly influenced by the bidding strategy employed by the BSP. A well-defined strategy is important to align activation decisions with market conditions, ensuring both profitability and compliance.

A preliminary aFRR activation strategy can be mathematically expressed to guide the decision-making process:

$$\beta_t^\uparrow = \begin{cases} 1 & \text{if } \lambda_t^{r, \text{act}^\uparrow} > \lambda_t^{\text{DA}} \\ 0 & \text{otherwise} \end{cases} \quad (2-41)$$

$$\beta_t^\downarrow = \begin{cases} 1 & \text{if } \lambda_t^{r, \text{act}^\downarrow} < \lambda_t^{\text{DA}} \text{ and } \lambda_t^{r, \text{act}^\downarrow} < 0 \\ 0 & \text{otherwise} \end{cases} \quad (2-42)$$

This strategy leverages the relationship between real-time activation prices ($\lambda_t^{r, \text{act}^\uparrow}$, $\lambda_t^{r, \text{act}^\downarrow}$) and day-ahead market prices (λ_t^{DA}). Activation is undertaken only when it is expected to

yield higher revenue compared to the day-ahead market. For upward activation, this occurs during price spikes in the real-time market, while for downward activation, only negative prices are considered to avoid incurring costs for providing energy.

This simple yet practical strategy allows realistic activation patterns to be derived from historical price data. While effective, it does not fully optimize aFRR profits or account for market uncertainties. The development of a more sophisticated bidding strategy is outside the scope of this thesis but could be explored in future work.

2-5 Passive imbalance

At the end of each ISP, there is a transaction between TenneT and the parties connected to the grid to account for deviations from the planned energy program. The imbalance price is equal to the prices of the activated FRR. If no activation occurs during the ISP, the imbalance price defaults to the mid-price. The link between the imbalance price and the FRR activation price serves as a regulatory measure to prevent imbalance abuse. High accepted bids for the FRR lead to high imbalance prices, creating a financial penalty for parties with a greater imbalance than the amount of FRR energy they have activated. This mechanism ensures that parties with large imbalances incur losses due to the elevated imbalance price.

Real-time data on ISP prices and volumes is available, enabling parties to evaluate the potential financial impact of their imbalance. Because of the connection between FRR prices and imbalance prices, there may be a financial incentive to intentionally create an imbalance under certain conditions. The availability of this information allows parties to assess whether deliberately increasing the imbalance in their portfolio could benefit the system overall. This practice, known as passive balancing, enables parties to contribute to grid stability without directly participating in ancillary markets.

When the day-ahead market decisions and imbalance decisions are considered independent, the following power balance equation applies:

$$P_t^{DA} + P_t^{\Delta} = P_t^{bat} - P_t^{H2} + P_t^{wind} \quad \forall t \in \mathcal{T}, \quad (2-43)$$

where P_t^{DA} is now a fixed parameters determined by the day-ahead offering.

Different prices are applied depending on whether there is a surplus or a deficit of energy. Consequently, the imbalance energy is divided into its positive and negative components:

$$P_t^{\Delta} = P_t^{\Delta+} - P_t^{\Delta-} \quad \forall t \in \mathcal{T}, \quad (2-44)$$

$$P_t^{\Delta+} \geq P_t^{\Delta} \quad \forall t \in \mathcal{T}, \quad (2-45)$$

$$P_t^{\Delta-} \geq -P_t^{\Delta} \quad \forall t \in \mathcal{T}, \quad (2-46)$$

$$P_t^{\Delta+} \leq M \cdot u_t^{imb} \quad \forall t \in \mathcal{T}, \quad (2-47)$$

$$P_t^{\Delta-} \leq M \cdot (1 - u_t^{imb}) \quad \forall t \in \mathcal{T}. \quad (2-48)$$

The revenue from imbalance decisions is modeled as follows:

$$\text{Revenue}_t^{imb} = P_t^{\Delta+} \lambda_t^{\Delta} + \Delta T - P_t^{\Delta-} \lambda_t^{\Delta} - \Delta T \quad (2-49)$$

where $\lambda_t^{\Delta+}$ and $\lambda_t^{\Delta-}$ are the imbalance prices for surplus and deficit, respectively usually given in [€/MWh].

Passive Imbalance and aFRR

When operating in the aFRR market and managing passive imbalance, a conservative approach is taken to ensure no imbalance is allowed during any aFRR activation. This means that whenever aFRR is activated, the balancing service provider (BSP) must completely eliminate the imbalance in the opposite direction, as well as avoid creating any new imbalance. This stricter modeling approach is expressed as follows:

$$P_t^{\Delta+} = 0 \quad \forall \beta_t^{\uparrow} \neq 0 \quad \text{or} \quad \beta_t^{\downarrow} \neq 0, \quad \forall t \in \mathcal{T}, \quad (2-50)$$

and

$$P_t^{\Delta-} = 0 \quad \forall \beta_t^{\uparrow} \neq 0 \quad \text{or} \quad \beta_t^{\downarrow} \neq 0, \quad \forall t \in \mathcal{T}. \quad (2-51)$$

This approach ensures that the BSP strictly adheres to system balancing requirements, minimizing the risk of financial penalties or operational disruptions. While this conservative modeling may reduce operational flexibility, it aligns with the goal of maintaining a stable grid during aFRR activations.

2-5-1 combined monetary

The total income on D-1 when combining the day-ahead and aFRR income is the following:

$$\text{Revenue}^{DA} = 96r^{\uparrow}\lambda^{r\uparrow} + 96r^{\downarrow}\lambda^{r\downarrow} + \sum_{t \in \mathcal{T}} P_t^{\text{net}} \Delta T \lambda_t^{DA} \quad (2-52)$$

The total extra income of the within-day revenue is:

$$\begin{aligned} \text{Revenue}^{WD} = \sum_{t \in \mathcal{T}} & \left(Q_t^{H2} \lambda_t^{H2} - z^{SU} C^{SU} + P_t^{\Delta+} \lambda_t^{\Delta+} \Delta T - P_t^{\Delta-} \lambda_t^{\Delta-} \Delta T \right. \\ & \left. \beta_t^{\uparrow} r^{\uparrow} \lambda_t^{r,act,\uparrow} \Delta T - \beta_t^{\downarrow} r^{\downarrow} \lambda_t^{r,act,\downarrow} \Delta T \right) \end{aligned} \quad (2-53)$$

Here we assume that the income of the hydrogen is received on the day itself.

2-6 Order of market clearance and optimization

The sequence in which market clearance occurs significantly influences the optimization process and the stages of decision-making. The clearance order is illustrated in Figure 2-3. Notably, aFRR capacity is cleared before the day-ahead market [13]. This sequence ensures that the required capacity is reserved, enabling more informed energy decisions in the day-ahead market.

From this figure, two distinct stages of optimization can be identified. The initial stage involves the formulation of decisions related to aFRR capacity and day-ahead energy offerings. The second stage focuses on the activation of capacity in response to passive imbalances.

In practice, the first stage may include multiple sub-stages due to the varying clearance times of different markets. While imbalance decisions could theoretically be considered during

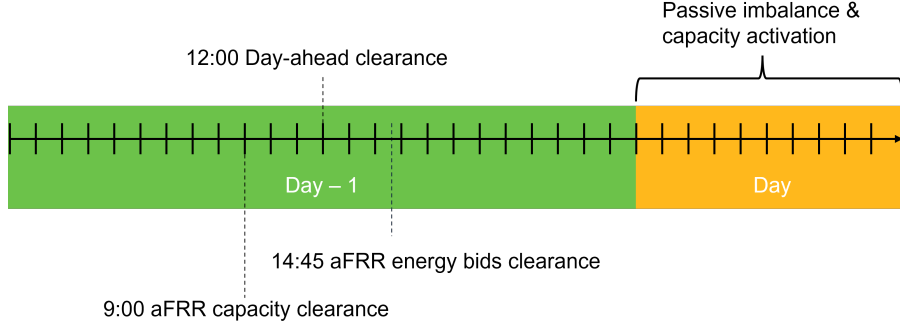


Figure 2-3: Clearance order of markets considered

this initial stage, accurately predicting prices over an extended time frame poses significant challenges. Consequently, the consideration of passive imbalance revenue is deferred to a stage closer to the real-time operation of the system. This approach is motivated by the inherent difficulty of accurately forecasting imbalance prices and volumes over extended time horizons. By postponing these decisions until closer to delivery, when real-time data and market conditions are better known, the optimization process can more effectively account for the dynamic nature of imbalance pricing. This ensures that the system remains flexible and responsive to real-time conditions, thereby improving overall performance and revenue optimization.

Furthermore, the set-points of various assets can be treated as second-stage variables, as they are adjustable throughout the day to respond to real-time conditions and requirements. While these set points are considered second-stage variables, their optimization occurs during the first stage to define the initial decision variables effectively.

2-7 Deterministic optimization model

In this section we collect all the constraints together to form the deterministic problem covering the multi-markets described in this chapter. This is referred to as the deterministic model, as no notation for uncertainty is included. The optimization problem is a mixed-integer linear program (MILP):

$$\begin{aligned} \max & \left(96r^{\uparrow} \lambda^{r^{\uparrow}} + 96r^{\downarrow} \lambda^{r^{\downarrow}} + \sum_{t \in \mathcal{T}} P_t^{\text{net}} \Delta T \lambda_t^{\text{DA}} + Q_t^{\text{H2}} \lambda_t^{\text{H2}} - z^{\text{SU}} C^{\text{SU}} \right. \\ & \left. + P_t^{\Delta+} \lambda_t^{\Delta+} \Delta T - P_t^{\Delta-} \lambda_t^{\Delta-} \Delta T + \beta_t^{\uparrow} r^{\uparrow} \lambda_t^{r, \text{act}, \uparrow} \Delta T - \beta_t^{\downarrow} r^{\downarrow} \lambda_t^{r, \text{act}, \downarrow} \Delta T \right) \end{aligned} \quad (2-54)$$

Subject to

Power balancing constraints:

$$P_t^{\text{DA}} = P_t^{\text{W}} - P_t^{\text{H2}} + P_t^{\text{bat}} - P_t^{\Delta} \quad (2-55)$$

$$r^{\uparrow} = r_t^{\uparrow, \text{bat}} + r_t^{\uparrow, \text{H2}} \quad (2-56)$$

$$r^\downarrow = r_t^{\downarrow, \text{bat}} + r_t^{\downarrow, \text{H2}} \quad (2-57)$$

$$P_t^{\text{DA}} + P_t^\Delta + r^\uparrow \leq \bar{P}^{\text{net}} \quad (2-58)$$

$$P_t^{\text{DA}} + P_t^\Delta - r^\downarrow \geq -\underline{P}^{\text{net}} \quad (2-59)$$

$$0 \leq P_t^W \leq P_t^{W,A} \quad (2-60)$$

State constraints for the electrolyzer:

$$z_t^{\text{su}} = 0, \text{ if } t = 0, \quad (2-61)$$

$$z_t^{\text{su}} \geq z_t^{\text{on}} - z_{t-1}^{\text{on}} - z_{t-1}^{\text{sb}}, \quad \forall t > 0 \quad (2-62)$$

$$z_{t-1}^{\text{off}} + z_t^{\text{sb}} \leq 1, \quad \forall t > 0 \quad (2-63)$$

$$z_t^{\text{on}} + z_t^{\text{off}} + z_t^{\text{sb}} = 1, \quad \forall t \quad (2-64)$$

Electrolyzer constraints:

$$Q_t^{\text{H2}} = \left(A(\hat{P}_t^{\text{H2}} - \beta_t^\uparrow r_t^{\uparrow, \text{H2}} + \beta_t^\downarrow r_t^{\downarrow, \text{H2}}) + Bz_t^{\text{on}} \right) \Delta T, \quad \forall t \in \mathcal{T} \quad (2-65)$$

$$\underline{P}^{\text{H2}} z_t^{\text{on}} \leq \hat{P}_t^{\text{H2}} \leq \bar{P}^{\text{H2}} z_t^{\text{on}}, \quad \forall t \in \mathcal{T} \quad (2-66)$$

$$P_t^{\text{H2}} = \hat{P}_t^{\text{H2}} + P^{\text{sb}} z_t^{\text{sb}}, \quad \forall t \in \mathcal{T} \quad (2-67)$$

$$\hat{P}_t^{\text{H2}} - r_t^{\uparrow, \text{H2}} \geq \underline{P}^{\text{H2}} z_t^{\text{on}}, \quad \forall t \in \mathcal{T} \quad (2-68)$$

$$\hat{P}_t^{\text{H2}} + r_t^{\downarrow, \text{H2}} \leq \bar{P}^{\text{H2}} z_t^{\text{on}}, \quad \forall t \in \mathcal{T} \quad (2-69)$$

Battery constraints:

$$\text{SOC}_{t=1}^{\text{bat}} = \text{SOC}^{\text{init}} + \sum_{t \in \mathcal{T}} \frac{P_{t,\omega}^{\text{bat}} - \beta_t^\uparrow r_t^{\uparrow, \text{bat}} + \beta_t^\downarrow r_t^{\downarrow, \text{bat}}}{P^{\text{bat}, \text{cap}}} \Delta T \quad (2-70)$$

$$\text{SOC}_t^{\text{bat}} = \text{SOC}_{t-1}^{\text{bat}} + \frac{P_{t,\omega}^{\text{bat}} - \beta_t^\uparrow r_t^{\uparrow, \text{bat}} + \beta_t^\downarrow r_t^{\downarrow, \text{bat}}}{P^{\text{bat}, \text{cap}}} \Delta T, \quad \forall t \in \mathcal{T} \setminus \{1\} \quad (2-71)$$

$$\text{SOC}^{\text{init}} + \sum_{t \in \mathcal{T}} \frac{P_{t,\omega}^{\text{bat}} - \beta_t^\uparrow r_t^{\uparrow, \text{bat}} + \beta_t^\downarrow r_t^{\downarrow, \text{bat}}}{P^{\text{bat}, \text{cap}}} \Delta T \leq \text{SOC}^{\text{final}} \quad (2-72)$$

$$\underline{\text{SOC}} \leq \text{SOC}_t^{\text{bat}} \leq \overline{\text{SOC}} \quad (2-73)$$

$$\text{SOC}_{t-1}^{\text{bat}} - \frac{(P_t^{\text{bat}} + r_t^{\uparrow, \text{bat}})}{P^{\text{bat}, \text{cap}}} \Delta T \geq \text{SOC}_t^{\text{min}}, \quad \forall t \in \mathcal{T} \setminus \{1\} \quad (2-74)$$

$$\text{SOC}^{\text{init}} - \frac{(P_{t=1}^{\text{bat}} + r_{t=1}^{\uparrow, \text{bat}})}{P^{\text{bat}, \text{cap}}} \Delta T \geq \text{SOC}_t^{\text{min}} \quad (2-75)$$

$$\text{SOC}_{t-1}^{\text{bat}} + \frac{(-P_t^{\text{bat}} + r_t^{\downarrow, \text{bat}})}{P^{\text{bat}, \text{cap}}} \Delta T \leq \overline{\text{SOC}}, \quad \forall t \in \mathcal{T} \setminus \{1\} \quad (2-76)$$

$$\text{SOC}^{\text{init}} + \frac{(-P_{t=1}^{\text{bat}} + r_{t=1}^{\downarrow, \text{bat}})}{P^{\text{bat}, \text{cap}}} \Delta T \leq \overline{\text{SOC}} \quad (2-77)$$

$$-\bar{P}^{\text{bat}, \text{ch}} \leq P_t^{\text{bat}} \leq \bar{P}^{\text{bat}, \text{dis}}, \quad \forall t \in \mathcal{T} \quad (2-78)$$

$$P_t^{\text{bat}} + r_t^{\downarrow, \text{bat}} \leq \bar{P}^{\text{bat}, \text{dis}} \quad (2-79)$$

$$-P_t^{\text{bat}} + r_t^{\uparrow, \text{bat}} \leq \bar{P}^{\text{bat}, \text{ch}} \quad (2-80)$$

Imbalance constraints:

$$P_t^\Delta = P_t^{\Delta+} - P_t^{\Delta-}, \quad \forall t \in \mathcal{T} \quad (2-81)$$

$$P_t^{\Delta+} \geq P_t^\Delta, \quad \forall t \in \mathcal{T} \quad (2-82)$$

$$P_t^{\Delta-} \geq -P_t^\Delta, \quad \forall t \in \mathcal{T} \quad (2-83)$$

$$P_t^{\Delta+} \leq M \cdot u_t^{imb}, \quad \forall t \in \mathcal{T} \quad (2-84)$$

$$P_t^{\Delta-} \leq M \cdot (1 - u_t^{imb}), \quad \forall t \in \mathcal{T} \quad (2-85)$$

Non-negative constraints:

$$r_t^\uparrow, r_t^\downarrow, P_t^W, P_t^{H2}, \text{SOC}_t^{\text{bat}}, \quad (2-86)$$

$$r_t^{\uparrow, \text{bat}}, r_t^{\downarrow, \text{bat}}, r_t^{\uparrow, H2}, r_t^{\downarrow, H2}, P_t^{\Delta+}, P_t^{\Delta-}, \hat{P}_t^{H2}, Q_t^{H2} \geq 0, \quad \forall t \in \mathcal{T}. \quad (2-87)$$

Binary constraints:

$$z_t^{\text{on}}, z_t^{\text{off}}, z_t^{\text{sb}} u_t^{imb} \in \{0, 1\}, \quad \forall t \in \mathcal{T}. \quad (2-88)$$

Remark on deterministic model

This model is somewhat simplistic and has inherent limitations. Combining imbalances in this way leads to arbitrage positions where energy is offered when it is known in advance that it cannot be delivered, which is not allowed in energy markets. To address this issue, an alternative model has been briefly analyzed. However, the primary purpose of this deterministic model is to summarize all constraints into a single reference framework and not to produce any of the results presented in this thesis.

2-8 Uncertainty in a two-stage model

Hybrid power plant optimization involves several uncertain elements that impact decision-making. These uncertainties arise from factors like energy prices, wind energy availability, and aFRR activation.

To address these uncertainties effectively, we extend the deterministic model to a two-stage model, which allows for better handling of uncertainty in decision-making.

2-8-1 Types of uncertainty

In the context of hybrid power plant optimization, various uncertainties influence the decision-making process. While this thesis focuses on specific uncertainties, many others exist in practice when additional markets and operational factors are considered. The key uncertainties present in our decision-making model can be broadly categorized as follows:

- **Operational uncertainties:**

- *Wind generation* ($P_t^{W,A}$): The availability of wind energy is inherently uncertain and subject to forecast errors.

- *aFRR activation* ($\beta_t^\uparrow, \beta_t^\downarrow$): The activation of automatic Frequency Restoration Reserves (aFRR) is unpredictable due to its dependence on real-time grid imbalances. These activations are decision-dependent in two ways: they rely on the choice of aFRR capacity in the first stage and are influenced by the bidding profile of aFRR energy bids.

- **Price uncertainties:**

- *Day-ahead energy prices* (λ_t^{DA}): These prices are uncertain but can be forecasted reasonably well, making them manageable in the optimization process [17].
- *aFRR capacity prices* ($\lambda_t^{r,\uparrow}, \lambda_t^{r,\downarrow}$): The prices for reserving aFRR capacity (up and down) are difficult to model due to the pay-as-bid system, where only average prices are published. For simplicity, these are assumed to be known [13].
- *aFRR activation prices* ($\lambda_t^{r,act,\uparrow}, \lambda_t^{r,act,\downarrow}$): The prices for activated aFRR (up and down) are volatile and depend on real-time market conditions. These prices are also influenced by the bidding profile of aFRR energy bids. With an activation strategy the minimal activation price received is known and is assumed as the forecasted value.
- *Imbalance prices* ($\lambda_t^{\Delta\uparrow}, \lambda_t^{\Delta\downarrow}$): These prices reflect the cost of balancing energy deviations and are highly unpredictable on the day-ahead stage [18]. However research has been done on short-term predictions which shows real-time forecasting is possible [19]. To not dive too deep into forecasting we assume the most recent imbalance price known and the others as unknown.
- *Hydrogen prices* (λ_t^{H2}): The market price for hydrogen can vary based on demand and supply conditions. Currently, we assume there is no established hydrogen market and use a stable price based on future predictions.

In this thesis, we focus primarily on **operational uncertainties** — particularly wind generation and aFRR activation — and include **day-ahead energy price uncertainty** due to its manageable complexity and to observe price uncertainty effects on the decision-making process. Other uncertainties, such as aFRR capacity prices, aFRR activation prices, imbalance prices, and hydrogen prices, are acknowledged but are not handled as uncertain but assumed to be known because they are either difficult to predict accurately or heavily influenced by bidding mechanics.

This distinction allows us to define the set of uncertain parameters as:

$$\xi = \left\{ \beta_t^\uparrow, \beta_t^\downarrow, P_t^{W,A}, \lambda_t^{DA} \mid t \in \mathcal{T} \right\}.$$

By concentrating on these uncertainties, the model aims to enhance the robustness of day-ahead decisions and real-time adjustments, providing a practical framework for managing variability inherent in renewable energy and reserve activation.

2-8-2 Definition of two-stage models

Hybrid power plant optimization often employs two-stage models to effectively handle uncertainty. As defined by [5], a generic two-stage model is structured as follows:

$$\begin{aligned}
& \min_{\mathbf{x}, \mathbf{y}_\xi} f^F(\mathbf{x}) + f^S(\mathbf{x}, \mathbf{y}_\xi, \boldsymbol{\xi}) \\
& \text{s.t. } \mathbf{h}^F(\mathbf{x}) = 0, \quad \mathbf{g}^F(\mathbf{x}) \leq 0, \\
& \quad \mathbf{h}^S(\mathbf{x}, \mathbf{y}_\xi, \boldsymbol{\xi}) = 0, \\
& \quad \mathbf{g}^S(\mathbf{x}, \mathbf{y}_\xi, \boldsymbol{\xi}) \leq 0.
\end{aligned} \tag{2-89}$$

With \mathbf{x} being the first-stage decisions, \mathbf{y}_ξ the second-stage decisions for uncertainty realization ξ . After solving the first stage, the second stage is formulated as:

$$\begin{aligned}
& \min_{\mathbf{y}} f^S(\mathbf{x}^*, \mathbf{y}, \boldsymbol{\xi}^*) \\
& \text{s.t. } \mathbf{h}^S(\mathbf{x}^*, \mathbf{y}, \boldsymbol{\xi}^*) = 0 \\
& \quad \mathbf{g}^S(\mathbf{x}^*, \mathbf{y}, \boldsymbol{\xi}^*) \leq 0.
\end{aligned} \tag{2-90}$$

With x^* being the first-stage decisions coming from the first stage, now parameters. And $\boldsymbol{\xi}^*$ being the realized uncertainty parameter.

2-8-3 Adapting the two-stage model for HPP optimization

In HPP optimization, the two-stage model is adapted to include discrepancies between the objectives of the first and second stages:

$$\begin{aligned}
& \text{First Stage: } f^{\text{DA}}(\mathbf{x}) + f^{\hat{S}}(\mathbf{x}, \mathbf{y}_\xi, \boldsymbol{\xi}) \\
& \text{Second Stage: } f^{\hat{S}}(\mathbf{x}^*, \mathbf{y}, \boldsymbol{\xi}^*) + f^{\text{imb}}(\mathbf{y}^{\text{imb}})
\end{aligned}$$

Where:

- $f^{\hat{S}}(\mathbf{x}, \mathbf{y}_\xi, \boldsymbol{\xi})$: Shared terms across objectives (e.g., hydrogen production, start-up cost, and aFRR capacity activation).
- $f^{\text{DA}}(\mathbf{x})$: Day-ahead specific terms in the first stage.
- $f^{\text{imb}}(\mathbf{y}^{\text{imb}})$: Imbalance adjustments unique to the second stage.

First- and second-stage decisions

The first-stage decision variables include the decisions made on the day before. Those being in this case the amount of energy offered in the DA market and the aFRR capacity market:

$$\mathbf{x} = \{P_t^{\text{DA}}, r_t^\uparrow, r_t^\downarrow \mid t \in \mathcal{T}\}.$$

Second-stage variables include real-time adjustments for imbalance and operational uncertainties:

$$\mathbf{y} = \{P_t^{\text{W}}, P_t^{\text{H2}}, P_t^{\text{bat}}, \text{SOC}_t^{\text{bat}}, r_t^{\uparrow, \text{bat}}, r_t^{\downarrow, \text{bat}}, r_t^{\uparrow, \text{H2}}, r_t^{\downarrow, \text{H2}}, z_t^{\text{on}}, z_t^{\text{off}}, z_t^{\text{sb}}, P_t^{\Delta+}, P_t^{\Delta-}, \hat{P}_t^{\text{H2}}, Q_t^{\text{H2}} \mid t \in \mathcal{T}\}.$$

Uncertainty parameters

The total set of uncertain parameters initially includes:

$$\xi = \left\{ \beta_t^\uparrow, \beta_t^\downarrow, P_t^{W,A}, \lambda_t^{\Delta\uparrow}, \lambda_t^{\Delta\downarrow}, \lambda_t^{H2}, \lambda_t^{DA}, \lambda_t^{r,\uparrow}, \lambda_t^{r,\downarrow}, \lambda_t^{r,act,\uparrow}, \lambda_t^{r,act,\downarrow} \mid t \in \mathcal{T} \right\}.$$

However, this is narrowed down to focus on operational uncertainty with the other uncertain parameters assumed to be known:

$$\xi = \left\{ \beta_t^\uparrow, \beta_t^\downarrow, P_t^{W,A}, \lambda_t^{DA} \mid t \in \mathcal{T} \right\}.$$

This refinement accounts for the challenges in forecasting aFRR activation and imbalance prices. The exclusion of imbalance revenue from the first stage avoids overly optimistic capacity allocation while ensuring a practical balance between day-ahead energy and aFRR capacity.

2-8-4 First-stage decision model

The first-stage optimization problem focuses on determining the day-ahead (DA) decision variables, including net power dispatch, upward and downward aFRR capacity, and hydrogen production. These decisions are made with the goal of maximizing expected revenue from the DA market, aFRR capacity payments, and hydrogen income. Since the actual hydrogen production depends on uncertain factors such as wind availability and aFRR activation, the first stage optimizes the expected hydrogen amount of $Q_t^{H2,exp}$ based on forecasted values.

The objective function is defined as:

$$\begin{aligned} \max \left(96r^\uparrow \lambda^{r\uparrow} + 96r^\downarrow \lambda^{r\downarrow} + \sum_{t \in \mathcal{T}} \left(P_t^{net} \Delta T \lambda_t^{DA} \right. \right. \\ \left. \left. + Q_t^{H2,exp} \lambda_t^{H2} - z^{SU,exp} C^{SU} \right) \right) \end{aligned} \quad (2-91)$$

Subject to:

Power balancing constraints:

$$P_t^{DA} = P_t^W - P_t^{H2} + P_t^{bat} \quad (2-92)$$

$$r^\uparrow = r_t^{\uparrow,bat} + r_t^{\uparrow,H2} \quad (2-93)$$

$$r^\downarrow = r_t^{\downarrow,bat} + r_t^{\downarrow,H2} \quad (2-94)$$

$$P_t^{DA} + r^\uparrow \leq \overline{P}^{net} \quad (2-95)$$

$$P_t^{DA} - r^\downarrow \geq -\underline{P}^{net} \quad (2-96)$$

Electrolyzer and battery Constraints:

See Equation 2-61 to Equation 2-80.

2-8-5 Second stage decision model

After solving this problem the second stage will consist of optimizing over the day itself. To account for any possible discrepancies and not get failed solves, we loosen the equality of the first stage variables using non-negative slack variables.

As optimizing again different activation parameters of aFRR can be inputted. As could be used in the case of forecasted activation and actual activation. Different activation parameters might render the problem infeasible. E.g. when the battery might be discharged more than expected due to many full upward activated aFRR. The battery might not be able to deliver more upward activated aFRR. To measure this we introduce slack variables for the aFRR equations as well.

$$r^\uparrow = r_t^{\uparrow, H2} + r_t^{\uparrow, bat} - s_t^{r\uparrow-} + s_t^{r\uparrow+} \quad (2-97)$$

$$r^\downarrow = r_t^{\downarrow, H2} + r_t^{\downarrow, bat} - s_t^{r\downarrow-} + s_t^{r\downarrow+} \quad (2-98)$$

- $s_t^{r\uparrow-}$: Accounts for any shortfall in the upward aFRR capacity.
- $s_t^{r\uparrow+}$: Accounts for any excess in the upward aFRR capacity.
- $s_t^{r\downarrow-}$: Accounts for any shortfall in the downward aFRR capacity.
- $s_t^{r\downarrow+}$: Accounts for any excess in the downward aFRR capacity.

with

$$s_t^{r\uparrow-}, s_t^{r\uparrow+}, s_t^{r\downarrow-}, s_t^{r\downarrow+} \geq 0 \quad \forall t \quad (2-99)$$

They are introduced in the objective with use of slack penalty, this forms the second stage optimization problem considering optimized first stage variables denoted with an asterisk.

$$\begin{aligned} \max \quad & \sum_{t \in \mathcal{T}} \left(Q_t^{H2} \lambda_t^{H2} - z^{SU} C^{SU} + P_t^{\Delta+} \lambda_t^{\Delta+} \Delta T - P_t^{\Delta-} \lambda_t^{\Delta-} \Delta T \right. \\ & \left. \beta_t^\uparrow r_t^{\uparrow, bat} \lambda_t^{r, act, \uparrow} \Delta T - \beta_t^\downarrow r_t^{\downarrow, bat} \lambda_t^{r, act, \downarrow} \Delta T \right. \\ & \left. - N(s_t^+ + s_t^- + s_t^{r\uparrow-} + s_t^{r\uparrow+} + s_t^{r\downarrow-} + s_t^{r\downarrow+}) \right) \end{aligned} \quad (2-100)$$

Subject to:

Power Balancing Constraints:

$$P_t^{DA*} + P_t^\Delta = P_t^W - P_t^{H2} + P_t^{bat} + s_t^+ - s_t^- \quad (2-101)$$

$$r_t^{\uparrow, *} = r_t^{\uparrow, H2} + r_t^{\uparrow, bat} - s_t^{r\uparrow-} + s_t^{r\uparrow+} \quad (2-102)$$

$$r_t^{\downarrow, *} = r_t^{\downarrow, H2} + r_t^{\downarrow, bat} - s_t^{r\downarrow-} + s_t^{r\downarrow+} \quad (2-103)$$

$$P_t^{DA*} + P_t^\Delta + r_t^{\uparrow, *} \leq \overline{P}^{net} \quad (2-104)$$

$$P_t^{DA*} + P_t^\Delta - r_t^{\downarrow, *} \geq -\underline{P}^{net} \quad (2-105)$$

Electrolyzer, Battery, and PImb Constraints:

See Equation 2-61 to Equation 2-85.

Now, with this definition of the two-stage structure, we can introduce uncertainties into the problem. Forecasts can be input into the first stage of the problem, while the realization of uncertain parameters in the second stage accounts for forecast errors. However, relying solely on forecasted values for uncertain parameters may not be sufficient, as forecast errors can significantly impact decision-making.

2-8-6 Forecasting and uncertainty management

Effective forecasting is critical for handling uncertainties in hybrid power plant operations, including predicting energy prices, renewable generation, and load demands. The literature outlines several forecasting techniques suitable for hybrid power systems. Time series models such as ARIMA (AutoRegressive Integrated Moving Average) are widely used for forecasting prices and demand due to their adaptability to trends and seasonal patterns. Additionally, regression-based models and machine learning approaches offer flexibility in capturing complex dependencies in high-dimensional data, which can be advantageous for market price forecasting [17].

For renewable generation forecasts, particularly wind and solar power, ensemble models combining statistical and physical methods are common. These models use real-time meteorological data to predict output fluctuations, allowing hybrid power plants to balance supply and demand effectively.

In hybrid systems, the quality of forecasts directly influences the choice of uncertainty management methods. Accurate forecasts are often sufficient for deterministic optimization approaches, whereas less reliable forecasts typically necessitate robust or stochastic optimization methods to account for uncertainty. While this thesis does not develop forecasting models, it assumes forecasted values as inputs to the optimization process and focuses on how these uncertainties are incorporated into the decision-making framework.

2-9 Iterative second-stage optimization through a shrinking horizon approach

To solve the second stage, multiple approaches can be taken. Either the uncertainty is assumed to be fully realized for the entire day, or it is revealed incrementally in steps. This distinction is important in setting up the optimization problem. While assuming all uncertainty is known a priori is valid and found in the literature [10], it is far less realistic. Such an assumption does not reflect the impulse-like behavior of activation energy and the inherent difficulty of predicting balancing energy.

To fairly compare different approaches, we evaluate their effectiveness in handling the disturbances caused by activation and the realization of uncertainty. To test the method, the second stage of the problem is reformulated into a shrinking-horizon approach.

This effectively transforms the problem into a multi-stage framework, where the optimization is solved iteratively over time steps with the ability to update the uncertainty. This iterative approach allows for testing the methods based on the principle of certainty gain [6].

At each iteration h , the shrinking horizon is defined by the set $\mathcal{H}_h = \{1, 2, \dots, T - h\}$, where $t^h \in \mathcal{H}_h$ represents the horizon indices. The optimization problem is solved over the subset $\mathcal{T}_h = \{h, h + 1, \dots, T\}$, which still uses indices t , ensuring that constraints apply consistently to the remaining time steps.

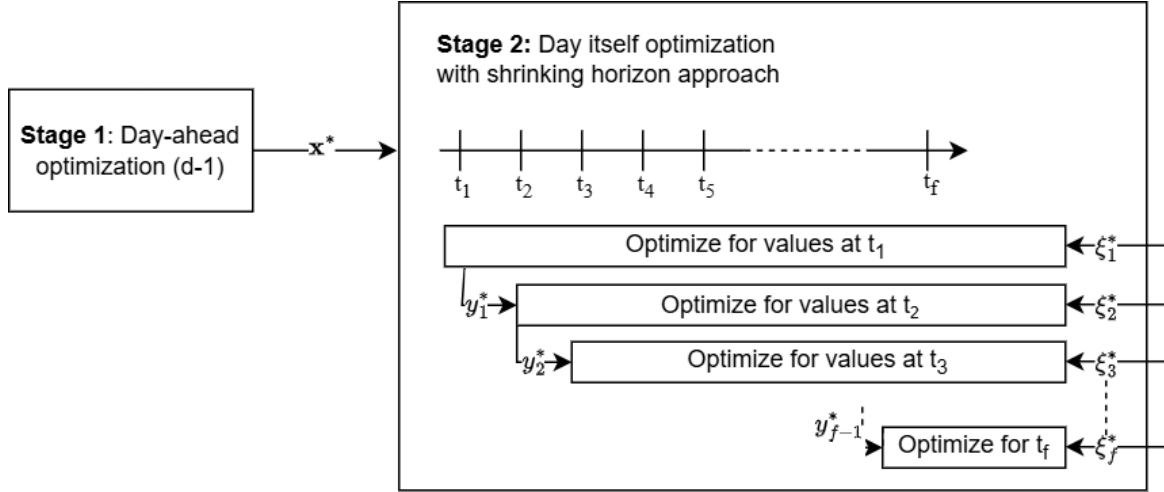


Figure 2-4: Shrinking horizon framework

2-9-1 Additional Constraints

Several additional constraints arise or are modified when optimizing using the shrinking horizon approach.

The first additional constraint fixes the initial state of the electrolyzer to account for ramp-up limits specific to state switching. The optimal state at the current time step t is set to the one found for $t + 1$ in the previous optimization step:

$$z_{t^h=1}^{\text{on}} = z_{t^h-1=2}^{\text{on},*}$$

The state of charge (SOC) at the next time step is calculated based on the previous optimal SOC value and the operational decisions made during the current optimization step, ensuring continuity in the SOC dynamics:

$$SOC_{t^h=0}^{\text{init}} = SOC_{t^h-1=1}^*$$

Besides, during the first steps of the horizon, the penalty N is increased to prioritize the validity of the solution for the first time step in cases where a valid solution for the entire timeline cannot be found. This makes N a time-dependent parameter vector:

$$\mathbf{N} = \{\alpha N, N, \dots, N\}.$$

2-10 Chapter summary: general modeling

This chapter presents a comprehensive model for the optimization of hybrid power plant operations across multiple energy markets. The fundamental components of the hybrid power plant, particularly the electrolyzer and battery, are defined using mathematical formulations and constraints. The electrolyzer is modeled with a three-state structure to capture its operational dynamics, including transitions between on, off, and standby states, with constraints ensuring that power consumption remains within specified limits. The battery model incorporates constraints related to the SOC and operational boundaries.

Furthermore, the integration of the Dutch aFRR market is addressed. The model incorporates capacity bidding, energy bids, and real-time activation strategies, ensuring that the plant's operations comply with market requirements. The passive imbalance system is included to represent deviations from planned energy schedules, capturing their financial implications and linking them to aFRR activations. Constraints are imposed to ensure that participation in the aFRR market does not lead to conflicting imbalances.

These components are assembled into a deterministic model, representing the hybrid power plant's behavior under fixed conditions. While deterministic modeling provides a foundational framework for decision-making, it is insufficient for capturing the inherent uncertainties associated with renewable energy generation, market prices, and reserve activation. To address these uncertainties, the deterministic framework is extended into a two-stage model. The first stage focuses on day-ahead decisions, including commitments to energy and allocations to reserves, while the second stage adjusts these decisions based on the realization of uncertain parameters.

The second stage employs a shrinking-horizon approach to enhance adaptability. This method enables iterative decision-making, allowing operational setpoints to be updated as new information becomes available throughout the day. The shrinking horizon framework improves the plant's ability to respond dynamically to uncertainty by permitting real-time adjustments.

To further address the challenges posed by uncertainty, the subsequent chapter introduces a stochastic programming approach. Stochastic programming extends the two-stage model by incorporating multiple scenarios that capture variations in wind generation, market prices, and aFRR activation. This approach optimizes day-ahead decisions to ensure consistency across scenarios while maintaining feasibility under a range of potential outcomes.

Approach 1: stochastic programming

Extending the fully deterministic model, which assumes known values for all parameters, stochastic programming introduces a framework for handling uncertainties. This chapter discusses the rationale for incorporating stochastic elements into the optimization model, detailing the formulation of a two-stage stochastic programming approach to manage uncertainties in production and pricing. The subsequent sections outline the model's formulation, the role of non-anticipativity constraints, and methods to optimize decisions under probabilistic variation.

3-1 Stochastic Model Framework

The framework of the approach is shown in Figure 3-1. The framework outlines the steps required in the stochastic programming approach. In the day-ahead decision stage, wind scenarios are generated to account for uncertainties in wind power availability, market pricing, and reserve energy activation. For a larger version see Appendix E.

The stochastic programming approach addresses uncertainties by considering multiple potential outcomes (scenarios). The process begins with collecting and processing historical wind data and forecasts to fit error forecasting models that quantify deviations between forecasted and actual wind power values. These models generate a range of wind scenarios to capture forecast uncertainties. Additionally, aFRR activation scenarios are created to account for potential upward and downward reserve activations, introducing further uncertainty related to grid stability.

In this framework, the uncertainties in wind power generation and reserve activation are treated as independent. Since the probabilities of aFRR activation scenarios are not known in advance, they are assigned equal probabilities. The combined scenario set is constructed by pairing these activation scenarios with the reduced wind scenarios, resulting in each combined scenario having a probability equal to the probability of the wind scenario divided by the number of activation scenarios. This independence assumption simplifies the modeling

process by avoiding the need for complex dependency structures while preserving computational feasibility.

In the day-ahead decision stage, the first-stage optimization problem is solved to determine optimal day-ahead energy bids and reserve capacity commitments. These decisions are inherently uncertain, as they are made before the actual wind and reserve activations are realized. The expected profit of these decisions is evaluated across all generated scenarios. When the first-stage variables are sent to the second stage the actual first-stage profit is calculated with the real market price data.

The framework transitions to the day-of-operation stage, where real-time decisions are adjusted as new information becomes available. At each time step $t = h$, actual wind values update the forecast starting point. This refined forecast undergoes scenario reduction to manage computational complexity while preserving essential stochastic characteristics.

Balancing reserve scenarios are updated accordingly, and the second-stage optimization problem is solved to determine real-time operational decisions, being the second-stage variables y . These second-stage decisions maintain consistency with the day-ahead plans. The process iterates through each time step until the 24-hour period concludes, at which point the final second-stage profit is calculated, combining day-ahead and real-time outcomes to determine total revenue.

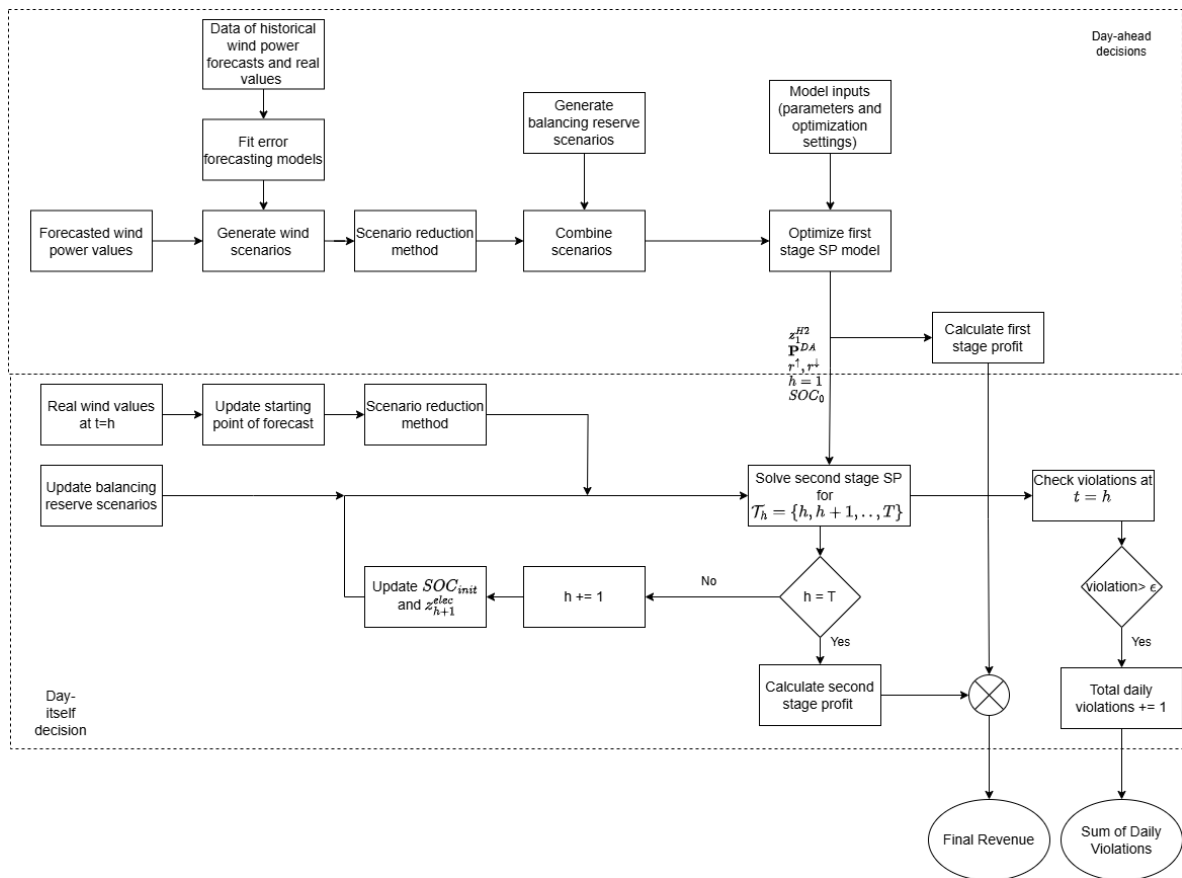


Figure 3-1: Stochastic programming framework

3-2 Two-Stage Stochastic Programming Model

With the framework explained we will now explain the steps in more detail. Looking at the optimization model and more specific ways of dealing with scenario generation and reduction.

3-2-1 Scenario programming definitions

Solving for uncertainty means we will be looking at the effect of uncertain parameters on the optimization problem. In a standard two-stage formulation this can be seen as:

$$\begin{aligned} \min_{\mathbf{x}, \mathbf{y}_\xi} \quad & f^F(\mathbf{x}) + \mathbb{E}_P \left[f^S(\mathbf{x}, \mathbf{y}_\xi, \boldsymbol{\xi}) \right] \\ \text{s.t.} \quad & \mathbf{h}^F(\mathbf{x}) = 0, \quad \mathbf{g}^F(\mathbf{x}) \leq 0, \\ & \mathbf{h}^S(\mathbf{x}, \mathbf{y}_\xi, \boldsymbol{\xi}) = 0, \\ & \mathbf{g}^S(\mathbf{x}, \mathbf{y}_\xi, \boldsymbol{\xi}) \leq 0. \end{aligned} \quad (3-1)$$

$$\mathbb{E}_P \left[f^S(\mathbf{x}, \mathbf{y}_\xi, \boldsymbol{\xi}) \right] \approx \sum_{\omega \in \Omega} \pi_\omega f^S(\mathbf{x}, \mathbf{y}_\omega, \boldsymbol{\xi}_\omega) \quad (3-2)$$

Each realization is paired with a probability π_ω , which can be defined in the following way [6]:

$$\pi_\omega = P(\omega \mid \boldsymbol{\xi} = \boldsymbol{\xi}(\omega)), \quad \text{where} \quad \sum_{\omega \in \Omega} \pi_\omega = 1 \quad (3-3)$$

Where ω is the scenario index with the set of scenarios $\Omega = \{1, \dots, N^\omega\}$ and $\boldsymbol{\xi}$ is the set of possible outcomes of the random variables.

The formulation in Equation 3-1 assumes a **risk-neutral perspective**, aiming to minimize the expected cost without prioritizing risk aversion. This approach simplifies the analysis. The introduction of large penalty values for the slack variables should penalize risk in a prioritizing matter.

Alternative risk-aware approaches, such as Conditional Value-at-Risk (CVaR) or Value-at-Risk (VaR), can be incorporated to emphasize tail risks [20]. These methods allocate greater weight to unfavorable scenarios, managing the potential impact of heavy-tailed distributions. However, the implementation of such measures requires prior knowledge of the distributional characteristics of uncertain parameters.

First-stage stochastic programming model

The first-stage problem is recast as a stochastic programming model as follows:

$$\max \left(96r^\uparrow \lambda^{r^\uparrow} + 96r^\downarrow \lambda^{r^\downarrow} + \sum_{\omega \in \Omega} \pi_\omega \left(\sum_{t \in \mathcal{T}} \left(P_t^{\text{DA}} \Delta T \lambda_{t,\omega}^{\text{DA}} + Q_{t,\omega}^{H2} \lambda_t^{H2} - z_{t,\omega}^{\text{SU}} C^{\text{SU}} \right) \right) \right) \quad (3-4)$$

Subject to

Power balancing Constraints:

$$P_t^{\text{DA}} = P_{t,\omega}^{\text{W}} - P_{t,\omega}^{\text{H2}} + P_{t,\omega}^{\text{bat}}, \quad \forall t \in \mathcal{T}, \omega \in \Omega \quad (3-5)$$

$$r_t^\uparrow = r_{t,\omega}^{\uparrow,\text{bat}} + r_{t,\omega}^{\uparrow,\text{H2}}, \quad \forall t \in \mathcal{T}, \omega \in \Omega \quad (3-6)$$

$$r_t^\downarrow = r_{t,\omega}^{\downarrow,\text{bat}} + r_{t,\omega}^{\downarrow,\text{H2}}, \quad \forall t \in \mathcal{T}, \omega \in \Omega \quad (3-7)$$

$$P_t^{\text{DA}} + r_t^\uparrow \leq \bar{P}^{\text{net}}, \quad \forall t \in \mathcal{T}, \omega \in \Omega \quad (3-8)$$

$$P_t^{\text{DA}} - r_t^\downarrow \geq -\underline{P}^{\text{net}}, \quad \forall t \in \mathcal{T}, \omega \in \Omega \quad (3-9)$$

Electrolyzer and battery Constraints:

See Equation 2-61 to Equation 2-80 with the additional ω index.

The full notation for the stochastic model can be found in Appendix F.

Role of non-anticipativity constraints

As can be seen in eqs. (3-5) to (3-9), not all variables include a index for the uncertainty set Ω . This is referred to as non-anticipativity constraints. This ensures that first-stage variables, such as P_t^{DA} , r_t^\uparrow , and r_t^\downarrow , remain the same across all scenarios. These variables do not depend on the scenario-specific index ω , as their decisions are made before the realization of uncertain parameters. This consistency is enforced by the following formulation:

$$\mathbf{x} = \mathbf{x}_\omega, \quad \forall \omega \in \Omega$$

Non-anticipativity constraints maintain the feasibility and robustness of the model in the presence of uncertainty by ensuring uniformity across scenarios.

3-2-2 Second-stage stochastic programming model

Furthermore the second-stage model is recast to a stochastic programming model

$$\max \sum_{\omega \in \Omega} \pi_\omega \left(\sum_{t \in \mathcal{T}} \left(Q_{t,\omega}^{\text{H2}} \lambda_t^{\text{H2}} - z_{t,\omega}^{\text{SU}} C^{\text{SU}} + P_{t,\omega}^{\Delta+} \lambda_t^{\Delta+} \Delta T - P_{t,\omega}^{\Delta-} \lambda_t^{\Delta-} \Delta T \right. \right. \\ \left. \left. + \beta_t^\uparrow r_t^\uparrow \lambda_t^{r,\text{act},\uparrow} \Delta T - \beta_t^\downarrow r_t^\downarrow \lambda_t^{r,\text{act},\downarrow} \Delta T \right) \right) \quad (3-10)$$

Subject to:

Power balancing Constraints:

$$P_t^{\text{DA},*} = P_{t,\omega}^{\text{W}} - P_{t,\omega}^{\text{H2}} + P_{t,\omega}^{\text{bat}} - P_{t,\omega}^{\Delta}, \quad \forall t \in \mathcal{T}, \omega \in \Omega \quad (3-11)$$

$$r_t^{\uparrow*} = r_{t,\omega}^{\uparrow,\text{bat}} + r_{t,\omega}^{\uparrow,\text{H2}}, \quad \forall t \in \mathcal{T}, \omega \in \Omega \quad (3-12)$$

$$r_t^{\downarrow*} = r_{t,\omega}^{\downarrow,\text{bat}} + r_{t,\omega}^{\downarrow,\text{H2}}, \quad \forall t \in \mathcal{T}, \omega \in \Omega \quad (3-13)$$

$$P_{t,\omega}^{\text{DA}} + P_{t,\omega}^{\Delta} + r_t^{\uparrow*} \leq \bar{P}^{\text{net}}, \quad \forall t \in \mathcal{T}, \omega \in \Omega \quad (3-14)$$

$$P_{t,\omega}^{\text{DA}} + P_{t,\omega}^{\Delta} - r_t^{\downarrow*} \geq -\underline{P}^{\text{net}}, \quad \forall t \in \mathcal{T}, \omega \in \Omega \quad (3-15)$$

Electrolyzer, battery and PImb constraints:

See Equation 2-61 to Equation 2-85 with the additional ω index.

The full notation for the stochastic model can again be found in Appendix F.

Shrinking horizon adaptation and non-anticipatory constraints

Depending on the uncertainty release mechanism discussed in section 2-9, the non-anticipatory constraints will vary. When uncertainty is released all at once, reformulating the problem into a stochastic programming model is unnecessary, as the model no longer contains uncertainty. However, under the shrinking horizon approach, the second-stage problem transforms into a multi-stage stochastic problem.

In this approach, the decisions at the current time step—corresponding to the first time step of the shrinking horizon—are enforced as non-anticipatory variables. This ensures that decisions at this step are scenario-independent and satisfy the following condition:

$$\mathbf{y}_{t_1} = \mathbf{y}_{t_1, \omega}, \quad \forall \omega \in \Omega,$$

where:

- t_1 is the **first element** of the time set T in the shrinking horizon.

This constraint ensures that the decision variable \mathbf{y}_{t_1} remains consistent across all scenarios ω in the scenario set Ω , thereby maintaining non-anticipativity at the current step.

Furthermore, as new information about incoming uncertainty becomes available, the set of scenarios can be regenerated to reflect the updated knowledge.

3-3 Scenario generation

In stochastic programming, scenario trees are essential for representing uncertainties in a manageable way, as continuous stochastic processes are often too complex to solve directly. However, the scenario count increases exponentially with the number of uncertain variables, making scenario reduction techniques or intelligent sampling methods necessary to maintain computational feasibility.

Several methods for scenario generation are established in the literature:

- **Sampling-based Methods:** Techniques such as Monte Carlo simulation are widely used for scenario generation due to their simplicity and efficiency. By sampling from known probability distributions, these methods create a range of potential outcomes that represent uncertainty comprehensively [21]. However, they are most effective when probability distributions are well-defined.

- **Forecasting-based Methods:** Time series models, including ARIMA, are frequently applied to generate scenarios for data that exhibit temporal dependencies, such as energy prices.

These models use historical data to simulate sample paths, which can be organized into scenario trees through clustering techniques [6]. Time series approaches require assumptions about the stationarity and distribution of variables, which may limit their applicability for complex or highly dynamic systems.

Scenario reduction methods

While generating a large number of scenarios can capture the full range of uncertainties in a stochastic model, this approach quickly becomes computationally demanding. To address this, scenario reduction methods are used to create a smaller subset of scenarios that retains the essential stochastic information of the original data.

One approach to scenario reduction involves probability distance measures, which quantify the similarity between two probability distributions. A common metric for this in stochastic programming is the Kantorovich distance, also known as the Wasserstein distance, which minimizes the "cost" of transforming one probability distribution into another [6]. This method allows the reduced scenario set to approximate the statistical characteristics of the full set while remaining computationally feasible.

Scenario reduction methods include forward and backward algorithms, as proposed by Dupacová et al. [22]. The backward algorithm progressively eliminates scenarios from the original set until the target size is reached, while the forward algorithm incrementally builds a reduced set by adding representative scenarios. Although these methods do not guarantee optimality, they have shown effective performance in practice [23]. The main limitation is that the size of the reduced set must be predefined, which can be challenging to estimate accurately. Previous research has shown that fast forward selection achieves excellent results with relatively low computational effort [24]. Based on these findings, fast forward selection is adopted as the scenario reduction technique for this optimization framework.

3-4 Challenges with reserve energy activation uncertainty

To form the scenarios for the reserve energy activation we either use a pessimistic activation approach. Meaning we assume in part of the scenarios that all up activation is activated and in another set of scenarios all down reserves are activated. And lastly we add a scenario where no activation occurs. The second approach is to generate a number of activation scenarios (N^A) with a specified number of random draws (N^{draws}) for both the up and down activation. The parameter of draws can be an approximation of the amount of activations linked to a certain activation strategy however when these activation will take place on the day is hard to impossible to say source. Covering the different combinations will lead to a huge amount of scenarios lower bounded by:

$$\text{Total possible distributions} \geq 2 \sum_{k=0}^x \binom{T}{k}$$

with x the maximum number of activations expected in the day, both up and down activation combined. $\binom{T}{k}$ is the binomial coefficient, representing the number of ways to choose k positions for 1's out of T positions.

Using the heuristic approach of all down and up, covers a large amount of scenario's and should be relatively robust to activation, it is difficult to use existing knowledge about the amount of activations and still have a robust solutions. For example, if we expect on a day 5 activation will occur, it is hard to create a pattern for to cover enough scenarios to be sure that the scenario programming will be robust.

3-5 Chapter summary: stochastic programming framework

This chapter builds upon the deterministic model by incorporating stochastic programming to address the inherent uncertainties associated with hybrid power plant operations. A two-stage framework is developed, incorporating scenarios that represent variability in renewable energy production, market prices, and reserve energy activation. The non-anticipativity constraints guarantee consistency in the initial stage of decision-making, while the scenario generation and reduction techniques ensure computational feasibility and accuracy. The shrinking horizon approach refines the two-stage model by enabling dynamic updates to the second-stage as uncertainties unfold.

Although stochastic programming provides a structured approach to managing uncertainty, its computational demands and reliance on probabilistic scenarios can restrict its practical applicability. These limitations prompt an investigation into robust optimization in the subsequent chapter, with a focus on resilience against worst-case scenarios that are not contingent on probabilistic assumptions.

Approach 2: adaptive robust optimization

Building upon the stochastic programming framework introduced in the previous chapter, this chapter transitions from scenario-based to bound-based uncertainty representation. While stochastic programming captures variability through probabilistic scenarios and ensures consistency in initial decisions with non-anticipativity constraints, its computational demands and reliance on scenario generation can limit practical applicability. These constraints motivate the exploration of robust optimization as an alternative approach.

Adaptive robust optimization (ARO) replaces scenarios with uncertainty sets, providing a framework that guarantees feasibility under all realizations within specified bounds. This approach is particularly relevant for hybrid power plants participating in capacity markets, where strict constraints demand resilient operational strategies. ARO adopts a two-stage structure, balancing initial (*here-and-now*) decisions with flexible (*wait-and-see*) adjustments to handle realized uncertainties.

This chapter introduces the ARO framework, highlighting its mathematical formulation and the definition of uncertainty sets. To address the complexity of solving ARO problems, a column-constraint generation algorithm is employed, iteratively refining solutions. Additionally, a shrinking horizon adaptation allows dynamic updates as new information becomes available, enabling robust decision-making in real-time.

By building on the principles of stochastic programming, ARO provides a complementary perspective, ensuring resilience against worst-case scenarios without relying on probabilistic assumptions.

4-1 ARO framework

Robust optimization is a methodology designed to ensure decision-making feasibility under uncertain conditions by optimizing for the worst-case realization within predefined uncertainty

sets. Unlike stochastic programming, which models uncertainty probabilistically through scenarios, robust optimization relies on deterministic bounds to encapsulate variability. This makes it particularly useful in applications where rare but extreme events can significantly impact feasibility and performance [25], [7].

The key advantage of robust optimization lies in its conservatism, which guarantees feasible solutions across all realizations within the uncertainty set. Commonly used uncertainty sets include box, polyhedral, and cardinality-constrained sets. Cardinality-constrained uncertainty sets, for example, limit the number of parameters that can simultaneously deviate, striking a balance between conservatism and practicality.

In the context of hybrid power plant operations, robust optimization is extended to adaptive robust optimization, where a two-stage structure enables preemptive and reactive decision-making. The first stage optimizes initial decisions (*here-and-now*), while the second stage adjusts decisions (*wait-and-see*) after uncertainty is realized.

As can be seen in Figure 4-1 there are a few key differences with the stochastic framework.

- **Use of uncertain bounds instead of scenarios:** Unlike the stochastic framework, which relies on multiple scenarios to represent uncertainty, this approach utilizes uncertain bounds to encapsulate the range of possible variations.
- **New solver algorithm for DA values:** A different solver algorithm is implemented to determine the Day-Ahead (DA) values. Needed to deal with the complexity of finding a robust solution.
- **Electrolyzer scheduling in the DA phase:** The scheduling of the electrolyzer is now conducted during the Day-Ahead phase, allowing for more robust decisions.

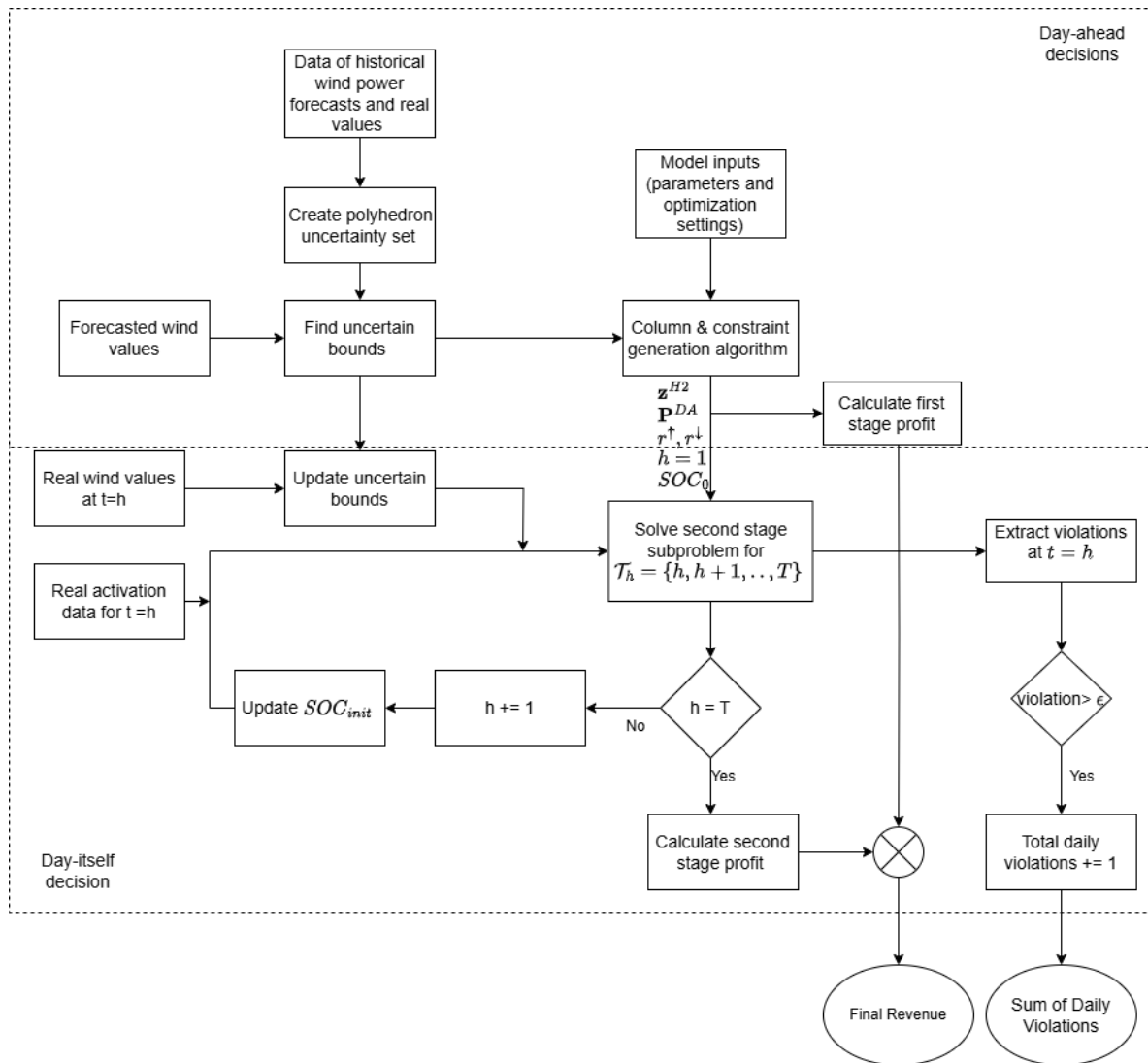


Figure 4-1: Robust optimization framework

4-2 Formulation for adaptive robust optimization model

The formulation of the ARO is as follows [7]:

$$\max_{\mathbf{x} \in \mathbf{X}} \left(f(\mathbf{x}) + \min_{\xi \in \Xi} \max_{y \in Y(\mathbf{x}, \xi)} f(\mathbf{x}, \mathbf{y}, \xi) \right) \quad (4-1)$$

This formulation captures the essence of adaptive robust optimization, which involves decision-making under uncertainty with two stages:

- **First Stage Decisions** (x): The first stage represents decisions that must be made before the uncertainty (ξ) is realized. These decisions are referred to as "here-and-now" decisions, as they set the basis for how the system should behave across uncertain conditions. Here, $x \in X$ represents these initial, robust decisions and is constrained by feasible set X , while $c^T x$ represents the immediate cost or revenue impact of those decisions.
- **Uncertainty Realization** ($\xi \in \Xi$): After making the initial decisions, uncertainty (ξ) is realized, represented by the set Ξ , which encapsulates all possible uncertain scenarios within defined bounds. The formulation seeks the worst-case realization within Ξ , indicated by the inner min operator, to ensure the solution remains feasible and as optimal as possible even under adverse conditions.
- **Second Stage (Adjustable) Decisions** (y): Following the realization of uncertainty, adjustable decisions y can be made to react optimally to the specific scenario that has occurred. These decisions are represented by $y \in Y(x, \xi)$, where the feasible set Y depends on both the first stage decisions and the realized uncertainty. The function $f(x, y, \xi)$ represents the objective or cost in the second stage, which the formulation seeks to maximize, given the constraints imposed by x and ξ .

In essence, this formulation balances between the first stage "here-and-now" decisions and the second stage "wait-and-see" adjustments, maximizing overall system performance while protecting against the worst-case scenarios within the defined uncertainty set Ξ .

4-2-1 Uncertainty set

For the robust optimization we need to define the uncertainty set. Multiple types uncertainty sets can be chosen with the most straightforward being the box uncertainty set, which can be extended to a polyhedron uncertainty set [25] [7]. The robustness of these box uncertainty can be controlled by introducing a robust budgets on the amount of deviations in the box, which is common in literature on robust energy offering [10], [26]. This is also referred to cardinality constrained uncertainty.

So to address uncertainty in wind power generation and reserve deployment, we employ a cardinality-constrained polyhedral set. This set ensures solution feasibility for all possible realizations of uncertain parameters within defined bounds while controlling conservativeness through user-defined budgets.

The wind-related uncertainty is modeled using variables $p_t^{W,A}$, representing the available wind power generation, bounded by:

$$p_t^{W,A} \in [\bar{P}_t^{W,A} - \hat{P}_t^{W,A,-}, \bar{P}_t^{W,A} + \hat{P}_t^{W,A,+}], \quad \forall t \in \mathcal{T}, \quad (4-2)$$

where $\bar{P}_t^{W,A}$ is the forecasted available wind power, and $\hat{P}_t^{W,A,\pm}$ denotes the maximum deviation. The uncertainty budget Γ^W limits the number of time periods t where deviations occur.

Similarly, the uncertainty in reserve deployment is modeled by fractional deployment variables $\beta_t^\uparrow \in [0, 1]$ and $\beta_t^\downarrow \in [0, 1]$ as introduced in subsection 2-4-2, representing upward and downward reserve activations, while being original fractional the worst-case uncertainty realization lies on the extreme vertices and thus the variables can be turned into binaries [10]. The uncertainty budget $\Gamma^{A\uparrow}$, and $\Gamma^{A\downarrow}$, control the number of periods where the HPP is called upon for reserves.

Mathematical Formulation

The uncertainty set is defined as:

$$\Xi = \left\{ (u_t^{W+}, u_t^{W-}, \beta_t^\uparrow, \beta_t^\downarrow) \mid \forall t \in \mathcal{T}, \text{ such that:} \right.$$

$$u_t^{W+}, u_t^{W-}, \beta_t^\uparrow, \beta_t^\downarrow \in \{0, 1\}, \quad (4-3)$$

$$p_t^{W,A} = \bar{P}_t^{W,A} - u_t^{W-} \hat{P}_t^{W,A} + u_t^{W+} \hat{P}_t^{W,A}, \quad (4-4)$$

$$u_t^{W+} + u_t^{W-} \leq 1, \quad (4-5)$$

$$\sum_{t \in \mathcal{T}} (u_t^{W+} + u_t^{W-}) \leq \Gamma^W, \quad (4-6)$$

$$\beta_t^\uparrow + \beta_t^\downarrow \leq 1, \quad (4-7)$$

$$\left. \sum_{t \in \mathcal{T}} \beta_t^\uparrow \leq \Gamma^{A,\uparrow}, \quad \sum_{t \in \mathcal{T}} \beta_t^\downarrow \leq \Gamma^{A,\downarrow} \right\}. \quad (4-8)$$

The uncertainty set is defined in (4-3) through (4-8) and models deviations in wind power generation and reserve activations under uncertainty. The available wind power $p_t^{W,A}$ is calculated using Equation 4-4. It accounts for nominal wind power $\bar{P}_t^{W,A}$ and deviations $\hat{P}_t^{W,A}$, which are applied through the binary variables u_t^{W+} and u_t^{W-} . Equation 4-5 enforces that upward and downward deviations in wind power cannot occur simultaneously at any time step t . The total number of periods with deviations in wind power is constrained by the budget Γ^W in Equation 4-6, which ensures that deviations remain within a predefined level. For reserve activations, Equation 4-7 guarantees mutual exclusivity between upward (β_t^\uparrow) and downward (β_t^\downarrow) activations within the same time step. The budgets for upward and downward reserve activations are separately defined in Equation 4-8, allowing flexibility to model asymmetry in the system's response capabilities. These budgets, $\Gamma^{A,\uparrow}$ and $\Gamma^{A,\downarrow}$, limit the maximum number of activations over the planning horizon.

This formulation balances conservativeness and profitability by controlling uncertainty budgets. Initial approaches used a single budget for reserve activations, but analysis of asymmetry in upward and downward activations led to a refined split-budget approach for better modeling accuracy. The initial framework employed a single uncertainty budget for activations. Based on insights from an activation analysis, this was refined to a split-budget approach to better reflect asymmetry between upward and downward activations.

4-2-2 ARO model formulation HPP

Now we reformulate the HPP optimization into the form of Equation 4-1. Forming the tri-level problem where in the upper level optimizing the revenue from the first-stage decisions, for simplification the electrolyzer-states are pre-scheduled during the DA stage. The middle level relates to the uncertainty of the wind and activation, trying to find the worst-possible outcome of the lower stage using the possible values within the uncertainty set. And the lower level maximizes the revenue from the day-within decisions on the imbalance market and minimizes losses due to violations of contracts.

$$\begin{aligned} \max_{x \in X} & \left\{ 96r^\uparrow \lambda^{r^\uparrow} + 96r^\downarrow \lambda^{r^\downarrow} + \sum_{t \in \mathcal{T}} P_t^{\text{net}} \Delta T \lambda_t^{DA} \right. \\ & + \min_{\xi \in \Xi} \max_{y \in Y(x, \xi)} \left(\sum_{t \in \mathcal{T}} Q_t^{H2} \lambda_t^{H2} - z^{SU} C^{SU} \right. \\ & \left. \left. + \beta_t^\uparrow r^\uparrow \lambda_t^{r, \text{act}, \uparrow} \Delta T - \beta_t^\downarrow r^\downarrow \lambda_t^{r, \text{act}, \downarrow} \Delta T \right) \right\} \end{aligned} \quad (4-9)$$

The constraints for the adaptive robust optimization problem are structured as follows:

- **First stage constraints:** Constraints Equation 2-61 - Equation 2-64 are in this case the only constraints specific to day-ahead decisions independent of second-stage variables. The first stage variables are: $\mathbf{x} = \{P_t^{DA}, r^\uparrow, r^\downarrow, z_t^{\text{on}}, z_t^{\text{off}}, z_t^{\text{sb}}, | t \in \mathcal{T}\}$.
- **Uncertainty set constraints:** Constraints Equation 4-3 - Equation 4-8 describe the uncertainty set with uncertain variables: $\xi = \{(u_t^{W+}, u_t^{W-}, \beta_t^\uparrow, \beta_t^\downarrow) | t \in \mathcal{T}\}$, setting bounds on possible variations in generation, and market conditions, ensuring robust performance across all feasible realizations of uncertainty.
- **Second-stage adjustable constraints:** Constraints Equation 2-101 - Equation 2-105 and Equation 2-65 - Equation 2-80 apply to the adjustable second-stage decisions: $\mathbf{y} = \{P_t^W, P_t^{H2}, P_t^{\text{bat}}, \text{SOC}_t^{\text{bat}}, r_t^{\uparrow, \text{bat}}, r_t^{\downarrow, \text{bat}}, r_t^{\uparrow, H2}, r_t^{\downarrow, H2}, \hat{P}_t^{H2}, Q_t^{H2} | t \in \mathcal{T}\}$. These constraints allow responsive adjustments based on the realization of uncertainty and include limits on battery response, hydrogen production adjustment and adjustment of the power flows to meet the equality constraints.

Robust bounds

Instead of dealing with uncertainty with using scenarios we optimize between uncertain bounds. The bounds can be made in multiple ways. This thesis assumes data driven methods so we have some data for the bounds. Multiple bound options have been considered. The first type was the use of a polyhedron convex hull. Using the map of forecasts to realization of power, we can draw a hull around the points and expect the forecast to be lower and upper bounded by the interpolation on this bound. However this came with the problem of values outside the bound. Also at higher wind-values less data is available meaning the bounds might not be covering all the data. A different approach commonly found in uncertainty characterization is the use of quantile regression [27]. Which allows the user to input certainty desired of which the data.

4-3 Column-constraint generation algorithm

As no state-of-the art solver can solve the two-layered robust optimization problem directly within reasonable amount of time, a specific solving method needs to be applied. As applied in [10] and described by [28], a column and constraint generation method can be applied to such problems. For here the problem is split in a master-subproblem and solved in the following way:

Algorithm 1 Iterative Master-Subproblem Algorithm with Separate Omega Update Steps

Step 1: Initialize parameters and structures

Set tolerance ε for convergence

Initialize bounds $UB \leftarrow \infty$, $LB \leftarrow -\infty$

Initialize iteration counter $k \leftarrow 0$

Initialize a random set of activation uncertainty and worst-case wind outcome

while $\frac{|UB-LB|}{|UB|} > \varepsilon$ **and** $k < \text{MAX_ITER}$ **do** **Step 2: Solve the master problem with updated constraints**

Define master problem using updated omega uncertainty set from previous iterations

Solve master problem to obtain first-stage decision variables, including fixed values $z^{on,*}$, $z^{sb,*}$, $r^{\uparrow,*}$, $r^{\downarrow,*}$, and $P^{DA,*}$

Step 3: Update the upper bound

$UB \leftarrow$ objective value of master problem

Step 4: Solve the subproblem using fixed values from master solution

Set bounds based on worst-case wind forecast realization

Define subproblem with dual formulation and solve to find zS_star

Step 5: Update the lower bound

Calculate start-up costs and day-ahead revenue $revenue_DA$

Update $LB \leftarrow \max\{LB, revenue_DA - \text{start-up costs} + zS_star\}$

Step 6: Check break conditions

if $\frac{|UB-LB|}{|UB|} \leq \varepsilon$ **or** $LB > UB$ **then break**

Step 7: Update iteration counter

$k \leftarrow k + 1$

Step 8: Update omega uncertainty variables and constraints

Modify omega uncertainty variables and add them to the master problem constraints to tighten the problem

Use this updated set of omega uncertainty in the next iteration of the master problem

Final Solution:

Return optimal values from step 2: $z^{on,*}$, $z^{sb,*}$, $r^{\uparrow,*}$, $r^{\downarrow,*}$, and $P^{DA,*}$

4-3-1 Master problem model

The master problem from the algorithm is a relaxed reformulation of Equation 4-9, where each iteration introduces a new set of constraints based on the realizations of uncertain variables obtained from the sub-problem. These additional constraints progressively tighten the feasible region. An auxiliary variable v is added which accounts for the worst-case revenue from the second stage. The master is defined as the following:

$$\max \left\{ \left(96r^{\uparrow}\lambda^{r^{\uparrow}} + 96r^{\downarrow}\lambda^{r^{\downarrow}} + v + \sum_{t \in T} P_t^{DA} \Delta T \lambda_t^{DA} \right) \right\} \quad (4-10)$$

Subject to:

$$v \leq \sum_{t \in \mathcal{T}} \left(r^\uparrow \lambda_t^\uparrow \Delta T \beta_{t,k}^\uparrow - r^\downarrow \lambda_t^\downarrow \Delta T \beta_{t,k}^\downarrow + Q_{t,k}^{H2} \lambda^{h2} \right) \quad \forall k \in \mathcal{K} \quad (4-11)$$

Power Balancing Constraints:

$$P_t^{\text{DA}} = P_{t,k}^{\text{W}} - P_{t,k}^{\text{H2}} + P_{t,k}^{\text{bat}} - P_{t,k}^\Delta, \quad \forall t \in \mathcal{T}, k \in \mathcal{K} \quad (4-12)$$

$$r^\uparrow = r_{t,k}^{\uparrow, \text{bat}} + r_{t,k}^{\uparrow, \text{H2}}, \quad \forall t \in \mathcal{T}, k \in \mathcal{K} \quad (4-13)$$

$$r^\downarrow = r_{t,k}^{\downarrow, \text{bat}} + r_{t,k}^{\downarrow, \text{H2}}, \quad \forall t \in \mathcal{T}, k \in \mathcal{K} \quad (4-14)$$

$$P_+^{\text{DA}} P_{t,k}^\Delta + r^\uparrow \leq \overline{P}^{\text{net}}, \quad \forall t \in \mathcal{T}, k \in \mathcal{K} \quad (4-15)$$

$$P_+^{\text{DA}} P_{t,k}^\Delta - r^\downarrow \geq -\underline{P}^{\text{net}}, \quad \forall t \in \mathcal{T}, k \in \mathcal{K} \quad (4-16)$$

Electrolyzer state constraints:

See Equation 2-61 to Equation 2-64.

Electrolyzer constraints:

$$Q_{t,k}^{\text{H2}} = \left(A(\hat{P}_{t,k}^{\text{H2}} - \beta_{t,k}^\uparrow r_{t,k}^{\uparrow, \text{H2}} + \beta_{t,k}^\downarrow r_{t,k}^{\downarrow, \text{H2}}) + Bz_{t,k}^{\text{on}} \right) \Delta T, \quad \forall t \in \mathcal{T}, k \in \mathcal{K} \quad (4-17)$$

$$\underline{P}^{\text{H2}} z_{t,k}^{\text{on}} \leq \hat{P}_{t,k}^{\text{H2}} \leq \overline{P}^{\text{H2}} z_{t,k}^{\text{on}}, \quad \forall t \in \mathcal{T}, k \in \mathcal{K} \quad (4-18)$$

$$P_{t,k}^{\text{H2}} = \hat{P}_{t,k}^{\text{H2}} + P^{\text{sb}} z_{t,k}^{\text{sb}}, \quad \forall t \in \mathcal{T}, k \in \mathcal{K} \quad (4-19)$$

$$\hat{P}_{t,k}^{\text{H2}} - r_{t,k}^{\uparrow, \text{H2}} \geq \underline{P}^{\text{H2}} z_{t,k}^{\text{on}}, \quad \forall t \in \mathcal{T}, k \in \mathcal{K} \quad (4-20)$$

$$\hat{P}_{t,k}^{\text{H2}} + r_{t,k}^{\downarrow, \text{H2}} \leq \overline{P}^{\text{H2}} z_{t,k}^{\text{on}}, \quad \forall t \in \mathcal{T}, k \in \mathcal{K} \quad (4-21)$$

Battery constraints:

$$\text{SOC}_{t=1,k}^{\text{bat}} = \text{SOC}^{\text{init}} + \sum_{t \in \mathcal{T}} \frac{P_{t,k}^{\text{bat}} - \beta_{t,k}^\uparrow r_{t,k}^{\uparrow, \text{bat}} + \beta_{t,k}^\downarrow r_{t,k}^{\downarrow, \text{bat}}}{P^{\text{bat}, \text{cap}}} \Delta T, \quad \forall k \in \mathcal{K} \quad (4-22)$$

$$\text{SOC}_{t,k}^{\text{bat}} = \text{SOC}_{t-1,k}^{\text{bat}} + \frac{P_{t,k}^{\text{bat}} - \beta_{t,k}^\uparrow r_{t,k}^{\uparrow, \text{bat}} + \beta_{t,k}^\downarrow r_{t,k}^{\downarrow, \text{bat}}}{P^{\text{bat}, \text{cap}}} \Delta T, \quad \forall t \in \mathcal{T} \setminus \{1\}, k \in \mathcal{K} \quad (4-23)$$

$$\text{SOC}^{\text{init}} + \sum_{t \in \mathcal{T}} \frac{P_{t,k}^{\text{bat}} - \beta_{t,k}^\uparrow r_{t,k}^{\uparrow, \text{bat}} + \beta_{t,k}^\downarrow r_{t,k}^{\downarrow, \text{bat}}}{P^{\text{bat}, \text{cap}}} \Delta T \leq \text{SOC}^{\text{final}}, \quad \forall k \in \mathcal{K} \quad (4-24)$$

$$\underline{\text{SOC}} \leq \text{SOC}_{t,k}^{\text{bat}} \leq \overline{\text{SOC}}, \quad \forall t \in \mathcal{T}, k \in \mathcal{K} \quad (4-25)$$

$$\text{SOC}_{t-1,k}^{\text{bat}} - \frac{(P_{t,k}^{\text{bat}} + r_{t,k}^{\uparrow, \text{bat}})}{P^{\text{bat}, \text{cap}}} \Delta T \geq \text{SOC}_{t,k}^{\text{min}}, \quad \forall t \in \mathcal{T} \setminus \{1\}, k \in \mathcal{K} \quad (4-26)$$

$$\text{SOC}^{\text{init}} - \frac{(P_{t=1,k}^{\text{bat}} + r_{t=1,k}^{\uparrow, \text{bat}})}{P^{\text{bat}, \text{cap}}} \Delta T \geq \text{SOC}_{t,k}^{\text{min}}, \quad \forall k \in \mathcal{K} \quad (4-27)$$

$$\text{SOC}_{t-1,k}^{\text{bat}} + \frac{(-P_{t,k}^{\text{bat}} + r_{t,k}^{\downarrow, \text{bat}})}{P^{\text{bat}, \text{cap}}} \Delta T \leq \overline{\text{SOC}}, \quad \forall t \in \mathcal{T} \setminus \{1\}, k \in \mathcal{K} \quad (4-28)$$

$$\text{SOC}^{\text{init}} + \frac{(-P_{t=1,k}^{\text{bat}} + r_{t=1,k}^{\downarrow, \text{bat}})}{P^{\text{bat}, \text{cap}}} \Delta T \leq \overline{\text{SOC}}, \quad \forall k \in \mathcal{K} \quad (4-29)$$

$$-\overline{P}^{\text{bat}, \text{ch}} \leq P_{t,k}^{\text{bat}} \leq \overline{P}^{\text{bat}, \text{dis}}, \quad \forall t \in \mathcal{T}, k \in \mathcal{K} \quad (4-30)$$

$$P_{t,k}^{\text{bat}} + r_{t,k}^{\downarrow,\text{bat}} \leq \bar{P}^{\text{bat,dis}}, \quad \forall t \in \mathcal{T}, k \in K \quad (4-31)$$

$$-P_{t,k}^{\text{bat}} + r_{t,k}^{\uparrow,\text{bat}} \leq \bar{P}^{\text{bat,ch}}, \quad \forall t \in \mathcal{T}, k \in K \quad (4-32)$$

Stochastic-robust hybrid approach to deal with price uncertainty

An extension is made to the master problem to explicitly account for market price uncertainty. This is achieved by modifying the objective function to maximize the expected value of profits across multiple scenarios ($\omega \in \Omega$), where each scenario is weighted by its probability (π_ω).

$$\max \left\{ \left(96r^{\uparrow}\lambda^{r\uparrow} + 96r^{\downarrow}\lambda^{r\downarrow} + \sum_{\omega \in \Omega} \pi_\omega \left(\sum_{t \in \mathcal{T}} P_t^{\text{net}} \Delta T \lambda_{t,\omega}^{DA} + v \right) \right) \right\} \quad (4-33)$$

It is important to note that this extension only modifies the objective function and does not directly affect the constraints of the master problem. The feasibility of the solution remains unchanged, as the constraints are not influenced by the stochastic extension.

4-3-2 Subproblem

The subproblem determines the worst-case realization of uncertainty and adjusts second-stage decisions accordingly. It is defined as follows:

$$\min_{\xi \in \Xi} \max_{y \in Y(x^*, \xi)} \left\{ \sum_{t \in \mathcal{T}} \left(Q_t^{H2} \lambda_t^{H2} - z^{SU} C^{SU} + P_t^{\Delta+} \lambda_t^{\Delta+} \Delta T - P_t^{\Delta-} \lambda_t^{\Delta-} \Delta T \right. \right. \\ \left. \left. + \beta_t^{\uparrow} r^{\uparrow,*} \lambda_t^{r,act,\uparrow} \Delta T - \beta_t^{\downarrow} r^{\downarrow,*} \lambda_t^{r,act,\downarrow} \Delta T \right) \right. \\ \left. - N \sum_{t \in \mathcal{T}} \left(s_t^+ + s_t^- + s_t^{r\uparrow-} + s_t^{r\uparrow+} + s_t^{r\downarrow-} + s_t^{r\downarrow+} \right) \right\}$$

Subject to

Power Constraints:

$$P_t^{DA,*} = P_t^W - P_t^{H2} + P_t^{\text{bat}} + s_t^+ - s_t^-, \quad : \mu_t^{\text{power}} \quad (4-34)$$

$$r^{\uparrow,*} = r_t^{\uparrow,\text{bat}} + r_t^{\uparrow,H2} + s_t^{\uparrow,+} - s_t^{\uparrow,-}, \quad : \mu_t^{\text{afrr-up}} \quad (4-35)$$

$$r^{\downarrow,*} = r_t^{\downarrow,\text{bat}} + r_t^{\downarrow,H2} + s_t^{\downarrow,+} - s_t^{\downarrow,-}, \quad : \mu_t^{\text{afrr-down}} \quad (4-36)$$

$$P_t^W \leq P_t^{W,A}, \quad : \mu_t^W \quad (4-37)$$

Battery Constraints:

$$\text{SOC}_t^{\text{bat}} = \text{SOC}_{t-1}^{\text{bat}} + \left(-P_t^{\text{bat}} - \beta_t^{\uparrow} r_t^{\uparrow,\text{bat}} + \beta_t^{\downarrow} r_t^{\downarrow,\text{bat}} \right) \frac{\Delta T}{\bar{P}^{\text{bat}}}, \quad : \mu^{\text{bat-state}} \quad (4-38)$$

$$\text{SOC}^{\text{init}} + \sum_{t \in \mathcal{T}} \left(\left(-P_t^{\text{bat}} - \beta_t^{\uparrow} r_t^{\uparrow,\text{bat}} + \beta_t^{\downarrow} r_t^{\downarrow,\text{bat}} \right) \frac{\Delta T}{\bar{P}^{\text{bat}}} \right) \geq \text{SOC}^{\text{final}}, \quad : \mu^{\text{bat-soc-final}} \quad (4-39)$$

$$\underline{\text{SOC}} \leq \text{SOC}_t^{\text{bat}} \leq \overline{\text{SOC}}, \quad : \mu^{\text{bat-state-LL}}, \mu^{\text{bat-state-UL}} \quad (4-40)$$

$$\text{SOC}_{t-1}^{\text{bat}} - \frac{r_t^{\uparrow, \text{bat}} - P_t^{\text{bat}}}{\overline{P}^{\text{bat}}} \Delta t \geq \underline{\text{SOC}}, \quad : \mu_t^{\text{bat-afrr-up}} \quad (4-41)$$

$$\text{SOC}_{t-1}^{\text{bat}} + \frac{r_t^{\downarrow, \text{bat}} - P_t^{\text{bat}}}{\overline{P}^{\text{bat}}} \Delta t \leq \overline{\text{SOC}}, \quad : \mu_t^{\text{bat-afrr-down}} \quad (4-42)$$

$$p_t^{\text{bat}} + r_t^{\uparrow, \text{bat}} \leq P^{\text{bat,dc,max}}, \quad : \mu_t^{\text{bat-afrr-up-rate}} \quad (4-43)$$

$$-p_t^{\text{bat}} + r_t^{\downarrow, \text{bat}} \leq P^{\text{bat,c,max}}, \quad : \mu_t^{\text{bat-afrr-down-rate}} \quad (4-44)$$

Electrolyzer Constraints:

$$p_t^{\text{H2}} \leq \overline{P}^{\text{H2}} z_t^{\text{on}} + P^{\text{H2,SB}} z_t^{\text{sb}}, \quad : \mu_t^{\text{elz-UL}} \quad (4-45)$$

$$p_t^{\text{H2}} \geq \underline{P}^{\text{H2}} z_t^{\text{on}} + P^{\text{H2,SB}} z_t^{\text{sb}}, \quad : \mu_t^{\text{elz-LL}} \quad (4-46)$$

$$Q_t^{\text{H2}} = \Delta t \left(A \left(p_t^{\text{H2}} - r_t^{\uparrow, \text{H2}} \beta_t^{\uparrow} + r_t^{\downarrow, \text{H2}} \beta_t^{\downarrow} \right) + B z_t^{\text{on}} \right), \quad : \mu_t^{\text{elz-prod}} \quad (4-47)$$

$$p_t^{\text{H2}} - r_t^{\uparrow, \text{H2}} \geq \underline{P}^{\text{H2}} z_t^{\text{on}} + P^{\text{H2,SB}} z_t^{\text{sb}}, \quad : \mu_t^{\text{elz-afrr-up}} \quad (4-48)$$

$$p_t^{\text{H2}} + r_t^{\downarrow, \text{H2}} \leq \overline{P}^{\text{H2}} z_t^{\text{on}} + P^{\text{H2,SB}} z_t^{\text{sb}}, \quad : \mu_t^{\text{elz-afrr-down}} \quad (4-49)$$

4-4 Solving the subproblem

To solve the subproblem, we adopt a dual-based approach for handling min-max optimization problems. This involves transforming the inner maximization into its dual form, enabling a tractable solution while preserving the problem's essential structure. The dual approach is chosen in line with the research of [10], as it avoids introducing additional binary variables that arise when using the KKT conditions for the inner problem.

By deriving the dual of the inner maximization, the problem is reformulated as a single minimization that accounts for worst-case scenarios. This dual formulation optimizes over both the uncertain variables and the dual variables, $\mu \in \mathcal{M}$. The mathematical representation of this dual problem is given by:

$$\begin{aligned} \min_{\xi \in \Xi, \mu \in \mathcal{M}} \left(\sum_{t \in \mathcal{T}} \left(P_t^{\text{net}} \mu_t^{\text{power}} - \underline{\text{SOC}} \mu_t^{\text{bat-state-LL}} + \overline{\text{SOC}} \mu_t^{\text{bat-state-UL}} \right. \right. \\ \left. \left. + \overline{P}^{\text{bat,dis}} \left(\mu_t^{\text{bat-UL}} + \mu_t^{\text{bat-afrr-up-rate}} \right) + \overline{P}^{\text{bat,ch}} \left(\mu_t^{\text{bat-LL}} + \mu_t^{\text{bat-afrr-down-rate}} \right) \right. \right. \\ \left. \left. + \left(\overline{P}^{\text{H2}} z_t^{\text{on},*,k} + z_t^{\text{sb},*,k} \right) \mu_t^{\text{elz-UL}} + \left(\underline{P}^{\text{H2}} z_t^{\text{on},*,k} + z_t^{\text{sb}} \right) \mu_t^{\text{elz-LL}} \right. \right. \\ \left. \left. + \Delta T \cdot A^{\text{H2}} \cdot z_t^{\text{on},*,k} \mu_t^{\text{elz-prod}} \right. \right. \\ \left. \left. + \left(\underline{P}^{\text{H2}} z_t^{\text{on},*,k} + z_t^{\text{sb},*,k} \right) \mu_t^{\text{elz-afrr-up}} \right. \right. \\ \left. \left. + \left(\overline{P}^{\text{H2}} z_t^{\text{on},*,k} + z_t^{\text{sb},*,k} \right) \mu_t^{\text{elz-afrr-down}} \right. \right. \\ \left. \left. + \overline{P}_t^{W,A} \mu_t^W - \hat{P}_t^{W,A,-} \mu_t^W u_t^{W-} + \hat{P}_t^{W,A,+} \mu_t^W u_t^{W+} \right. \right. \\ \left. \left. + r_t^{\uparrow} \mu_t^{\text{afrr-up}} + r_t^{\downarrow} \mu_t^{\text{afrr-down}} \right) \right) \end{aligned}$$

$$\begin{aligned}
& + \sum_{t \in \mathcal{T}, t > 0} \left(-SOC_t^{min} \mu_t^{\text{bat-afrr-up}} + \overline{SOC} \mu_t^{\text{bat-afrr-down}} \right) \\
& + \sum_{t \in \mathcal{T}} \left(\lambda_t^{r\uparrow} r^{\uparrow} \Delta T - \lambda_t^{r\downarrow} r^{\downarrow} \Delta T \right) \\
& + \left(SOC^{final} - SOC^{init} \right) \mu^{\text{bat-soc-final}} \\
& + SOC^{init} \mu_0^{\text{bat-state}} + \left(-\underline{SOC} + SOC^{init} \right) \mu_0^{\text{bat-afrr-up}} + \left(-SOC^{init} + \overline{SOC} \right) \mu_0^{\text{bat-afrr-down}}
\end{aligned}$$

subject to

$$\mu_t^{\text{bat-state}} - \mu_t^{\text{bat-state-LL}} + \mu_t^{\text{bat-state-UL}} = 0, \quad t = |\mathcal{T}| \quad (4-50)$$

$$\mu_t^{\text{bat-state}} - \mu_{t+1}^{\text{bat-state}} - \mu_t^{\text{bat-state-LL}} + \mu_t^{\text{bat-state-UL}} - \mu_{t+1}^{\text{bat-afrr-up}} + \mu_{t+1}^{\text{bat-afrr-down}} = 0, \quad \forall t < |\mathcal{T}| - 1 \quad (4-51)$$

$$\begin{aligned}
& \frac{\Delta T \mu_t^{\text{bat-state}}}{\overline{P}^{\text{bat}}} + \mu_t^{\text{power}} + \mu_t^{\text{bat-afrr-up-rate}} - \mu_t^{\text{bat-afrr-down-rate}} \\
& - \mu_t^{\text{bat-LL}} + \mu_t^{\text{bat-UL}} \\
& + \frac{\mu_t^{\text{bat-afrr-up}}}{\overline{P}^{\text{bat}}} - \frac{\mu_t^{\text{bat-afrr-down}}}{\overline{P}^{\text{bat}}} - \frac{\Delta T \mu^{\text{bat-soc-final}}}{\overline{P}^{\text{bat}}} = 0, \quad \forall t \in \mathcal{T}
\end{aligned} \quad (4-52)$$

$$\frac{\mu_t^{\text{bat-state}} \beta_t^{\uparrow} \Delta T}{\overline{P}^{\text{bat}}} - \frac{\mu_t^{\text{bat-afrr-up}} \Delta T}{\overline{P}^{\text{bat}}} + \mu_t^{\text{bat-afrr-up-rate}} - \frac{\mu^{\text{bat-soc-final}} \beta_t^{\uparrow} \Delta T}{\overline{P}^{\text{bat}}} + \mu_t^{\text{afrr-up}} \geq 0, \quad \forall t \in \mathcal{T} \quad (4-53)$$

$$-\frac{\mu_t^{\text{bat-state}} \beta_t^{\downarrow} \Delta T}{\overline{P}^{\text{bat}}} + \frac{\mu_t^{\text{bat-afrr-down}} \Delta T}{\overline{P}^{\text{bat}}} + \mu_t^{\text{bat-afrr-down-rate}} + \frac{\mu^{\text{bat-soc-final}} \beta_t^{\downarrow} \Delta T}{\overline{P}^{\text{bat}}} + \mu_t^{\text{afrr-down}} \geq 0, \quad \forall t \in \mathcal{T} \quad (4-54)$$

$$-\mu_t^{\text{power}} + \mu_t^{\text{elz-UL}} + \mu_t^{\text{elz-LL}} - \Delta T A^{\text{H2}} z_{t,k}^{\text{on},*} \mu_t^{\text{elz-prod}} + \mu_t^{\text{elz-afrr-up}} + \mu_t^{\text{elz-afrr-down}} = 0, \quad \forall t \in \mathcal{T} \quad (4-55)$$

$$\mu_t^{\text{elz-prod}} \geq \lambda_t^{\text{H2}}, \quad \forall t \in \mathcal{T} \quad (4-56)$$

$$-\mu_t^{\text{elz-afrr-up}} + \mu_t^{\text{afrr-up}} + A^{\text{H2}} \mu_t^{\text{elz-afrr-up}} \beta_t^{\uparrow} z_{t,k}^{\text{on},*} \geq 0, \quad \forall t \in \mathcal{T} \quad (4-57)$$

$$\mu_t^{\text{elz-afrr-down}} + \mu_t^{\text{afrr-down}} - A^{\text{H2}} \mu_t^{\text{elz-afrr-down}} \beta_t^{\downarrow} z_{t,k}^{\text{on},*} \geq 0, \quad \forall t \in \mathcal{T} \quad (4-58)$$

$$\mu_t^{\text{W}} + \mu_t^{\text{power}} \geq 0, \quad \forall t \in \mathcal{T} \quad (4-59)$$

$$\mu_t^{\text{power}} \geq -N, \quad \forall t \in \mathcal{T} \quad (4-60)$$

$$-\mu_t^{\text{power}} \geq -N, \quad \forall t \in \mathcal{T} \quad (4-61)$$

$$\mu_t^{\text{afrr-up}} \geq -N, \quad \forall t \in \mathcal{T} \quad (4-62)$$

$$-\mu_t^{\text{afrr-up}} \geq -N, \quad \forall t \in \mathcal{T} \quad (4-63)$$

$$\mu_t^{\text{afrr-down}} \geq -N, \quad \forall t \in \mathcal{T} \quad (4-64)$$

$$-\mu_t^{\text{afrr-down}} \geq -N, \quad \forall t \in \mathcal{T} \quad (4-65)$$

$$\begin{aligned} & \mu_t^{\text{bat-state-LL}}, \mu_t^{\text{bat-state-UL}}, \mu_t^{\text{bat-afrr-up}}, \mu_t^{\text{bat-afrr-down}}, \mu_t^{\text{bat-afrr-up-rate}}, \mu_t^{\text{bat-afrr-down-rate}}, \\ & \mu_t^{\text{elz-UL}}, \mu_t^{\text{elz-afrr-down}}, \mu_t^{\text{afrr-up}}, \mu_t^{\text{afrr-down}}, \mu_t^{\text{W}} \geq 0, \quad \forall t \in \mathcal{T} \\ & \mu^{\text{bat-soc-final}}, \mu_t^{\text{elz-LL}}, \mu_t^{\text{elz-afrr-up}} \leq 0, \quad \forall t \in \mathcal{T}. \end{aligned} \quad (4-66)$$

While solving this subproblem, it is observed that there are bi-linear terms present in both the objective function and the constraints. Although a solver like Gurobi is capable of handling mixed-integer nonlinear programming (MINLP) problems, this approach is undesirable due to its negative impact on solving speed. Consequently, these terms are reformulated as described in [10] to improve computational efficiency for example in:

$$\underline{\mu}^{\text{W}} \cdot u_t^{\text{W}-} \leq w_t^{\text{wind-}} \leq \bar{\mu}^{\text{W}} \cdot u_t^{\text{W}-} \quad (4-67)$$

$$\underline{\mu}^W \cdot (1 - u_t^{W-}) \leq \mu_t^W - w_t^{\text{wind-}} \leq \bar{\mu}^W \cdot (1 - u_t^{W-}) \quad (4-68)$$

,

With the lower and upper bounds being equal to a value M , depending on whether the dual variables are negative, positive, or unbounded, the reformulation allows the dual variable to be free when the binary is 0, and when the binary equals 1, the dual takes the value of the replacing variable. Care should be taken to choose these values appropriately, as they influence the stability and convergence rate. The value should be at least larger than the penalty N to ensure correct penalization of infeasible solutions.

While simplified, the problem still consists of a large number of binary variables, which may prevent the optimization problem from finding a solution within a desirable time frame. To address this, a time limit is set. However, to ensure the algorithm finds a solution with some guarantees of optimality, a minimum MIP gap is set for the lower bound to be updated.

4-5 Shrinking horizon adaptation ARO

The shrinking horizon adaptation is applied to the ARO framework to dynamically manage uncertainty and refine second-stage decisions. By updating the optimization problem at each time step with real-time information, this approach enables robust adjustments to operational strategies, particularly in the presence of passive imbalance.

We assume that the imbalance price for the current time step is known, as well as whether reserve activation occurs and in which direction. Additionally, we impose tight bounds on imbalance during reserve activation, ensuring no imbalance occurs in the system under these conditions. These assumptions allow passive imbalance to serve as an adaptive tool for leveraging leftover wind energy when no reserve activation occurs. By incorporating these assumptions, the shrinking horizon framework dynamically adjusts to updated information, ensuring robust and efficient operations.

Introducing passive imbalance at the first time step creates an adopted subproblem namely:

$$\min_{\xi \in \Xi} \max_{y \in Y(x^*, \xi)} \sum_{t \in \mathcal{T}} \left(Q_t^{H2} \lambda_t^{H2} - z^{SU} C^{SU} + \beta_t^{\uparrow, *, k} r_t^{\uparrow, *, k} \lambda_t^{r, act, \uparrow} \Delta T - \beta_t^{\downarrow, *, k} r_t^{\downarrow, *, k} \lambda_t^{r, act, \downarrow} \Delta T \right) + P^\Delta \lambda^\Delta \Delta T \quad (4-69)$$

Subject to

Constraints Equation 4-35 - Equation 4-37

$$P_t^{DA, *, k} = P_t^W - P_t^{H2} + P_t^{\text{bat}} - P^\Delta \lambda^\Delta + s_t^+ - s_t^- \quad : \mu_t^{\text{power}}, t = 0 \quad (4-70)$$

$$P_t^{DA, *, k} + P_t^\Delta + r_t^{\uparrow, *, k} \leq \bar{P}^{\text{net}}, \quad : \bar{\mu}_t^{\text{net}} \forall t \in \mathcal{T} \quad (4-71)$$

$$P_t^{DA, *, k} + P_t^\Delta - r_t^{\downarrow, *, k} \geq -\underline{P}^{\text{net}}, \quad : \underline{\mu}_t^{\text{net}} \forall t \in \mathcal{T} \quad (4-72)$$

And for the battery and electrolyzer constraints see Equation 4-38 - Equation 4-49.

The imbalance is not split as it is in the other problems. As this would require again the use of a binary variable to split the balance and this leads to problems deriving the dual solution. This does lead to a discrepancy, and in the post-processing of the second stage revenue the true revenue will be calculated using the split balance price system to make it a fair comparison with the other methods.

The adopted sub-problem is solved the same way as in section 4-4, with the extra constraints added to the dual. With the incoming uncertainty at $t = h$, the real values for the uncertainty are used and the uncertain available wind power is replaced with the real available wind power. To achieve new values for the battery, the solution from the dual is put into the original primal.

4-6 Chapter summary: ARO Framework

This chapter introduces a adaptive robust optimization framework designed to address the inherent uncertainties associated with HPP portfolio management. In contrast to stochastic programming, which is based on probabilistic scenarios, ARO employs uncertainty sets to optimize under specified uncertainty budgets. These uncertainty budgets allow the user to control the conservatism of the solution. In the ARO framework, wind uncertainty is represented through the use of bounds rather than scenarios. This approach is particularly useful for meeting strict constraints in capacity markets and dealing with the uncertain nature of activation, where very little information is available beforehand.

To solve the ARO problem, a column-constraint generation algorithm is employed. This iterative method subdivides the problem into two parts: a master problem, which determines robust first-stage decisions, and a subproblem, which identifies the worst-case realizations and refines the constraints. The iterative process continues until a convergence criterion is met.

The chapter also introduces a shrinking horizon adaptation, where a receding horizon approach allows for real-time updates as new information becomes available. Passive imbalance is added to the subproblem, and the dual is adjusted accordingly. This imbalance mechanism is used to manage deviations when no reserve activation occurs, utilizing leftover wind energy for adjustments.

In the next chapter, a case study is presented to evaluate the effectiveness of the ARO framework. The case study applies both the stochastic programming and ARO approaches to a hybrid power plant under realistic conditions. By comparing these two methods, the case study highlights their respective advantages, trade-offs, and performance in managing uncertainty and ensuring robust operational decisions.

Chapter 5

Case study

This chapter explores the performance of the different optimization approaches in managing uncertainty for hybrid power plants participating in energy markets. Specifically, we investigate how these methods handle uncertainty, focusing on their ability to ensure robust operations while maximizing revenue. By applying data-driven uncertainty optimization, we aim to provide practical insights into the behavior of hybrid power plants under varying conditions.

The case study evaluates the two distinct optimization frameworks: stochastic programming and adaptive robust optimization. These frameworks are tested against benchmark approaches, deterministic forecasting (DF) and perfect information (PI), to assess their strengths and limitations. Through this comparative analysis, we examine how each method balances robustness with revenue generation, addressing key challenges in market participation and operational flexibility.

The overarching objective is to demonstrate the trade-offs inherent in each approach, providing a comprehensive understanding of their suitability for hybrid power plant management under real-world uncertainty.

5-1 set-up

5-1-1 Power plant set-up and assumptions

A hybrid power plant is used with the following specifications¹:

- **Wind turbines capacity:** 22 MW
- **Electrolyzer capacity:** 10 MW

¹The values of the total wind capacity and battery are roughly based on an existing Dutch hybrid power plant [29]

- Values for production curve based on TNOs EMERGE model values from [30]
- **Total battery storage capacity:** 10 MW
- **Grid connection:** 22 MW

Besides the assumptions on the model parameter we have some important assumptions and simplification in the model.

Model assumptions

- **Component assumptions**
 - The **electrolyzer** state needs to be scheduled at least one time-step before the time of uncertainty realization.
 - The **electrolyzer** can reach its desired working points with in the time delta.
 - The **electrolyzer** dynamics are fully linear in the on-state.
 - The **battery** dynamics are linear and no energy is lost due to efficiency and no degradation occurs
 - The **wind turbine** operates based on forecasted and real wind power values without curtailment limits.
- **Market assumptions**
 - All energy offered on the **day-ahead market** is sold at the market clearing price.
 - All energy offered at **capacity market** is sold at average capacity price of that day.
 - **Passive imbalance** prices of the current time step are perfectly forecasted and known, and with that we restrict the passive imbalance at other time steps to be 0
 - Activation of aFRR is known at the current time step and is assumed to be either full or none.
 - While aFRR is activated no other imbalance is allowed.
- **Further model assumptions**
 - The **costs** of components are ignored and the objective is focused on revenue, cold starts of the electrolyzer are, however, penalized to avoid unrealistic state switching

Table 5-1 summarizes the key parameters and settings used for the stochastic programming (SP) and robust optimization (RO) methods in this case study. In Appendix A the values of the assets are shown. The optimization was run using Gurobi.

Table 5-1: Model Parameters for SP and RO Base Models.

Parameter	Value/Description
Common Parameters	
Optimization Feasibility Tolerance (Gurobi)	1.00×10^{-4}
Data	2020-2022
SP Base Model	
Timelimit	600s
Gurobi MIPGap	0.01
Number of non-reduced wind scenarios generated	1000
RO Base Model	
CCGA: tolerance (Γ^{CCGA})	0.02
CCGA: MAX_ITER	50
Gurobi Feasibility Tolerance	1.00×10^{-4}
Gurobi MIPGap	0.02
TimeLimit iteration	300s
Robust bounds: quantiles	[0.01, 0.99]
General Parameters	
λ^{H2}	3 euro/KG
N	10000
α (shrinking horizon penalty adjustment at $t^h = 1$)	100

5-2 Data gathering and preparation

Data for the Dutch energy market case study was sourced from ENTSO-E and TenneT. ENTSO-E, the association of European electricity transmission system operators, plays a critical role in coordinating the operation, planning, and development of Europe's electricity grid. It facilitates cross-border electricity flows and supports the integrated energy market across 36 countries, contributing significantly to the energy transition [31].

To train the model on historical patterns and evaluate its predictive performance, data from 2020 to 2022 was used as the training set, while data from 2023 served as the test set. This separation enables an assessment of how well the model generalizes to new data, simulating its applicability to future energy market predictions.

5-2-1 Market prices and DA price forecasts

The capacity market prices are assumed to be known during the optimization. These prices, available on ENTSO-E, are reported as daily averages with no associated price spread. Additionally, the pay-as-bid nature of the market complicates the development of reliable forecasts. As a result, forecasting capacity market prices is not pursued in this study. The activation prices and passive imbalance prices are also assumed to be known and taken from ENTSO-E.

In contrast, significant research has been conducted on forecasting day-ahead (DA) electricity prices, which are known for their relatively high predictability. However, DA price forecasts

were not available for the case-study period. To address this, a forecasting method from the EPF toolbox was adapted [17].

To forecast day-ahead (DA) market prices, we employ the Lasso Estimated AutoRegressive with Exogenous variables (LEAR) model. The LEAR model is a parameter-rich ARX (AutoRegressive with eXogenous inputs) model that leverages the Least Absolute Shrinkage and Selection Operator (LASSO) for implicit feature selection. By applying LASSO, the model eliminates redundant or irrelevant features, making it particularly suitable for datasets with a large number of predictors, which is common in electricity price forecasting.

The exogenous inputs are the historical day-ahead prices of the previous three days and one week ago (D-1, D-2, D-3, D-7). The historical DA prices are combined with the total load forecast, scheduled generation both available on ENTSO-E [31] with lags D, D-1, D-7.

The price scenarios were randomly generated using random sampling on the error distribution and then added to the forecast to cover a wider range in prices.

5-2-2 Wind data gathering and analysis

Wind power data was collected from ENTSO-E, which provides both forecasted and actual wind power generation for the entire Netherlands. Additionally, the annual total wind energy production capacity was obtained. By normalizing the forecasted and actual wind power data with the total wind capacity in the Netherlands, a factor representing the fraction of available wind power for the case-study power plant was derived.

Analysis of the wind forecasts revealed a significant bias toward overestimation, with forecasted wind power often exceeding the actual values on the day of delivery. Such a bias can have a substantial impact on the performance of robust optimization algorithms, as it may lead to overly conservative decisions or misrepresentation of uncertainty. The bias was removed using a linear regression model. More on details on this bias can be found Appendix D.

5-2-3 Real-time aFRR activations

For the real activations we know a couple things. We extract the following three things. First the price for the activation at the time instance. Secondly the total amount of capacity acquired for that instance. And the amount of energy used. We then calculate the percentage of energy used and we can couple that to the amount of capacity activated in our system.

So we modify Equation 2-41 and Equation 2-42 as we introduce an activation threshold parameter, τ^{act} that relates with percentage of the total aFRR reserves is used to our system. Because we decided to have it binary we say that from a x amount of capacity used with the price above our minimum price

We introduce the following:

- $r_t^{\text{used},\%}$: Percentage of aFRR used at time t , defined as:

$$r_t^{\text{used},\%} = \frac{r_t^{\text{used},\text{nationwide}}}{r_t^{\text{available},\text{nationwide}}}$$

where:

- $r_t^{\text{used,nationwide}}$: Total aFRR activated nationwide at time t .
- $r_t^{\text{total,available}}$: Total aFRR available nationwide at time t .

The modified conditions for aFRR activation are given as follows:

Upward Activation (β_t^\uparrow):

$$\beta_t^\uparrow = \begin{cases} 1 & \text{if } \lambda_t^{\text{r,act}\uparrow} > \lambda_t^{\text{DA}} \text{ and } r_t^{\text{used,\%}} \geq \tau^{\text{act}}, \\ 0 & \text{otherwise.} \end{cases}$$

Downward Activation (β_t^\downarrow):

$$\beta_t^\downarrow = \begin{cases} 1 & \text{if } \lambda_t^{\text{r,act}\downarrow} < \lambda_t^{\text{DA}} \text{ and } \lambda_t^{\text{r,act}\downarrow} < 0 \text{ and } r_t^{\text{used,\%}} \geq \tau^{\text{act}}, \\ 0 & \text{otherwise.} \end{cases}$$

While in reality if the price is above your asking price it means your aFRR energy bid is supposed to be activated, the experiments are run on hourly basis it is sampled from the last hour which is assumed to extrapolate for the whole hour and we don't consider partly activation. Thus setting the activation limit to exactly the price can result in too much activation, and with that a highly unlikely case. For the base case we set that value to **0.1**. This value can be adjusted to simulate different strategies which allow for more or less activations without relying too much on the high range of activation prices. The relation between the daily amount of activations in both directions and the activation threshold is given in Figure 5-1

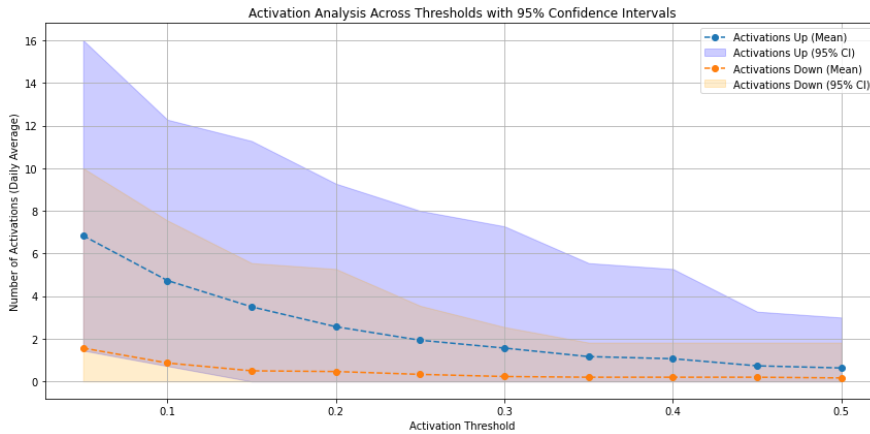


Figure 5-1: The relation between activation threshold (τ^{act}) and the amount of daily activations within a 95% confidence interval based on activation data from 2020 till 2022.

For a value threshold value of **0.1** the historical maximum amount of up activation equals approximately 12 with a 97.5% certainty. And for the downward activation around a maximum of 8 with a 97.5% certainty.

5-2-4 Scenario generation available wind power

To generate wind scenarios, we first analyze the forecast error, the difference between real and forecasted wind values, by examining its statistical properties. This initial analysis helps determine whether an ARIMA model is suitable for capturing the patterns in the error.

Our analysis begins by filtering out the outlier in the errors using the Mahalanobis distance. The Mahalanobis distance measures how far a point is from the center of a data distribution, accounting for correlations among variables, making it useful for identifying outliers. checking for stationarity, a key requirement for ARIMA modeling. Using the Augmented Dickey-Fuller test, we confirm that the error series is stationary.

Next, we investigate the correlation structure of the error. The autocorrelation plot (see Figure 5-2) does not show a clear seasonal pattern across the day. However, both the autocorrelation and partial autocorrelation plots indicate that errors are correlated across lags, suggesting that the size of previous errors influences subsequent ones. Moreover, the PACF cuts off after one lag, implying that an AR(1) model will likely capture the main patterns in the error series.

Based on these insights, we select an AR(1) model within the ARIMA framework to simulate wind error scenarios. While the focus is not on optimizing scenario generation, this approach provides a practical method for representing forecast errors in our analysis.

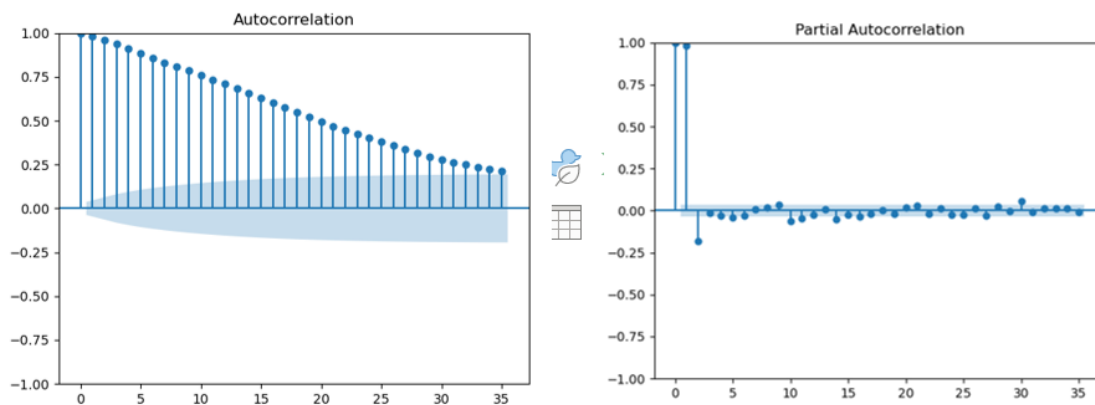


Figure 5-2: Autocorrelation (left) and partial-autocorrelation (right) of the available wind power errors

Using this fitted AR(1) model, we generate 1000 different available wind power trajectories, as shown in Figure 5-3, each initially assigned an equal probability. Subsequently, we employ the fast forward scenario reduction procedure outlined in section 3-3 to compress these scenarios into a smaller set with adjusted probabilities. The amount of scenario reduction is a tunable parameter that provides flexibility in balancing computational requirements with scenario spread in the resulting model.

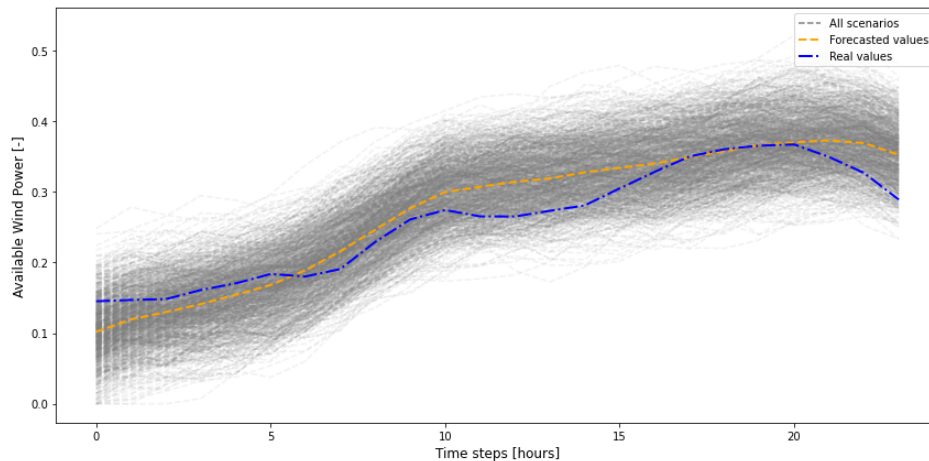


Figure 5-3: Example of 1000 scenarios for the fraction of available wind power on 2023-11-01, plotted with the original forecast and actual fraction of available wind power.

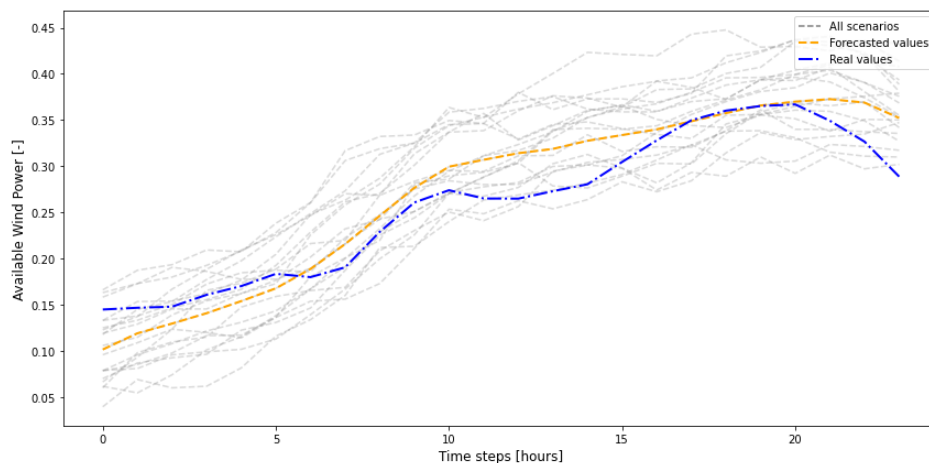


Figure 5-4: Example of 20 reduced scenarios for the fraction of available wind power wind-power on 2023-11-01, plotted with the original forecast and actual fraction of available wind power.

Wind scenarios in shrinking horizon approach

With uncertainty realization we assume knowledge of the current time-step of the wind and activation. With this new information, new scenarios are formed in the same manner as previously described. But now the starting point for all scenarios is the same, being the real available wind power at $t=h$. An example can be found in Appendix D.

5-2-5 Robust bounds for available wind power

For the robust optimization approach, we work with robust intervals instead of scenarios. Multiple options for robust prediction intervals can be taken. the first iteration of the bound was done with just using the convex hull. However when values are outside of the hull with

more extreme data coming in, it becomes messy. The data should be projected on the hull at some point, which also shows another shortcoming of the convex hull. At points where the data is more sparse the bounds become tighter instead of wider which would be more sensible because less data suggest less certainty of the bounds. The second option of quantile regression was then implemented which allowed control over the conservativeness and showed the desired behavior on the extreme vertices of the hull. In the end to benefit of the convex hull and the better performance of RQ at less dense data, a conservative combination was chosen as:

$$P^{W,A+} = \max(CH, RQ^{99\%}) \quad (5-1)$$

$$P^{W,A-} = \min(CH, RQ^{1\%}), \quad (5-2)$$

and the resulting bounds shown in Figure 5-5.

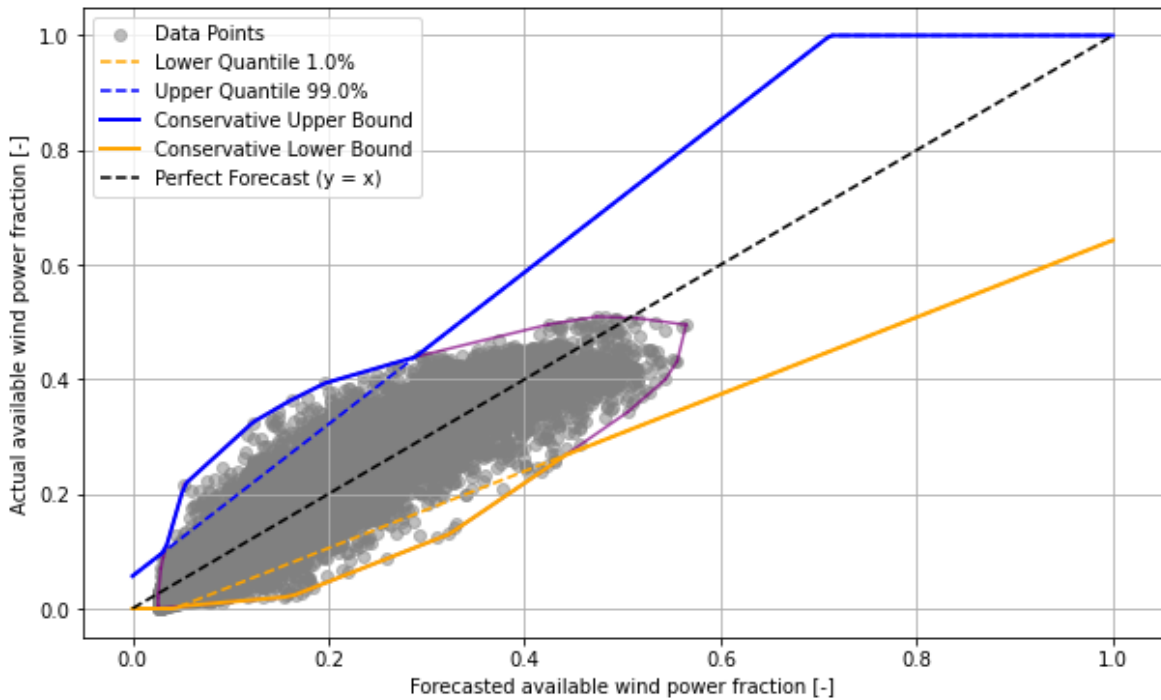


Figure 5-5: Robust bounds for the fraction of available wind power wind power being a combination of quantile regression and convex hull, using training data from 2020 till 2022.

Robust bounds in shrinking horizon approach

With uncertainty realization we assume knowledge of the current timestep of the wind and activation. This leads to the ability of updating the bounds. Having dynamic robust bounds instead of relying on the convex hull. For this we assume that the original robust bounds are truly robust. For the new robust bounds we take the worst known difference between errors and use that iteratively on the current real wind till it intersects with the original bound. An example can be found in Appendix D.

5-3 Metrics

For the results, we analyze focusing primarily on **revenue** and **violations**.

- **Revenue:** Total revenue is the main metric for evaluating monetary performance. However, to highlight the workings of different approaches, the first-stage and second-stage revenues will also be investigated independently.
 - With the first-stage revenue (FSR) being: $\left(96r^\uparrow\lambda^{r^\uparrow} + 96r^\downarrow\lambda^{r^\downarrow} + \sum_{t \in \mathcal{T}} P_t^{\text{net}} \Delta T \lambda_t^{DA}\right)$
 - And second-stage revenue (SSR): $\sum_{t \in \mathcal{T}} \left(Q_t^{H2} \lambda_t^{H2} - z^{SU} C^{SU} + P_t^{\Delta+} \lambda_t^{\Delta+} \Delta T - P_t^{\Delta-} \lambda_t^{\Delta-} \Delta T - \beta_t^\uparrow r^\uparrow \lambda_t^{r,act,\uparrow} \Delta T - \beta_t^\downarrow r^\downarrow \lambda_t^{r,act,\downarrow} \Delta T\right)$
- **Violations:** This metric focuses on the slack variables at $t = 0$ in the shrinking horizon approaches. Slack is identified after optimization and flagged as a violation if any of the slack variables exceeds the error tolerance of $\epsilon = 10^{-6}$. Any slack at the current time step is counted as a violated time step. Violations can occur due to either:
 - Not having the required capacity available at the current time step, or
 - Failing to balance the power equation.

In real life, violations of contract requirements would be penalized, but it is hard to directly link these violations to monetary values. Too many violations could result in exclusion from the capacity market, leading to a loss of income, in addition to direct monetary penalties for failing to meet aFRR activation requirements. Such risks highlight the importance of maintaining compliance with aFRR activation requirements [13]. We can formulate the daily amount of violations using an indicator function as:

$$\text{Daily Violations} = \sum_{h \in \mathcal{H}} \mathbf{1} \left(\max_{i \in \{+, -, r^\uparrow+, r^\uparrow-, r^\downarrow+, r^\downarrow-\}} s_h^{(i)} > \epsilon \right)$$

5-3-1 Benchmarks: Deterministic Forecasting (DF) and Perfect Information (PI)

To establish a baseline, we use deterministic forecasting (DF) and perfect information (PI) as benchmarks. These benchmarks serve as reference points to evaluate the performance of the stochastic programming and adaptive robust optimization approaches.

- **Deterministic Forecasting:** This approach uses forecasted values for uncertain parameters, such as wind power and aFRR activation, to make decisions. It represents the case where decisions are based solely on available forecasts.
- **Perfect Information:** This approach uses real values for uncertain parameters, assuming perfect hindsight. However, to ensure a fair comparison, the PI approach is constrained to the same flow of information as the other methods. This means it cannot anticipate future states of the passive imbalance market or other uncertain factors beyond what is assumed known at the time of decision-making in the other approaches.

These benchmarks provide insight into the trade-offs between relying on forecasts and having access to perfect information. While DF demonstrates the limitations of forecast accuracy, PI highlights the theoretical maximum performance achievable under perfect conditions.

We will analyze the effect of different hyper-parameters and model choices on the approaches. For the case study, we begin with a comparison over a month of data, followed by a closer examination of a single week to illustrate more detailed differences between the approaches and their inherent uncertainties. Accounting for this inherent uncertainty is crucial to ensuring a fair comparison of different hyper-parameters and model choices.

5-4 Case study A: monthly analysis

For the monthly analysis, we use a base case configuration with parameters provided in Table 5-2. The activation budgets are derived from the observed activations in Figure 5-1, while the wind budget is set to 24. This wind budget accounts for days where the actual wind is consistently below the forecasted available wind throughout the day. While this is a conservative choice, it is intended to produce a robust solution.

This setup allows us to gain general insights into model performance, focusing on the behavior under different market scenarios and identifying overall trends. To isolate the effects of operational uncertainty, market price uncertainty is excluded from this analysis. The fraction of available wind power utilized during the month is illustrated in Figure 5-6.

Table 5-2: Model parameters for SP and RO base models.

Parameter	Value/Description
Common Parameters	
Activation threshold	0.1
SP Base Model	
Amount of wind scenarios (N^W)	20
Activation scenarios (N^A)	[all_up, all_down, zero] (pessimistic activation approach) : $\begin{bmatrix} \beta^\uparrow \\ \beta^\downarrow \end{bmatrix} = \begin{bmatrix} 1 & 1 & \dots & 1 \\ 0 & 0 & \dots & 0 \end{bmatrix}, \begin{bmatrix} 0 & 0 & \dots & 0 \\ 1 & 1 & \dots & 1 \end{bmatrix}, \begin{bmatrix} 0 & 0 & \dots & 0 \\ 0 & 0 & \dots & 0 \end{bmatrix}$
Day-ahead prices	perfect information assumed
RO Base Model	
Wind budget (Γ^W)	24
Activation budget up ($\Gamma^{A,\uparrow}$)	15
Activation budget down ($\Gamma^{A,\downarrow}$)	8
Day-ahead prices	perfect information assumed

5-4-1 Results base case

The results of the base case model comparison are presented in Table 5-3. As expected the PI model achieves the highest total revenue, followed by the DF model. In contrast, RO and SP models yield significantly lower revenues.

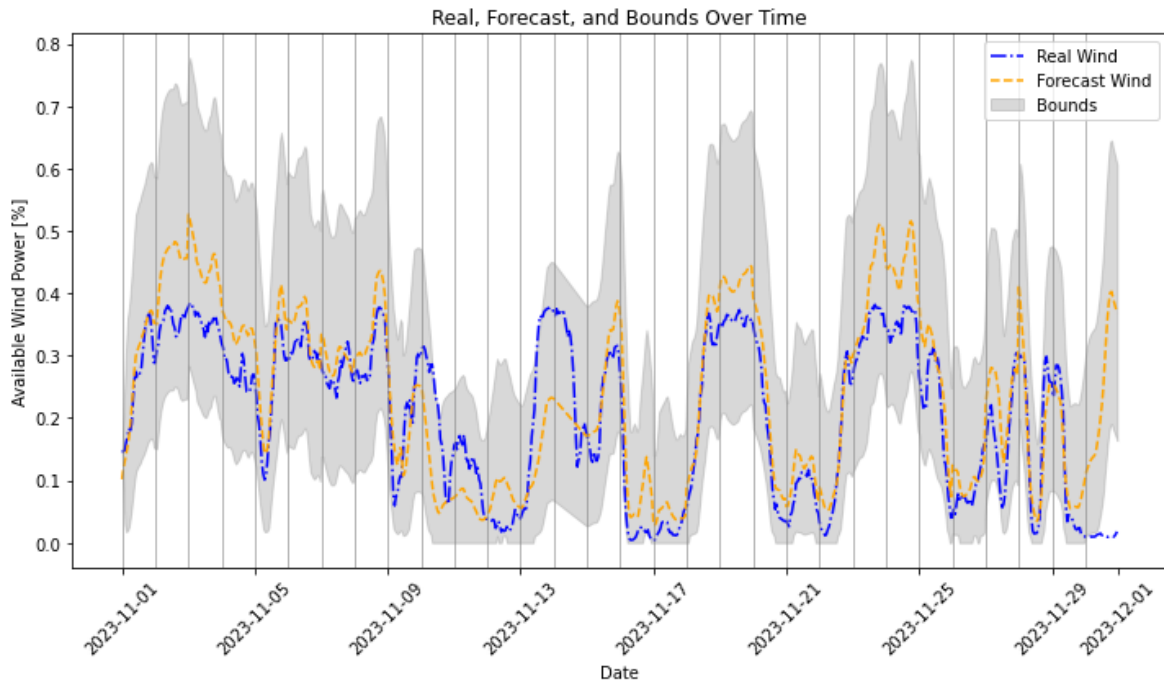


Figure 5-6: Forecast of the fraction of available wind power wind power with its robust bounds for 2023-11, plotted with the original forecast and actual fraction of available wind power.

A key observation is the trade-off between revenue and constraint violations. The DF model incurs 111 violations, demonstrating that its higher revenue is achieved at the cost of not fully adhering to constraints. In comparison, the PI, RO, and SP models exhibit no violations, highlighting their ability to maintain feasibility under the given constraints.

Analyzing the revenue components, the DF model relies predominantly on its FSR and achieves the lowest SSR. The PI model balances its FSR and SSR, resulting in the highest total revenue while adhering to all constraints. The RO model achieves the highest SSR and lowest FSR, reflecting a conservative first stage decision that focuses on mitigating risks in the first stage and capitalizing on profitable scenarios in the second stage. Contrarily, the SP model achieves a higher FSR than SSR.

Table 5-3: Comparison of Model Revenues and Violations Using Base Case

Model	Total FSR	Total SSR	Total Revenue	Total Violations (out of 720)
DF	748,514.80	76,974.55	825,489.35	111.00
PI	564,986.67	291,176.16	856,162.83	0.00
RO	268,108.71	330,355.18	598,463.90	0.00
SP	364,020.03	208,966.93	572,986.96	0.00

Looking at a more detailed revenue breakdown shown in Figure 5-7, the following things can be found. Firstly DF shows difference in using imbalance as a tool or penalty. Achieving more profit on the DA market but this is largely due to overestimation of wind and its ability to provide aFRR services. Due to this overestimation it achieves unfavorable balancing positions

leading to a loss in revenue. Secondly it can be observed that far less energy is committed to DA with RO, which is consequently utilized during the second-stage, explaining the higher SSR with respect to SP.

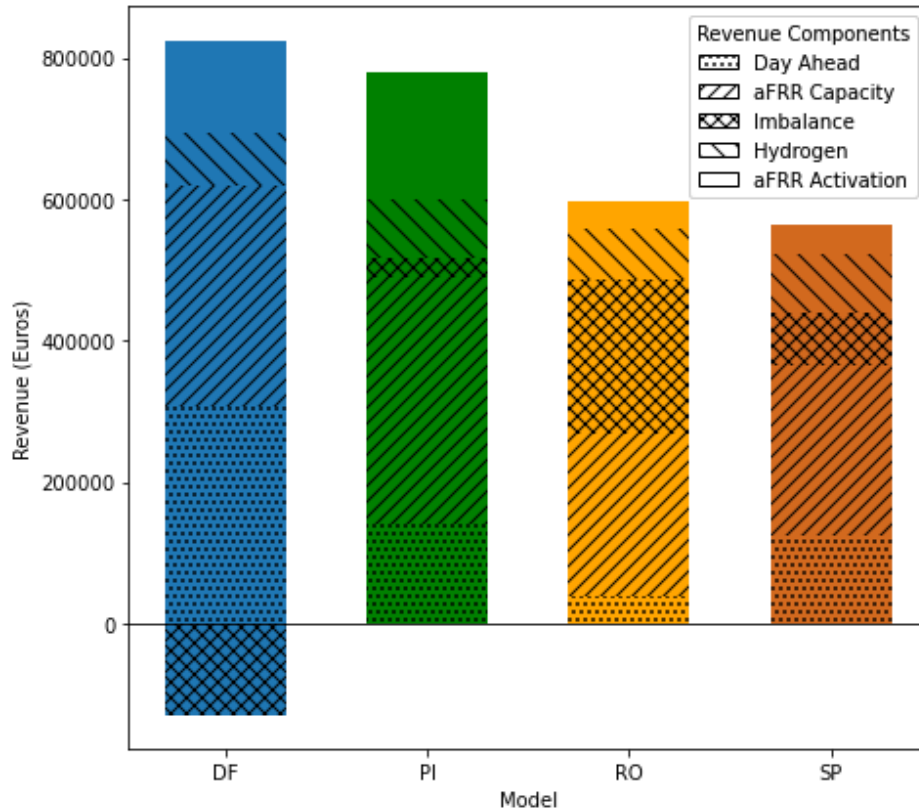


Figure 5-7: Revenue distribution for the different approaches using base case parameters for November 2023

Figure 5-8 illustrates the participation in aFRR up capacity and the corresponding regulation price for different models (SP, RO, DF, and PI). The figure highlights differences in strategy between models, particularly in how they manage uncertainty and operational challenges associated with high aFRR up capacity commitments. The following can be observed:

- The SP model avoids committing to high aFRR up capacity levels due to the difficulty in consistently delivering the required energy. This is particularly challenging under scenarios requiring continuous up activation.
- The RO model demonstrates higher participation in aFRR up capacity in comparison to SP, especially during periods of higher regulation prices. This reflects its ability to manage uncertainty more flexibly compared to SP, albeit with higher risks.
- The PI model serves as a benchmark, reliably aligning its participation with high capacity prices, due to the absence of forecast errors in activation and wind.

Figure 5-9 shows the participation in aFRR down capacity and the corresponding regulation price for the same models. It demonstrates the practical constraints of the system, such as

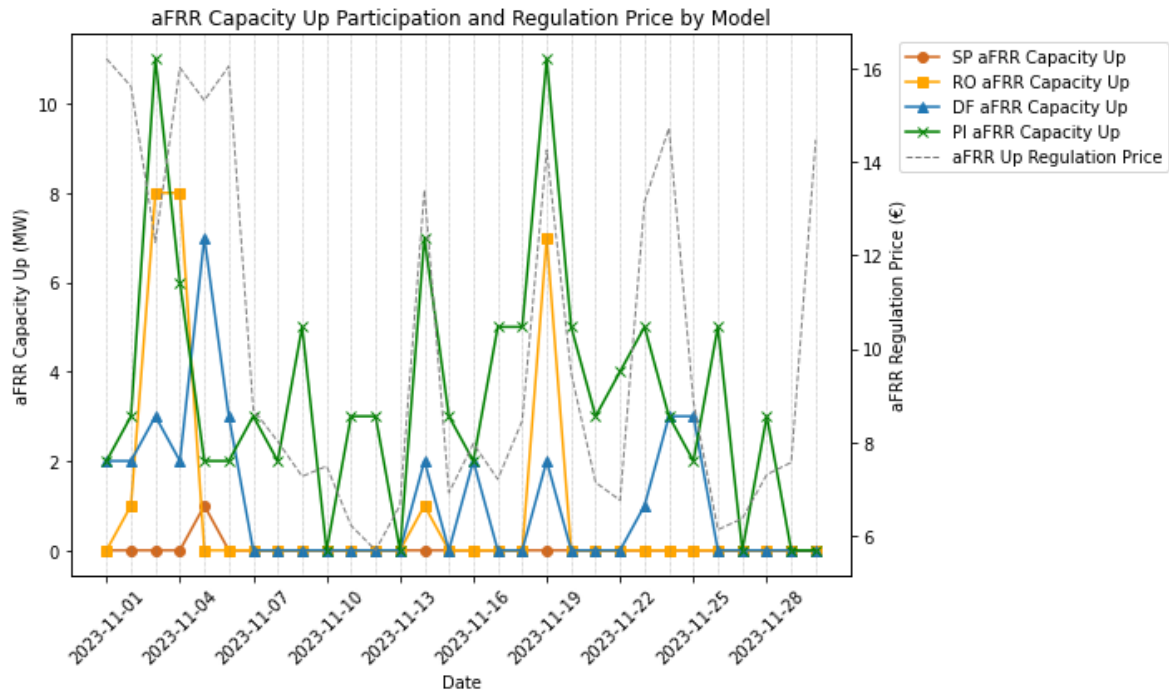


Figure 5-8: AFRR up capacity for November 2023, for the 4 different approaches.

capacity limits for the battery and hydrogen systems, and how these affect the ability to participate in aFRR down capacity. The following can be observed:

- The SP model exhibits higher utilization of aFRR down capacity compared to RO, showing its ability to maximize participation within practical system constraints.
- The aFRR down capacity is capped at a practical limit of 12 MW across all models, representing the system's operational boundary. Which consists of the combination of the hydrogen system's maximum capacity ($r_t^{\uparrow, H2, max} = 8.5$ MW) and the battery's practical limit of 4 MW, determined by its initial and final SOC.
- The dashed gray line representing the aFRR down regulation price demonstrates periods of high financial incentives. The robust optimization shows the highest sensitivity to market price fluctuations.

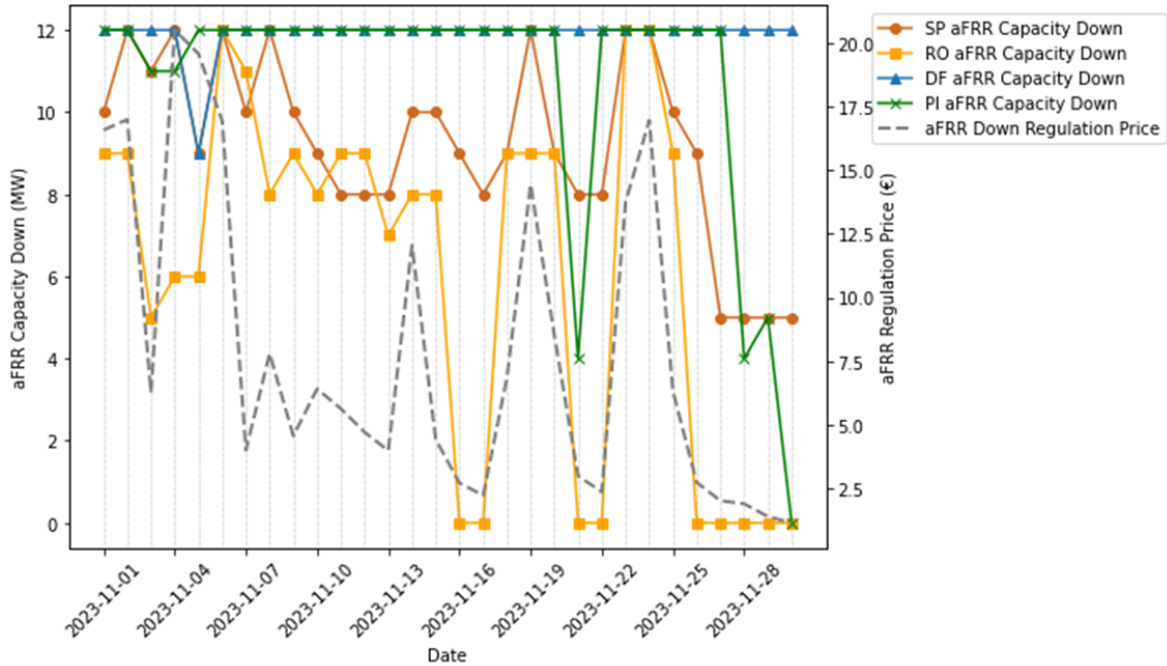


Figure 5-9: AFRR down capacity for November 2023, for the 4 different approaches.

5-4-2 Monthly Results Excluding Passive Imbalance

The ability to rebalance the portfolio within the same day limits the evaluation of the robustness of the first-stage solution. To assess the robustness of these solutions, the passive imbalance is excluded by enforcing $P_t^\Delta = 0 \quad \forall t \in T$, and the models are rerun. The results are presented alongside the original values with passive imbalance in Table 5-4.

Model	Total FSR	Total SSR	Total Revenue	Violations (out of 720)
DF (benchmark)	748,514.80	76,974.55	825,489.35	111.00
PI (benchmark2)	564,986.67	291,176.16	856,162.83	0.00
RO	268,108.71	330,355.18	598,463.90	0.00
SP	364,020.03	208,966.93	572,986.96	0.00
DF (No PImb)	757,732.16	179,009.46	936,741.62	557.00
PI (No PImb)	564,986.67	259,476.43	824,463.09	0.00
RO (No PImb)	270,135.51	150,447.05	420,582.57	22.00
SP (No PImb)	362,524.23	155,832.72	518,356.95	78.00

Table 5-4: Combined values for both regular and (NO PImb) models.

The comparison reveals several key findings. The DF benchmark achieves a higher total revenue in the absence of passive imbalance but incurs significantly more contract violations (557 out of 720). The increase in revenue is attributed to the model's inability to "buy" energy in the passive imbalance system to adjust for overly optimistic decisions in the first-stage. The second thing we notice is that the robust optimization now performs worse in terms of profit compared to SP, but has a significantly lower amount of contract violations to the

SP counterpart. These findings demonstrate the value of robust optimization in ensuring operational reliability under stricter conditions.

A more detailed breakdown of the revenue and violations distribution, as shown in Figure 5-10, reveals that the majority of violations for both the RO and SP approaches occur on 2023-11-30. Specifically, 15 out of 22 violations for RO and 19 out of 78 total violations for SP are concentrated on this day. Referring to Figure 5-6, this corresponds to a day when the actual available wind power significantly deviated from the forecasted values, even falling outside the robust bounds. This discrepancy exemplifies a rare tail event. When passive imbalance is included, such a substantial deviation can be compensated for. However, in its absence, both approaches struggle to manage the extreme mismatch effectively.

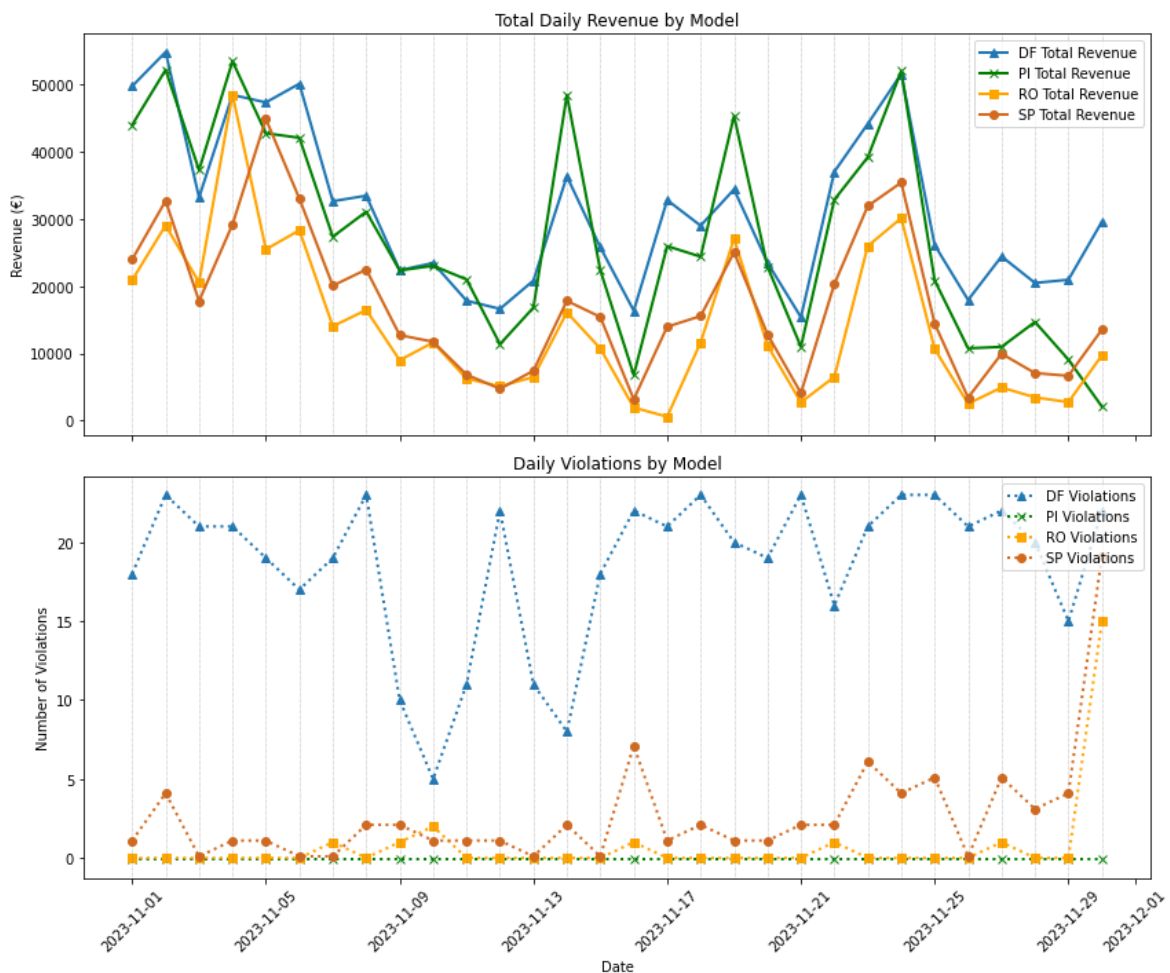


Figure 5-10: Detailed breakdown of daily revenues and violations for November 2023. The figure highlights the trade-offs between revenue generation and operational constraints across different optimization approaches.

5-5 Case study B: weekly runs for parameter sensitivity analysis

For the second case study, we use 7 days of data, each run approximately 20 times, to capture the randomness induced by the methods. The first 7 days of November provide a spread of uncertainty, including cases where the forecast is optimistic, thus testing model robustness. The wind data is shown in Figure 5-11. Besides that the activations are plotted in Figure 5-12

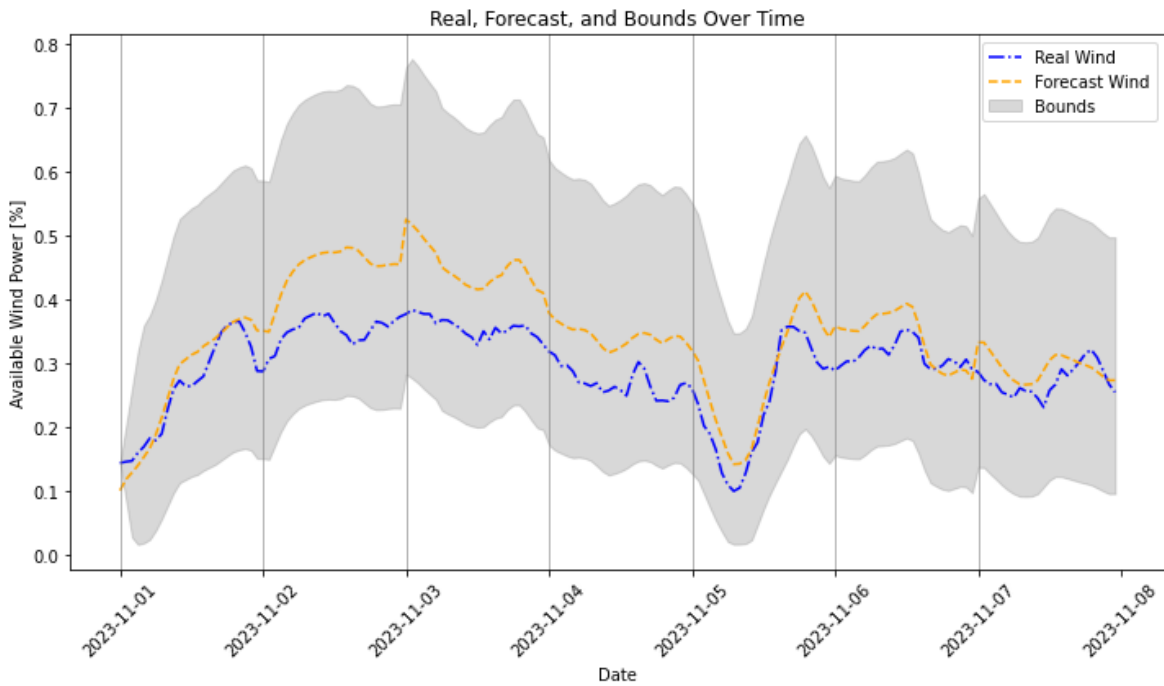


Figure 5-11: Forecast of the fraction of available wind power with its robust bounds for the first week of November 2023, plotted with the original forecast and actual fraction of available wind power.

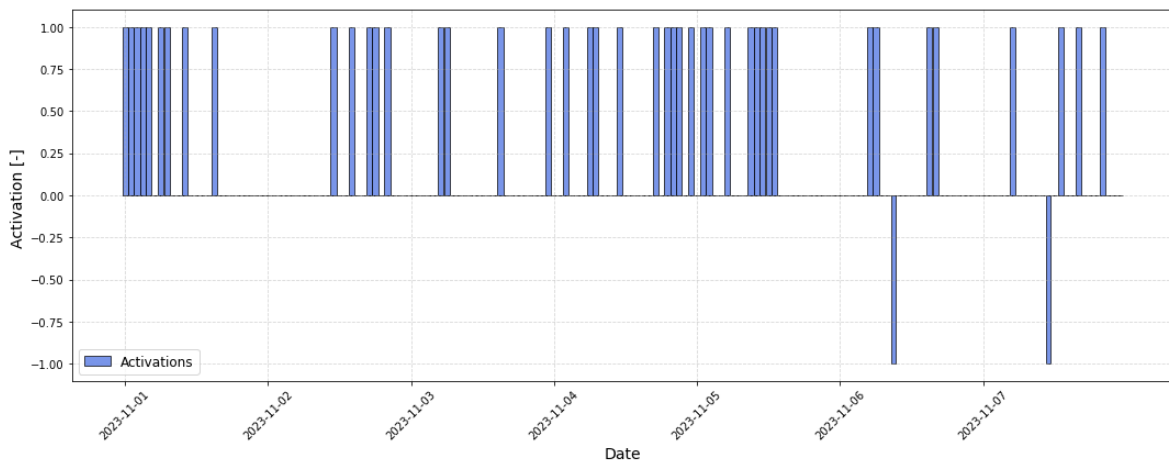


Figure 5-12: Weekly activation profiles activation = 1 equals up activation ($\beta^\uparrow = 1$), activation = -1 equal down activation $\beta^\downarrow = 1$

5-5-1 benchmarks results

We compare the performance of DF and PI benchmarks, both with and without passive imbalance. The results are summarized in Table 5-5.

The analysis reveals that DF consistently produce higher first-stage revenues compared to PI, which is due to the wind forecast power being overly optimistic in this week. However, PI scenarios slightly surpass DF in total revenue due to improved second-stage performance, not loosing to revenue to unwanted imbalance. Interestingly, excluding passive imbalance (No PImb) enhances second-stage revenues for DF, yet this improvement comes at the cost of increased violations. These findings underscore the trade-off between revenue optimization and operational reliability, with passive imbalance playing a critical role in balancing these outcomes.

Table 5-5: Revenue statistics under deterministic forecast and perfect information (in kEuro).

Model	FSR (kEuro)	SSR (kEuro)	Total (kEuro)	Violations (out of 168)
DF	205.53 ± 3.17	73.70 ± 15.45	279.22 ± 15.91	63.90 ± 4.63
PI	181.12	102.33	283.46	0.00 ± 0.00
DF - No PImb	203.85 ± 2.98	79.79 ± 8.96	283.64 ± 10.65	137.80 ± 6.03
PI - No PImb	181.12	93.85	274.97	0.00 ± 0.00

5-5-2 Stochastic programming parameter analysis

SP: impact of uncertain market prices

We investigate the effect of market price uncertainty on SP models. The results are shown in Table 5-6. Using perfect information, we can see in the first stage there is revenue to be gained in the first-stage. However including price scenarios with random sampling on the error distribution has minimal effect on the total revenue.

Table 5-6: Revenue statistics for different SP price models (in kEuro).

Model	FSR (kEuro)	SSR (kEuro)	Total (kEuro)	Violations (out of 168)
SP - Base Case, Forecasted Price	153.19 ± 1.55	61.74 ± 4.47	214.93 ± 3.69	0.00 ± 0.00
SP - Base, Perfect Price Info (PI price)	156.36 ± 1.61	60.78 ± 4.51	217.13 ± 4.30	0.05 ± 0.22
SP - Base, Price Scenarios	155.26 ± 1.11	59.64 ± 5.74	214.89 ± 5.02	0.00 ± 0.00

SP: impact of amount of wind scenarios

The impact of varying amounts of wind scenarios on the SP models is analyzed in this section. Results are summarized in Table 5-7, which highlights the variation in revenues under high and low wind scenarios.

The results show that a higher number of wind scenarios results in lower FSRs, indicating that the more wind scenarios are considered, the more conservative the first-stage solution becomes. The increased SSR is attributed to more energy being available for use in the passive imbalance markets.

Table 5-7: Revenue statistics for high wind and low wind scenarios (in kEuro).

Model	FSR (kEuro)	SSR (kEuro)	Total (kEuro)	Violations (out of 168)
SP - High Wind ($N^W = 40$) (PI price)	150.23 \pm 0.90	67.32 \pm 6.17	217.55 \pm 5.51	0.00 \pm 0.00
SP - Low Wind ($N^W = 10$) (PI price)	157.59 \pm 0.45	59.42 \pm 2.51	217.00 \pm 2.70	0.00 \pm 0.00

SP: random activation patterns

This section explores the influence of varying the number of random activation patterns and draws on the SP models. The results are detailed in Table 5-8.

Increasing the number of scenarios and draws significantly reduces the standard deviation of revenues, indicating improved consistency. However, achieving higher total revenues is associated with fewer draws, which in turn leads to a notable increase in violations.

Table 5-8: Revenue statistics for random activation patterns (in kEuro).

Model	FSR (kEuro)	SSR (kEuro)	Total (kEuro)	Violations (out of 168)
SP - $N^a = 5$, $N^{draws} = 8$ (PI price)	170.25 \pm 2.02	124.84 \pm 14.50	295.08 \pm 14.01	29.00 \pm 2.33
SP - $N^a = 5$, $N^{draws} = 15$ (PI price)	170.08 \pm 1.67	83.97 \pm 11.61	254.05 \pm 10.99	15.30 \pm 4.35
SP - $N^a = 10$, $N^{draws} = 15$ (PI price)	167.26 \pm 1.90	70.06 \pm 6.04	237.32 \pm 4.86	5.50 \pm 0.93

SP: passive imbalance not included

The impact of excluding passive imbalance on the SP models is analyzed in this section. The findings, as presented in Table 5-9, demonstrate the following trends. Removing passive imbalance leads to reduced total revenues. Additionally, the base case without passive imbalance results in lower second-stage revenues and a higher incidence of violations compared to models that incorporate passive imbalance. However, the relative increase in violations from the base case to the random activation scenarios is more significant when passive imbalance is allowed. Specifically, violations rise from an average of 0 to 5.5 when passive imbalance is included, whereas the increase is smaller, from 14.8 to 16.5, when passive imbalance is excluded. This highlights the stronger stabilizing effect of passive imbalance in mitigating violations under random activation patterns.

Table 5-9: Revenue statistics for SP models without passive imbalance (in kEuro).

Model	FSR (kEuro)	SSR (kEuro)	Total (kEuro)	Violations (out of 168)
SP - Base Case (No PImb, PI price)	156.86 \pm 0.89	31.74 \pm 0.47	188.60 \pm 0.74	14.80 \pm 5.41
SP - 10 Scenarios, 15 Draws (No PImb, PI price)	165.52 \pm 1.96	53.99 \pm 10.23	219.51 \pm 10.69	16.50 \pm 4.12

SP: additional metric of managed activations

An additional metric of aFRR activation managed (AM) and not managed (ANM) is introduced, and the results for the different SP model parameters are shown in Table 5-10. The first observation is that models with random activation scenarios, instead of pessimistic activation scenarios, have significantly more AM, indicating a higher volume of aFRR capacity

sold. The second observation is that not all violations originate from activations that are not managed.

Table 5-10: Comparison of Stochastic Programming Models with Additional Metrics.

Model	Total AM \pm std	Total ANM \pm std	Violations \pm std (out of 168)
SP - Base Case, Forecast Price	9.43 \pm 2.14	0.00 \pm 0.00	0.00 \pm 0.00
SP - Perfect Price Info	11.80 \pm 2.65	0.05 \pm 0.22	0.05 \pm 0.22
SP - Price Scenarios	3.85 \pm 3.51	0.00 \pm 0.00	0.00 \pm 0.00
SP - High Wind (Base Activations)	6.67 \pm 4.12	0.00 \pm 0.00	0.00 \pm 0.00
SP - Low Wind (Base Activations)	10.00 \pm 0.00	0.00 \pm 0.00	0.00 \pm 0.00
SP - $N^a = 5$, $N^{draws} = 8$	30.33 \pm 3.01	15.83 \pm 1.65	29.00 \pm 2.33
SP - $N^a = 5$, $N^{draws} = 15$	29.60 \pm 5.19	9.30 \pm 1.95	15.30 \pm 4.35
SP - $N^a = 10$, $N^{draws} = 15$	33.38 \pm 4.81	4.25 \pm 1.04	5.50 \pm 0.93
SP - Base Case, (No PImb)	11.00 \pm 0.00	0.00 \pm 1.26	14.80 \pm 5.41
SP - $N^a = 10$, $N^{draws} = 15$ (No PImb)	26.25 \pm 2.50	6.75 \pm 2.38	16.50 \pm 4.12

5-5-3 ARO parameter analysis

For the weekly results we focus on impact of the uncertainty budgets. The robust budgets $\Gamma^{A,\uparrow}$, $\Gamma^{A,\downarrow}$, and Γ^W define the allowable uncertainty in activation up, activation down, and wind scenarios, respectively. The different cases tested are shown in Table 5-11

Table 5-11: Comparison of models and budgets

Model	$\Gamma^{A,\uparrow}$	$\Gamma^{A,\downarrow}$	Γ^W
HAHW (High Act. high wind)	15	8	24
MAHW (Med. act. high wind)	8	4	24
MAMW (Med. act. med wind,)	8	4	12
LAHW (Low Act. high wind)	2	2	24
LALW (Low Wind, Low Act.)	2	2	6

For each combination of budgets we evaluate two primary sets of scenarios: one where passive imbalance is include and another where it is excluded. As shown in the monthly results, including passive imbalance ensures that deviations are managed to comply with aFRR contracts, typically resulting in no violations. In contrast to scenario programming, we focus more on the cases excluding passive imbalance to illustrate where the robustness of the first-stage solution begins to break down.

From the results presented in Table 5-12 and Table 5-15, we observe the following:

- **Revenue performance:**

- Models with lower robust budgets, such as RO - LALW, achieve the highest total revenue (275.30 ± 21.04 k€). This is due to more aggressive first-stage decisions enabled by lower conservatism in the uncertainty budget.
- Passive imbalance exclusion leads to significantly lower total revenue. Which is most clear in the higher budgets. This shows that more conservative decisions in the first stage open up more opportunities in the second-stage to rebalance for profit.

- **Violations:**

- No violations occur when passive imbalance is included, demonstrating the model's robustness in meeting aFRR contracts, with the ability to rebalance regardless the budget.
- Excluding passive imbalance increases violations, particularly for RO No PImb - LALW, which records 18.95 ± 3.55 violations due to the low uncertainty budget.

- **Activations managed (AM) and activations not managed (ANM):**

- Total AM is highest for models with lower budgets, such as RO - LALW (43.20 ± 4.02), reflecting more aggressive offering on the aFRR capacity market.

- In scenarios excluding passive imbalance, the ANM increases, particularly for RO No PImb - LALW (4.60 ± 1.39). What is interesting to see is that the AM is still high. Showing that the violations not necessarily only happen during activations. Violations besides activation not managed include not being able to deliver promised capacity if it was asked at that moment, which is less severe in terms of violating aFRR contracts but still highly unfavorable.

Table 5-12: Comparison of Robust Optimization Models with Key Metrics (in kEuro).

Model	Total FSR (k€)	Total SSR (k€)	Total Revenue (k€)	Violations (out of 168)
RO - HAHW	111.29 ± 1.01	150.68 ± 4.98	261.97 ± 3.99	0.00 ± 0.00
RO - MAHW	115.50 ± 0.89	144.13 ± 2.41	259.63 ± 1.68	0.00 ± 0.00
RO - MAMW	114.66 ± 4.12	142.52 ± 14.62	257.18 ± 10.81	0.00 ± 0.00
RO - LAHW	117.53 ± 1.56	155.82 ± 10.44	273.35 ± 8.93	0.00 ± 0.00
RO - LALW	121.84 ± 3.30	153.46 ± 24.14	275.30 ± 21.04	0.00 ± 0.00
RO No PImb - HAHW	111.32 ± 0.86	76.64 ± 4.61	187.96 ± 3.79	1.00 ± 0.00
RO No PImb - MAHW	115.28 ± 0.88	71.67 ± 3.44	186.95 ± 2.60	0.95 ± 0.22
RO No PImb - MAMW	116.14 ± 1.55	79.95 ± 6.57	196.09 ± 5.04	0.40 ± 0.63
RO No PImb - LAHW	117.53 ± 1.08	100.89 ± 7.83	218.42 ± 7.09	0.00 ± 0.00
RO No PImb - LALW	121.15 ± 1.62	121.81 ± 9.42	242.96 ± 8.28	18.95 ± 3.55

Table 5-13: Comparison of Robust Optimization Models with Additional Metrics.

Model	Total AM \pm std	Total ANM \pm std	Total Violations \pm std (out of 168)
RO - HAHW	20.80 ± 5.67	0.00 ± 0.00	0.00 ± 0.00
RO - MAMW	17.20 ± 3.78	0.00 ± 0.00	0.00 ± 0.00
RO - LAHW	23.90 ± 6.30	0.00 ± 0.00	0.00 ± 0.00
RO - LAHW	40.50 ± 5.40	0.00 ± 0.00	0.00 ± 0.00
RO - LALW	43.20 ± 4.02	0.00 ± 0.00	0.00 ± 0.00
RO No PImb - HAHW	20.65 ± 5.08	0.00 ± 0.00	1.00 ± 0.00
RO No PImb - MAMW	18.60 ± 4.28	0.00 ± 0.00	0.95 ± 0.22
RO No PImb - MAMW	24.93 ± 4.06	0.07 ± 0.26	0.40 ± 0.63
RO No PImb - LAHW	41.50 ± 3.76	0.00 ± 0.00	0.00 ± 0.00
RO No PImb - LALW	40.40 ± 1.39	4.60 ± 1.39	18.95 ± 3.55

ARO: Impact of market price uncertainty

During the main case study results perfect price information was used to not convolute the results as the focus of the study was on operational uncertainty. However the extension in Equation 4-33 was implemented and tested on one of the models. The week data suggests an improvement on using price scenarios over not using price scenarios, but looking closer at the daily data it was inconclusive. The different prices of the forecast and scenarios programming lead to different optima of the CCGA which resulted in either very high difference of the total revenue due to uncertain effect of activation.

Table 5-14: Comparison of RO models on including DA price uncertainty with main metrics. CCGA: tolerance of 0.04

Model	Total FSR	Total SSR	Total Rev (k€)	Total Violations (out of 168)
RO No PImb - HAHW	112.26 ± 0.66	72.79 ± 3.24	185.04 ± 2.69	1.00 ± 0.00
RO No PImb - HAHW - Price Forecasts	117.88 ± 0.54	72.54 ± 1.59	190.41 ± 1.17	0.93 ± 0.46
RO No PImb - HAHW - Price Scens	117.46 ± 0.51	74.34 ± 4.12	191.80 ± 3.71	0.71 ± 0.47

Table 5-15: Comparison of RO models on including DA price uncertainty with additional Metrics.

Model	Total MA ± std	Total ANM ± std
RO No PImb - HAHW	16.80 ± 3.79	0.00 ± 0.00
RO No PImb - HAHW - Forecast	10.20 ± 0.77	0.07 ± 0.26
RO No PImb - HAHW Price Scens	10.59 ± 1.66	0.00 ± 0.00

5-5-4 Computational times

We first present the computation times for the different configurations of the SP framework. The results are shown in Table 5-16. Only the results are shown for where the model parameter resulted in a different amount of total scenarios, as it was found while running the case study that this dedicated the average run time. There seems to be a linear relation correlation between the run time and total scenarios. The run times are acceptable for the application of offering.

Table 5-16: Computation times for SP scenarios.

Model	Total Scenarios	Average Run Time/Day (sec)
SP - Base	60	498.19 ± 71.17
SP - Low Wind ($n^W = 10$) (Base Activations)	30	228.73 ± 32.68
SP - 5 Random aFRR Scenarios - 15 Draws	100	761.82 ± 108.83
SP - 10 Random aFRR Scenarios - 15 Draws	200	1,442.75 ± 206.11

The computation times for different robust optimization models are summarized in Table 5-17. The RO MAMW model has the highest average run time and standard deviation out of the RO models. Lowering the amount of activation budget decreases the search space, however higher budgets typically result in tighter constraints in the column and constraint algorithm and with that faster convergence times. This is also evident in the case of LALW and LAHW.

Table 5-17: Computation times for RO scenarios.

Model	Average Run Time/Day (sec)
RO HAHW	60.27 ± 12.84
RO MAHW	70.55 ± 29.77
RO MAMW	216.76 ± 55.13
RO LAHW	41.50 ± 7.60
RO LALW	108.49 ± 56.34

In comparison, the robust optimization approach outperforms the stochastic programming approach in terms of computation time. While the benchmarks' running times were not tracked, they were estimated to be on the order of a few seconds per day. It is important to note that the run times refer to the total simulation time for an entire day, and for each model, the running time includes both the first and second stage.

Considering the market clearance order in Figure 2-3, the current run times for both approaches appear to fit within the day-ahead clearance timeframe. Observations from the model runs suggest that most model versions produce day-within setpoints at a sufficient rate, except for the SP model with 200 total scenarios. With an average run time of 1,442.75 seconds, the first stage solution and the first few scenarios contribute significantly to the overall run time. In the second stage optimization, each horizon step is realistically around 15 minutes. Ideally, a decision would need to be made within the first 5 minutes of the decision interval, which is nearly achieved in this case. However, the primary focus of this thesis is not computational times but the methods needed to be computationally trackable, as shown for this particular case study.

5-6 Discussion of case study results and model limitations

5-6-1 Start-up costs

Start-up costs were included to encourage more realistic electrolyzer behavior. During the analysis of the case study results, the effects of these start-up costs were found to be minimal and were thus largely ignored. The start-up cost was set at 500, scaled from literature [3]. This assumption was not explicitly verified and may have been overly restrictive, potentially limiting the electrolyzer's operational flexibility. Future studies focused on detailed economic impact should revisit and refine this assumption to better capture the trade-offs between start-up costs and dynamic operational behavior.

5-6-2 Performance CCGA

It was noticed during running that the CCGA would sometimes take longer than the set timelimit to converge or find a valid MILP solution to the dual subproblem. This is due to the large number of binary variables, which makes the problem hard to converge. A slight deviated version of the CCGA algorithm was created to handle cases where MILP would not converge in a suitable time. The timelimit of 300s was not optimized to avoid suboptimal

solution but they were rare and sometimes dependent on how much computing power was left on the laptop. For a better assessment of performance, a more stable running environment should be chosen.

Notably, the results in Table 5-12 show significant variability in some models, such as RO - MAMW, which has a high standard deviation. The box plot in Figure 5-13 illustrates large discrepancies in revenue across different days, with notable outliers on 2023-11-05.

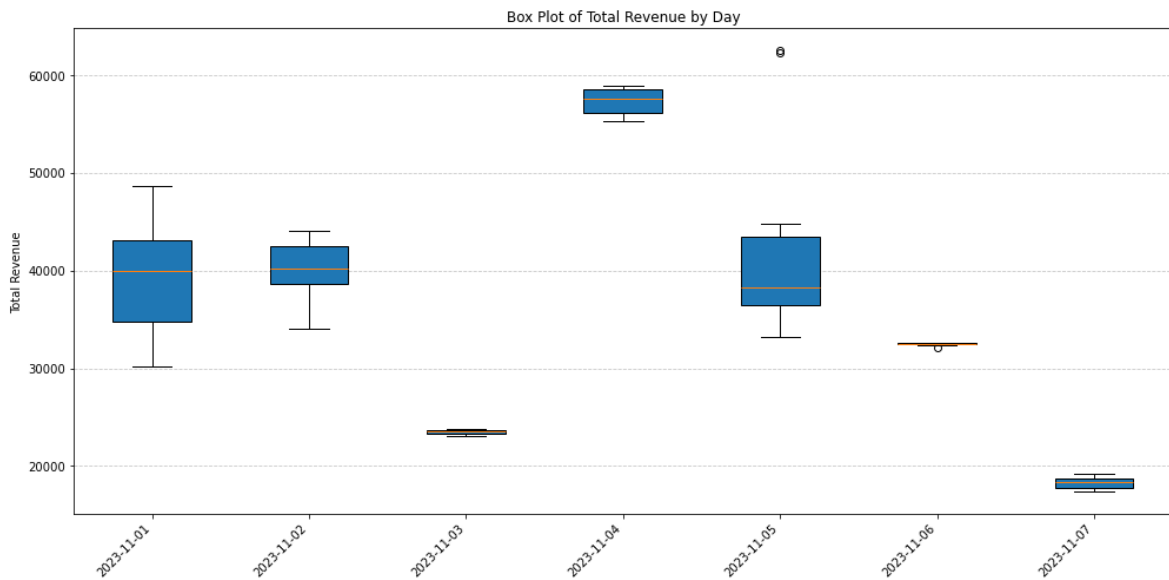


Figure 5-13: Box plot of total revenue for each day in the first week of November 2023. Values created using the RO MAMW model

The days with a high spread of total revenue are also the days with high prices coinciding with activations of aFRR up, as illustrated in Figure 5-13 and Figure 5-14. This phenomenon can be attributed to the CCGA having multiple optima, where a few MW difference in aFRR capacity can have a significant impact on the second-stage revenue and with that on the total revenue. However, this uncertainty in activation prices is not currently captured. An extension to stochastic activation prices could potentially capture higher activation prices and should be investigated.

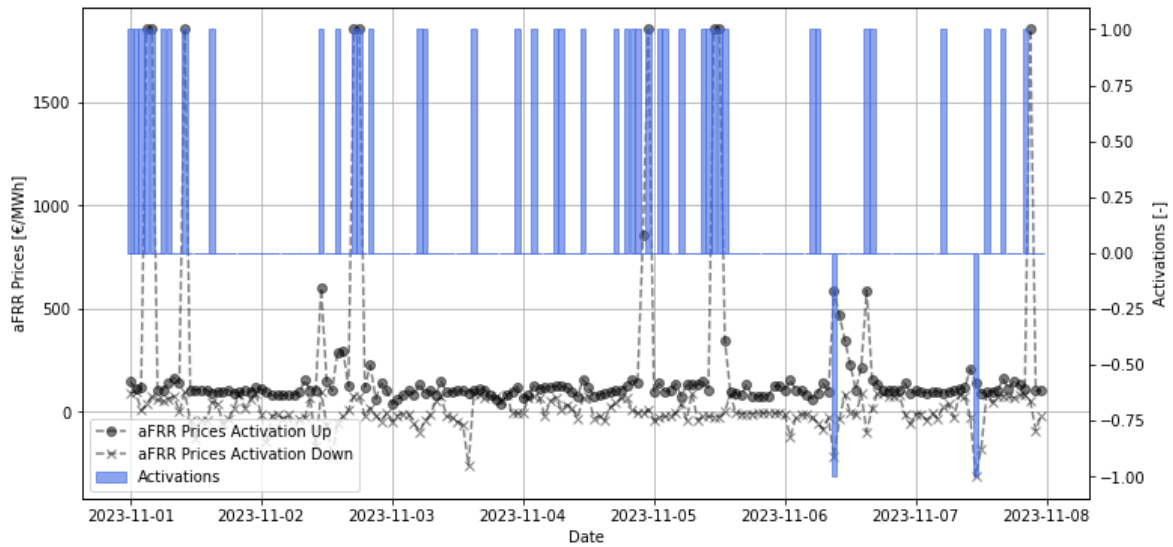


Figure 5-14: aFRR activations vs activation prices of the first week of November 2023. The left axis shows the aFRR prices and on the right the real activation throughout the with activation = 1 equals up activation ($\beta^\uparrow = 1$), activation = -1 equal down activation ($\beta^\downarrow = 1$)

5-6-3 Passive imbalance impact and price uncertainty

The case study assumes perfect knowledge of imbalance prices at the current horizon time-step, an assumption that warrants reconsideration. In practice, imbalance price data is provided every minute, allowing for forecasts of the final imbalance price within each settlement period. As the period progresses, the certainty of these forecasts increases. Incorporating real-time forecasting of imbalance prices into the model would provide a more realistic representation of market dynamics and improve decision-making under uncertainty.

5-6-4 Impact of aFRR activation energy

The current aFRR activation is modeled on an hourly basis under the assumption of full hourly activation, which is unrealistic for two key reasons. First, aFRR activation is inherently a 15-minute product. The current approach samples prices from these 15-minute intervals and extrapolates them over the entire hour. Consequently, a high price observed during a single 15-minute period is extended to the full hour, disproportionately influencing the total daily revenue.

Second, the assumption of full activation is not reflective of real-world operations. A more realistic approach would involve matching the activation strategy to a merit order, as illustrated in . Such an approach would allow for a more accurate estimation of activated aFRR volumes. This adjustment is particularly relevant when implementing a 15-minute offering framework, which could enable either a more precise economic assessment or real-time operational experiments simulating the plant's response to aFRR requests.

Furthermore, incorporating this refinement would provide an opportunity to explore optimal bidding strategies, potentially improving the plant's participation in the market and its overall performance.

5-6-5 Limited impact of DA price uncertainty

While the original scope of the study also included managing DA market price uncertainty, the resulting data were inconclusive. To avoid further complicating the results of the robust optimization, perfect price information was assumed for the DA prices. In the stochastic optimization analysis, as discussed in section 5-5-2, it was shown that perfect price information provided an additional value of approximately 2.36k€, which corresponds to a 1.5% increase in profit. However, a creating scenarios with random sampling on the error distribution, while increasing first-stage profit, led to a decrease in total profit. This suggests the presence of underlying dynamics that influence profit but are either not well modeled or insufficiently captured in the current framework.

For robust optimization, the master problem was briefly extended to a stochastic hybrid approach, but proved inconclusive in dealing with price uncertainty. A possible explanation lies in the risk-neutral optimization of the objective function, since the random sampling resulted in a mean price equal to the forecast. This might have made the approach ineffective in improving the solution.

Additionally, Figure 5-7 demonstrates that the overall impact of DA price uncertainty on revenue is relatively low. A greater integration of renewable energy sources could potentially influence the amount of DA energy offered, thereby amplifying the impact of DA market price uncertainty on the overall outcomes.

5-6-6 Risk neutral stochastic programming

The current stochastic problem is set-up in a risk neutral way. While this might not be the best naming for it. As violations are not allowed in the scenario programming, every possible scenario put in should at least find a suitable solutions. In that way negating risk. An alternative would be to allow the model to deviate from the equality constraint using the before mentioned slack variables. The penalty of the slack variables could then be used as risk measure. This could be done in combination with a conditional value at risk method, which would allow to penalize losses more than revenue. However the focus was to create a way to deal with the strict constraint of balancing and thus this method was not applied.

5-6-7 Case study limitations

As outlined in section 5-1-1, the models and case study rely on several simplifying assumptions, which play a crucial role in shaping the results and should be carefully considered when interpreting them.

First, the inclusion of additional realistic operational constraints, such as ramp rates for wind turbines and more accurate battery operation models, could significantly affect the results. For example, these constraints may reduce the flexibility of the battery or electrolyzer, potentially leading to less optimal or more conservative decisions. The omission of these constraints suggests that the current results may represent a best-case scenario in terms of operational flexibility.

Furthermore, costs such as net tariffs, asset maintenance, and degradation are not accounted for in this analysis. These costs can have a substantial impact on net revenue. Therefore,

while the results provide an estimate of gross revenue, they do not fully reflect the net financial outcomes. When applying these findings to real-world scenarios, these additional costs should be incorporated to provide a comprehensive view of profitability.

Despite these limitations, the results demonstrate the potential of the proposed hybrid power plant optimization approaches and their relevance to different market structures. The methods explored offer valuable insights into possible strategies for participation in day-ahead and balancing markets, even if the exact revenue figures should be interpreted with caution.

While the assumptions simplify the analysis and enhance computational tractability, they also indicate that the results are indicative rather than definitive. Real-world applications should carefully integrate additional constraints and costs to ensure that strategies remain viable under practical conditions.

5-7 Chapter summary: case study

This chapter explores two case studies that evaluate the performance of the SP and ARO frameworks in managing uncertainty for hybrid power plants participating in energy markets. The focus is on balancing revenue generation with operational robustness under real-world uncertainty. The results are benchmarked against with DF and PI approaches.

5-7-1 Methods

Case Study A: Monthly Analysis

The monthly analysis uses November 2023 data to compare the performance of SP and ARO against the benchmarks. For SP, wind and activation scenarios were generated, and the real day-ahead prices were used instead of forecast. For ARO, uncertainty budgets ($\Gamma^W, \Gamma^{A,\uparrow}, \Gamma^{A,\downarrow}$) defined the allowable deviations in wind power and activations. Robust bounds for wind power were derived from quantile regression and convex hull methods. The models were evaluated both with and without passive imbalance to assess the robustness of first-stage solutions.

Case Study B: Weekly Runs for Parameter Sensitivity Analysis

The weekly analysis focused on the first seven days of November 2023, with 20 runs per day to account for variability in scenarios. This analysis investigated the impact of hyperparameters such as wind and activation budgets, the number of scenarios, and the inclusion of passive imbalance. Activation patterns and price scenarios were also evaluated to understand their influence on model outcomes. Computational times for each approach were tracked to assess their feasibility within market clearance timeframes.

5-7-2 Results and insights

Case Study A: Monthly Analysis

The PI benchmark achieved the highest total revenue (€856,162.83) with no violations, followed by DF, which generated €825,489.35 in total revenue but incurred 111 out of 720 possible violations. SP and ARO produced lower revenues (€572,986.96 and € 598,463.90, respectively) but maintained feasibility under all constraints. When passive imbalance was

excluded, DF showed a significant increase in violations (557 out of 720), while SP accumulated 78 violations and ARO registered only 22, demonstrating a more conservative yet reliable approach overall.

Case Study B: Weekly Runs for Parameter Sensitivity Analysis

The weekly results highlighted trade-offs between conservatism and revenue generation. In terms of revenue the SP models benefited from introducing activation scenarios, with revenues decreasing as the number of activation patterns increased. Random activation came at the cost of longer computation times and increased amount of violations. ARO models demonstrated flexibility in adapting to uncertainty budgets; lower budgets ($\Gamma^W, \Gamma^{A,\uparrow}, \Gamma^{A,\downarrow}$) led to higher revenues but also increased violations when passive imbalance was excluded. However the increase in violations was only noticeable when both the wind and activation budgets were set to low values for the cases where passive imbalance was excluded, highlighting the robustness of the approach. Including price scenarios improved revenues for both SP and ARO models, particularly under high uncertainty in market conditions. Computational times were acceptable for market operations, with ARO models consistently solving faster than SP models, which scaled linearly with the number of scenarios.

The case studies demonstrated the effectiveness of SP and ARO methods in managing uncertainty for hybrid power plants. ARO methods provide robust solutions with lower violation rates, making them ideal for conservative decision-making under strict operational constraints. Benchmarks highlighted the importance of balancing conservatism and revenue generation, with PI offering a theoretical upper bound and DF exposing the risks of relying solely on forecasts.

Conclusions and future work

6-1 Conclusions

This thesis addresses the central research question: *How can we effectively manage the portfolio of a hybrid power plant, including wind turbines, photovoltaic cells, batteries, and electrolyzers, for participation in the day-ahead market and the Dutch balancing market, using a tractable data-driven optimization approach?*

The research was guided by two main objectives.

The first objective focused on developing a comprehensive model for hybrid power plants operating within the Dutch multi-market environment, emphasizing interactions with aFRR reserves and activations. This was achieved through modeling of electrolyzers, batteries, and power balance constraints, with each asset's role in capacity bidding and reserve activation explicitly defined. Unlike generic capacity allocation methods, this approach provided a clearer representation of asset-specific contributions, ensuring compliance with market requirements. The study specifically modeled the Dutch aFRR capacity market, where binding contracts require aFRR capacity to be available for every hour of the day. Failure to manage activation or to have the committed capacity available results in a violation of the contract. These violations were represented as slack variables, serving as a metric to evaluate the robustness of first-stage decisions and their ability to maintain reliable performance under uncertainty. To further validate the practicality of the framework, a shrinking horizon approach was implemented, enabling real-time updates and providing a more realistic simulation of aFRR activation uncertainties.

The second objective focused on addressing uncertainties using real-world market data through the development and application of optimization frameworks. Two complementary optimization methods were explored: stochastic programming and adaptive robust optimization. The stochastic programming approach managed uncertainties by generating scenarios for renewable generation, market prices and aFRR activation. The stochastic programming approach demonstrated effectiveness for situations where uncertainties follow a known or estimable distribution. It provided valuable insights but revealed limitations in its ability to consistently manage activation uncertainties, particularly under random or highly variable patterns.

In contrast, the adaptive robust optimization framework took a conservative approach using robust bounds on wind generation and market activations, leveraging duality theory to solve the inner problem of the CCGA. This methodology effectively minimized violations and ensured compliance with strict market requirements, demonstrating its strength in dealing with scenarios characterized by high uncertainty. However, the conservative nature of this approach also revealed trade-offs, including reduced first-stage revenue potential and reduced flexibility in operational scheduling. The reduced flexibility in the current robust approach stems from the reliance of classical CCGA on duality, which precludes the inclusion of binary variables in the subproblem. This constraint led to the pre-scheduling of binary variables such as the electrolyzer states, reducing operational flexibility of the framework.

The case study, utilizing real-world market and operational data from 2023, provided several key insights into the performance of the proposed optimization frameworks:

- **Effective uncertainty management with passive imbalance:** Both the stochastic and robust optimization frameworks demonstrated the ability to successfully manage hybrid power plant offerings under uncertainty when passive imbalance was allowed, achieving zero violations across all tested scenarios and delivering reasonable revenue levels compared to the benchmarks of using only forecasts or perfect information.
- **Limitations of Stochastic optimization:** The stochastic optimization framework achieved satisfactory results only under pessimistic activation scenarios and with the inclusion of passive imbalance. However, its performance with respect to violations deteriorated significantly when either pessimistic activation was replaced with a random activation scenarios or passive imbalance was removed, underscoring its sensitivity to these conditions.
- **Performance of robust optimization:** The robust optimization approach consistently outperformed the stochastic framework in terms of profit when passive imbalance was permitted. This outcome was attributed to its more conservative first-stage decisions, which allowed for greater exploitation of favorable passive imbalance conditions. Additionally, the robust optimization framework demonstrated higher revenues with zero violations during the first week of November compared to SP, effectively leveraging upward activation capacity and with that the potential high upward activation prices. Lastly an increase in violations was only noticeable when both the wind and activation budgets were set to low values for the cases where passive imbalance was excluded, highlighting the robustness of the approach.

This work contributes to the field of hybrid power plant management by presenting a framework for navigating uncertainty in dynamic market participation. It emphasizes the balance between profitability, reliability, and adaptability, providing a basis for further research into hybrid power plant operations and their role in integrating renewable energy into the energy system.

6-2 Future work

Address current limitations

Future work should begin by addressing the limitations identified in the case study, as these present opportunities to refine and expand the framework. A key area for improvement is the analysis of uncertainties in parameters currently assumed to be known, such as imbalance price uncertainty, and explicitly modeling aFRR activation price uncertainty. Additionally, the model should incorporate higher-fidelity representations of system components. For example, separate charging and discharging variables for the battery, along with efficiency losses, should be introduced. Similarly, the nonlinearity of the electrolyzer could be modeled to better capture its real-world behavior. Although this would introduce binaries to the second stage, robust optimization theory provides methods to derive exact solutions for non-linear second-stage optimization in finite steps [32] [33].

Include higher time resolution and improve day coupling

The current model employs an hourly resolution, amplifying the influence of high-price events on daily results. In reality, price fluctuations typically occur within shorter intervals, such as 15 minutes. Adopting a 15-minute resolution would better reflect real-world dynamics. While averaging was considered, the system's ability to switch balancing states—and consequently price directions—within an hour made this approach infeasible. A rolling horizon framework could be introduced to manage the increased computational demands of this finer resolution, preserving the 15-minute granularity for intra-day decisions while using first-stage decisions as references for subsequent stages.

Implementing a rolling horizon approach could also address the current issue of decoupled days. The existing shrinking horizon resets every 24 hours, creating discontinuities in battery state-of-charge and electrolyzer dynamics. In practice, operations flow seamlessly between days, with known working points and accurate initial battery states. Although the current model partially accounts for this by enforcing a minimum final state-of-charge equal to the starting point, it does not consider factors such as electrolyzer cold starts. A rolling horizon framework would improve continuity by integrating decisions across multiple days, aligning more closely with real-world operations.

However, this approach must address the 12-hour gap caused by the timing of day-ahead market commitments, particularly with a 24-hour rolling horizon. Resolving this gap will be critical to achieving realistic and effective integration of intra-day and day-ahead decisions.

Increase market choices and optimize market offering strategy

This thesis focused on integrating the DA market, aFRR, and passive imbalance into the hybrid power plant model. However, this approach excludes other key markets such as mFRR and FCR, which could further enhance the plant's profitability and balancing capabilities. The current analysis limited rebalancing options to using imbalance prices and energy only when aFRR was not activated, primarily to simplify the model.

In practice, the intraday market provides critical opportunities for real-time responses to uncertainty. Incorporating this market would allow the plant to make additional decisions at each timestep, enabling continuous rebalancing throughout the day. Leveraging the intraday market effectively could significantly reduce rebalancing costs compared to relying solely on imbalance prices. A more comprehensive model that integrates the intraday market would provide robust solutions, minimizing violations while ensuring compliance with contractual obligations.

Additionally, the plant's offering profiles could be optimized to better align with market dynamics. Currently, offering profiles are not explicitly modeled, and the market clearing price is assumed for the DA market. By tailoring offering profiles, the plant could more effectively address DA market price uncertainty and improve profitability.

Include price maker dynamics

The current assumption that the hybrid power plant acts as a price taker may be valid for smaller plants, but as the plant's size and offered capacities increase, this assumption becomes less realistic. Incorporating price-maker dynamics would account for the plant's influence on market prices. However, this inherently introduces non-linearity, making it computationally challenging to integrate into a robust optimization framework. Existing research has explored price-maker dynamics in the context of offering reserve energy through stochastic programming [34], with more recent advancements addressing robust price-maker dynamics [35]. Extending robust optimization to include price-maker dynamics in reserve markets would be a valuable and intriguing direction for future research.

Appendix A

Appendix: asset parameters used

Parameters for the assets:

Table A-1: Electrolyzer Parameters.

Parameter	Value/Description
Size	1.00×10^1 MW (Capacity)
OptPercent	28% (Optimum operation point as % of capacity)
MinPercent	15% (Minimum power needed as % of capacity)
SBPercent	1% (Stand-by power as % of capacity)
Pressure	30 bar (Cell pressure)
Temperature	90 C (Cell temperature)
Current	5000 A/m ² (Cell current density)
Area	0.2 m ² (Cell area)
NSegments	1 (Number of linear segments)

Table A-2: Battery Parameters.

Parameter	Value/Description
SOC ^{init}	50% (Initial state of charge)
P _{max} ^c	50% (Max storage charging power as % of size)
P _{max} ^{dc}	50% (Max storage discharging power as % of size)
ChargeFinal	50% (Imposed charge at final time step)
MinSOC	0.1 (Minimum state of charge)
MaxSOC	0.9 (Maximum state of charge)

Table A-3: General Parameters.

Parameter	Value/Description
$\underline{P}^{\text{net}}$	22
$\overline{P}^{\text{net}}$	22

Appendix B

Appendix: old models

B-1 old model with a higher fidelity

While the model had some higher fidelity at some point due to modelling choices they are left out, making the choice to test a more advanced optimization approach.

$$SOC_t^{bat} = SOC_{t-1}^{bat} + \left(\frac{P_t^{bat\ in} - P_t^{bat\ out}}{\text{Bat capacity}} \right) \cdot \Delta T \quad (\text{B-1})$$

Final State of Charge Constraint Ensures the final state of charge of the battery meets or exceeds a specified level, considering the entire operational period.

$$SOC^{bat\ init} + \sum_{t \in T} \left(\frac{(P_t^{bat\ in} - P_t^{bat\ out}) \cdot T}{\text{Bat capacity}} \right) \geq SOC^{bat\ final} \quad (\text{B-2})$$

The total powerbalance of the battery consists of the following components

$$P_t^{bat} = P_t^{bat,out} - P_t^{bat,in} - P_t^{bat,loss,in} - P_t^{bat,loss,out} \quad (\text{B-3})$$

First setpoints between zero and one are used as an optimization variable as:

$$P_t^{bat,in} \leq sp_t^{b,in} \cdot \eta_{bat} \cdot P^{b,ch,max} \quad (\text{B-4})$$

$$P_t^{bat,out} \leq sp_t^{b,out} \cdot \eta_{bat} \cdot P^{b,dis,max} \quad (\text{B-5})$$

Battery Output Limit Constraint Specifies the maximum power output from the battery, determined by the output setpoint, battery efficiency, and maximum discharge power. Battery Input Losses Constraint Calculates losses associated with charging the battery, taking into account the efficiency and maximum charge power.

$$P_t^{bat\ out} = S_t^{bat,out} \cdot \eta^{eff\ bat} \cdot P^{bat\ dis\ max} \quad (\text{B-6})$$

Battery Output Losses Constraint Determines losses during battery discharge, incorporating the efficiency and maximum discharge power.

$$P_t^{\text{bat loss out}} = S_t^{\text{bat,out}} \cdot (1 - \eta^{\text{eff bat}}) \cdot P^{\text{bat dis max}} \quad (\text{B-7})$$

Battery input constraint with big M ensures that the battery input power does not exceed a large constant M when the battery is operational.

$$P_t^{\text{bat in}} \leq M \cdot u_t^{\text{bat}} \quad (\text{B-8})$$

Battery Output Constraint with Big M Limits battery output power with the help of a large constant M, accounting for the operational status of the battery.

$$P_t^{\text{bat out}} \leq M \cdot (1 - u_t^{\text{bat}}) \quad (\text{B-9})$$

B-1-1 electrolyzer old constraints for allowing storage

For the hydrogen storage the following constraints are added

$$\begin{aligned} Q_t^{\text{H2,prod}} &= Q_t^{\text{H2,out,direct}} + SOS_t^{\text{in}} & \forall t \in \mathcal{T}, \\ Q_t^{\text{H2,out,total}} &= Q_t^{\text{H2,out,direct}} + SOS_t^{\text{out}} & \forall t \in \mathcal{T}, \\ SOS_t^{\text{out}} &\leq SOS^{\text{out limit}} & \forall t \in \mathcal{T}, \\ P_t^{\text{comp}} &= K^{\text{comp}} SOS_t^{\text{in}} & \forall t \in \mathcal{T}, \\ SOS_{t=1} &= SOS^{\text{ini}} + SOS_{t=1}^{\text{in}} - SOS_{t=1}^{\text{out}} \\ SOS_t &= SOS_{t-1} + SOS_t^{\text{in}} - SOS_t^{\text{out}} & \forall t \in \mathcal{T} \setminus \{1\}, \\ SOS_t &\leq SOS^{\text{cap}} & \forall t \in \mathcal{T}. \end{aligned} \quad (\text{B-10})$$

B-1-2 old electrolyzer segmentation

In the original model of the electrolyzer from [3], a higher fidelity model is used that adjusts to the non-linearity of the electrolyzer production curve.

$$Q_t^{\text{H2,prod}} = \sum_{s \in \mathcal{S}} \left(A_s \hat{P}_{ts}^e + B_s z_{ts}^h \right) \quad \forall t \in \mathcal{T}, s \in \mathcal{S} \quad (\text{B-11})$$

Setting power bounds for segments and ensuring only one active segment at a time.

$$\underline{P}_s z_{ts}^h \leq \hat{P}_{ts}^e \leq \bar{P}_s z_{ts}^h \quad \forall t \in \mathcal{T}, s \in \mathcal{S}. \quad (\text{B-12})$$

$$z_t^{\text{on}} = \sum_{s \in \mathcal{S}} z_{t,s}^h \quad \forall t, s \in \mathcal{S} \quad (\text{B-13})$$

$$P^{\text{H2}} = \sum_{s \in \mathcal{S}} \hat{P}_{ts}^e + P^{\text{sb}} z_t^{\text{sb}} \quad \forall t \in \mathcal{T}, s \in \mathcal{S} \quad (\text{B-14})$$

Appendix: robust optimization

C-1 Full reformulation

Complimentary activation up battery SOC constraints

$$\underline{\mu}^{\text{SOC}} \cdot \beta_t^\uparrow \leq w_t^{\text{up-soc}} \leq \bar{\mu}^{\text{SOC}} \cdot \beta_t^\uparrow \quad (\text{C-1})$$

$$\underline{\mu}^{\text{SOC}} \cdot (1 - \beta_t^\uparrow) \leq \mu_t^{\text{bat-state}} - w_t^{\text{up-soc}} \leq \bar{\mu}^{\text{SOC}} \cdot (1 - \beta_t^\uparrow) \quad (\text{C-2})$$

Complimentary activation up final battery SOC constraints

$$\underline{\mu}^{\text{SOC-final}} \cdot \beta_t^\uparrow \leq w_t^{\text{up-final}} \leq \bar{\mu}^{\text{SOC-final}} \cdot \beta_t^\uparrow \quad (\text{C-3})$$

$$\underline{\mu}^{\text{SOC-final}} \cdot (1 - \beta_t^\uparrow) \leq -w_t^{\text{up-final}} \leq \bar{\mu}^{\text{SOC-final}} \cdot (1 - \beta_t^\uparrow) \quad (\text{C-4})$$

Complimentary activation up electrolyzer constraints

$$\underline{\mu}^{\text{elz-prod}} \cdot \beta_t^\uparrow \leq w_t^{\text{up-elz}} \leq \bar{\mu}^{\text{elz-prod}} \cdot \beta_t^\uparrow \quad (\text{C-5})$$

$$\underline{\mu}^{\text{elz-prod}} \cdot (1 - \beta_t^\uparrow) \leq \mu_t^{\text{elz-prod}} - w_t^{\text{up-elz}} \leq \bar{\mu}^{\text{elz-prod}} \cdot (1 - \beta_t^\uparrow) \quad (\text{C-6})$$

Complimentary activation down battery SOC constraints

$$\underline{\mu}^{\text{SOC}} \cdot \beta_t^\downarrow \leq w_t^{\text{down-soc}} \leq \bar{\mu}^{\text{SOC}} \cdot \beta_t^\downarrow \quad (\text{C-7})$$

$$\underline{\mu}^{\text{SOC}} \cdot (1 - \beta_t^\downarrow) \leq \mu_t^{\text{bat-state}} - w_t^{\text{down-soc}} \leq \bar{\mu}^{\text{SOC}} \cdot (1 - \beta_t^\downarrow) \quad (\text{C-8})$$

Complimentary activation down final battery SOC constraints

$$\underline{\mu}^{\text{SOC-final}} \cdot \beta_t^\downarrow \leq w_t^{\text{down-final}} \leq \bar{\mu}^{\text{SOC-final}} \cdot \beta_t^\downarrow \quad (\text{C-9})$$

$$\underline{\mu}^{\text{SOC-final}} \cdot (1 - \beta_t^\downarrow) \leq -w_t^{\text{down-final}} \leq \bar{\mu}^{\text{SOC-final}} \cdot (1 - \beta_t^\downarrow) \quad (\text{C-10})$$

Complimentary activation down electrolyzer constraints

$$\underline{\mu}^{\text{elz-prod}} \cdot \beta_t^\downarrow \leq w_t^{\text{down-elz}} \leq \bar{\mu}^{\text{elz-prod}} \cdot \beta_t^\downarrow \quad (\text{C-11})$$

$$\underline{\mu}^{\text{elz-prod}} \cdot (1 - \beta_t^\downarrow) \leq \mu_t^{\text{elz-prod}} - w_t^{\text{down-elz}} \leq \bar{\mu}^{\text{elz-prod}} \cdot (1 - \beta_t^\downarrow) \quad (\text{C-12})$$

To assure running stability while running large sum of data partly unsupervised, a few extra steps were implemented to deal with the possibility of a MILP solution not converging in appropriate time. The algorithm is sketched here but is less complete for the other steps than algorithm 1. It checks if the subproblem is solving okay and if not check if the objective value is converging while not being optimal according to the MIP gap yet.

Algorithm 2 Iterative Algorithm with Timeout and Stabilization Checks

Step 1: Initialization

Set tolerance ε , bounds $UB \leftarrow \infty$, $LB \leftarrow -\infty$, iteration counter $k \leftarrow 0$, and other parameters (MAX_ITER, TIMEOUT, MAX_STABLE_ITER, STABILITY_THRESHOLD)

Initialize random uncertainty set and timeout_counter $\leftarrow 0$

while $\frac{|UB-LB|}{|UB|} > \varepsilon$ **and** $k < \text{MAX_ITER}$ **do Step 2: Solve Master Problem**

Define and solve master problem with updated uncertainty set, extracting fixed values $z_{\text{on_fixed}}$, $z_{\text{sb_fixed}}$, $a_{\text{frr_capacity_up_fixed}}$, $a_{\text{frr_capacity_down_fixed}}$, and energy_export_da

Update $UB \leftarrow$ objective value of master problem

Step 3: Solve Subproblem

Define bounds and solve subproblem to compute zS_{star}

subproblem times out but provides a solution Skip LB update, increment timed-out_counter, and continue to next step using the second stage uncertain values to create a new column.
no solution is found Increment timed-out_counter, but don't add a new column

Update $LB \leftarrow \max\{LB, \text{revenue_DA} - \text{start-up costs} + zS_{\text{star}}\}$

Reset timeout_counter

Step 4: Check Stabilization

Track zS_{star} in a rolling window of MAX_STABLE_ITER

if Changes in zS_{star} over the last MAX_STABLE_ITER steps $<$ STABILITY_THRESHOLD **then Terminate early and accept the current bounds.**

Step 5: Update Uncertainty and Iteration

Modify uncertainty set and update constraints for next iteration

Increment iteration counter k

Appendix D

Appendix: results

D-1 Observation wind data

The available wind-forecast was slightly biased, indicated some type of systematic forecasting error in the data gathered from ENTSO-E. The data was detrended using a linear regression model. The original wind error can be found in

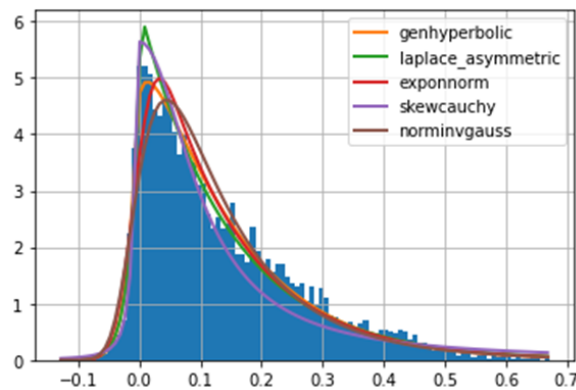


Figure D-1: Available Wind power error of $\hat{P}^{w,A} - P^{w,A}$, with different distributions plotted on it

In Figure D-2 and Figure D-3 example is given how both methods are adjusted to real incoming wind power data.

D-2 SP weekly case study results

First we use 7 days of data. Where we run each day approximately 20 times to capture the randomness induced by the methods. The first 7 days of November give a reasonable spread

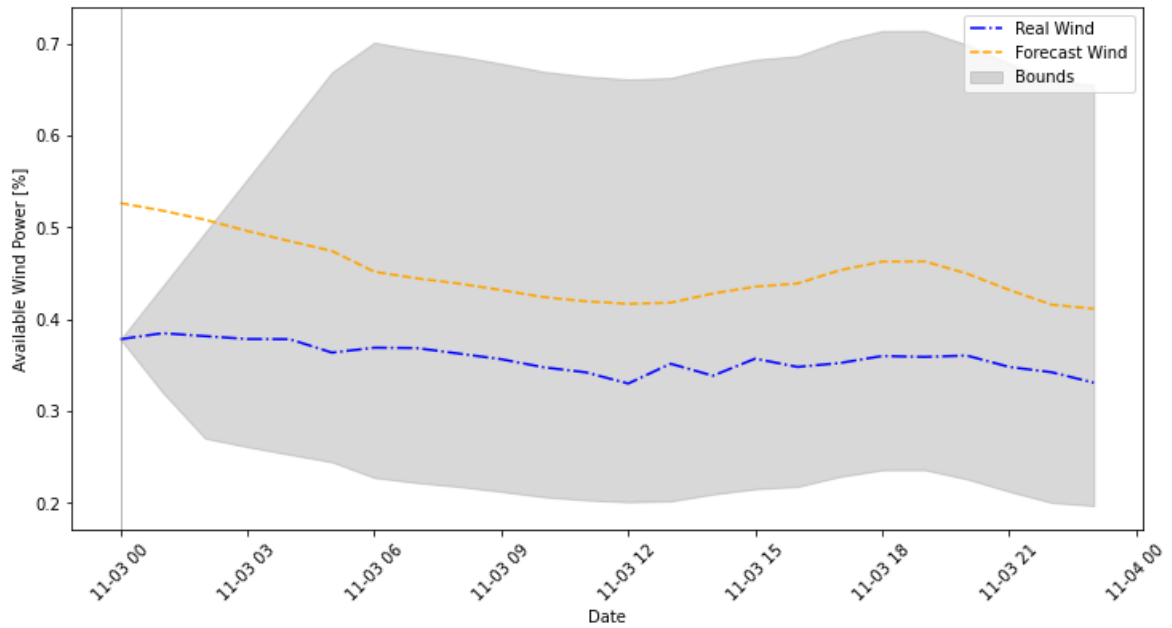


Figure D-2: Example of robust bounds adjusted to incoming wind power data

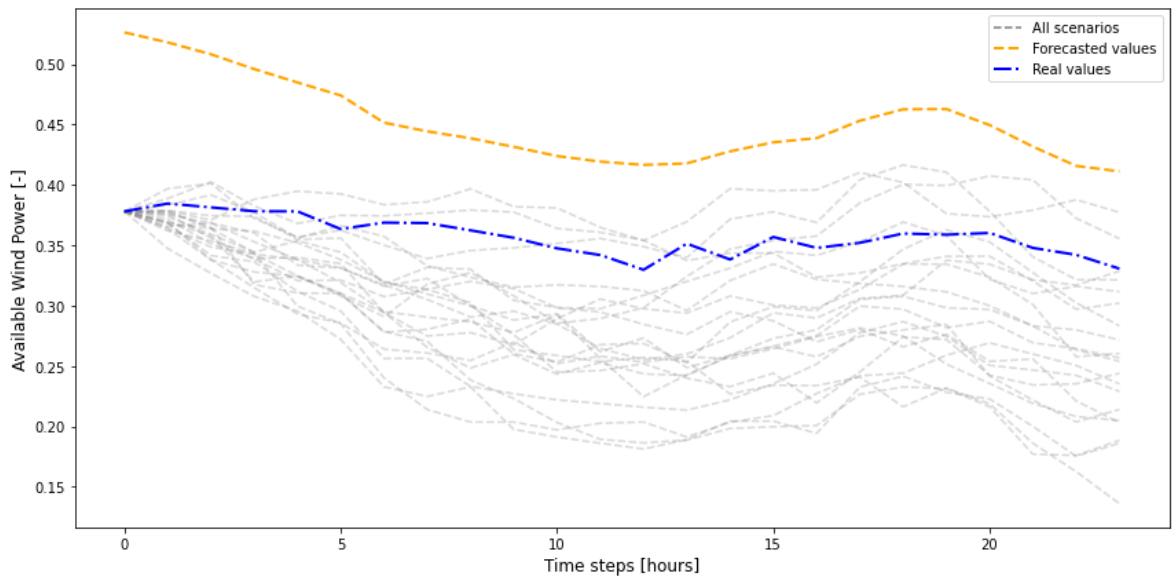


Figure D-3: Example of adjusted wind scenarios to incoming wind power data

of uncertainty with days where the forecast is optimistic which is tests for robustness of the model.

D-2-1 SP week results: DA prices

Base Forecasted Price

Table D-1: Performance metrics for the scenario *Base Forecasted Price* (Revenue and Violations).

Date	FSR Mean	FSR Std	SSR Mean	SSR Std	Total Revenue Mean	Total Revenue Std	Violations Mean	Violations Std
1-11-2023	19,493.58	1,022.67	22,491.92	2,908.74	41,985.50	2,001.56	0	0
2-11-2023	30,880.59	263.47	-2,052.79	1,240.51	28,827.80	994.09	0	0
3-11-2023	16,196.00	524.04	3,370.03	599.24	19,566.03	200.05	-	-
4-11-2023	26,707.44	165.82	4,971.98	791.83	31,679.42	645.54	-	-
5-11-2023	21,346.53	1,060.90	15,231.81	3,584.61	36,578.34	3,186.84	-	-
6-11-2023	26,832.05	285.83	7,981.89	301.66	34,813.94	114.37	-	-
7-11-2023	11,729.39	647.99	9,747.47	246.01	21,476.86	453.09	-	-
Total	153,185.57	1,553.09	61,742.31	4,469.72	214,927.88	3,688.96	-	-

Table D-2: Additional metrics for the scenario *Base Forecasted Price* (Activation managed and not managed).

Date	Total AM	Total AM Std	Total ANM	Total ANM Std
1-11-2023	0	0	0	0
2-11-2023	0	0	0	0
3-11-2023	0	0	0	0
4-11-2023	7.43	2.14	0	0
5-11-2023	1.00	0	0	0
6-11-2023	1.00	0	0	0
7-11-2023	1.00	0	0	0
Total	9.43	2.14	0	0

Perfect Price Info

Table D-3: Performance metrics for the scenario *Perfect Price Info* (Revenue and Violations).

Date	FSR Mean	FSR Std	SSR Mean	SSR Std	Total Revenue Mean	Total Revenue Std	Violations Mean	Violations Std
1-11-2023	19,737.64	597.01	22,462.95	2,441.47	42,200.59	2,767.65	-	-
2-11-2023	30,868.07	509.28	-1,874.97	3,847.27	28,993.10	3,353.23	-	-
3-11-2023	16,105.57	446.16	3,692.70	495.97	19,798.27	139.12	-	-
4-11-2023	27,509.90	184.95	6,690.20	274.45	34,200.10	105.69	0.05	0.22
5-11-2023	23,483.86	579.71	11,974.21	1,552.84	35,458.07	1,277.80	-	-
6-11-2023	26,882.37	391.53	8,118.57	373.91	35,000.93	153.81	-	-
7-11-2023	11,771.68	1,123.91	9,712.02	428.45	21,483.70	716.26	-	-
Total	156,359.09	1,613.29	60,775.67	4,505.94	217,134.76	4,300.65	0.05	0.22

Table D-4: Additional metrics for the scenario *Perfect Price Info* (Activation managed and not managed and Computation Time).

Date	Total AM	Total AM Std	Total ANM	Total ANM Std	Comp Time Mean	Comp Time Std
1-11-2023	0.45	2.01	-	-	486.41	15.21
2-11-2023	-	-	-	-	483.75	14.63
3-11-2023	-	-	-	-	490.22	6.68
4-11-2023	8.95	0.22	0.05	0.22	480.10	6.48
5-11-2023	0.40	1.79	-	-	482.12	6.12
6-11-2023	1.00	-	-	-	477.43	5.34
7-11-2023	1.00	-	-	-	587.32	65.90
Total	11.80	2.65	0.05	0.22	3,487.35	71.51

Price Scenario

Table D-5: Performance metrics for the scenario *Price Scenario* (Revenue and Violations).

Date	FSR Mean	FSR Std	SSR Mean	SSR Std	Total Revenue Mean	Total Revenue Std	Violations Mean	Violations Std
1-11-2023	19,931.70	416.31	20,777.75	2,552.29	40,709.45	2,487.44	-	-
2-11-2023	30,735.83	496.62	-1,255.50	2,725.46	29,480.33	2,258.19	-	-
3-11-2023	15,878.48	202.08	3,705.27	268.71	19,583.74	138.54	-	-
4-11-2023	26,755.01	161.22	4,968.57	698.51	31,723.58	554.11	-	-
5-11-2023	23,242.05	981.77	13,929.43	4,370.01	37,171.48	3,409.35	-	-
6-11-2023	26,855.81	374.83	7,935.29	310.64	34,791.09	168.73	-	-
7-11-2023	11,856.44	556.08	9,577.10	239.43	21,433.54	440.38	-	-
Total	155,255.32	1,109.43	59,637.90	5,736.24	214,893.22	5,019.19	-	-

Table D-6: Additional metrics for the scenario *Price Scenario* (Activation managed and not managed and Computation Time).

Date	Total AM	Total AM Std	Total ANM	Total ANM Std	Comp Time Mean	Comp Time Std
1-11-2023	-	-	-	-	299.04	138.06
2-11-2023	-	-	-	-	310.97	200.14
3-11-2023	-	-	-	-	313.72	199.41
4-11-2023	-	-	-	-	304.76	182.23
5-11-2023	1.85	3.51	-	-	258.39	9.83
6-11-2023	1.00	-	-	-	254.21	8.01
7-11-2023	1.00	-	-	-	445.42	72.94
Total	3.85	3.51	-	-	2,186.50	710.02

D-2-2 SP week results: wind scenarios

SP Low Wind

Table D-7: Performance metrics for the scenario *SP Low Wind* (Revenue and Violations).

Date	FSR Mean	FSR Std	SSR Mean	SSR Std	Total Revenue Mean	Total Revenue Std	Violations Mean	Violations Std
1-11-2023	20,706.14	766.38	18,346.51	1,989.14	39,052.65	1,334.28	-	-
2-11-2023	31,393.74	185.58	-4,328.68	644.84	27,065.06	483.17	-	-
3-11-2023	16,903.24	247.91	2,776.70	393.60	19,679.94	154.28	-	-
4-11-2023	26,925.83	137.79	3,944.92	465.59	30,870.76	334.79	-	-
5-11-2023	21,265.58	1,052.20	21,889.65	2,491.02	43,155.23	2,009.76	-	-
6-11-2023	27,369.01	279.28	7,482.74	337.02	34,851.75	130.68	-	-
7-11-2023	13,022.94	242.22	9,305.03	145.10	22,327.97	106.72	-	-
Total	157,586.48	445.28	59,416.89	2,509.89	217,003.36	2,699.21	-	-

Table D-8: Additional metrics for the scenario *SP Low Wind* (Activation managed and not managed and Computation Time).

Date	Total AM	Total AM Std	Total ANM	Total ANM Std	Comp Time Mean	Comp Time Std
1-11-2023	-	-	-	-	255.10	2.31
2-11-2023	-	-	-	-	256.46	0.48
3-11-2023	-	-	-	-	260.67	2.92
4-11-2023	-	-	-	-	255.61	0.97
5-11-2023	8.00	-	-	-	258.93	8.69
6-11-2023	1.00	-	-	-	253.66	0.91
7-11-2023	1.00	-	-	-	326.64	26.55
Total	10.00	-	-	-	1,867.07	26.98

Dataset Analysis

Table D-9: Performance metrics for high wind scenario (Revenue and Violations).

Date	FSR Mean	FSR Std	SSR Mean	SSR Std	Total Revenue Mean	Total Revenue Std	Violations Mean	Violations Std
1-11-2023	19,276.04	791.99	933.88	3,517.79	20,209.92	2,894.81	0	0
2-11-2023	30,009.89	700.86	-40,639.63	3,828.68	-10,629.74	3,417.83	0	0
3-11-2023	15,324.24	224.63	746.29	537.73	16,070.53	520.11	0	0
4-11-2023	26,622.24	147.45	6,439.72	1,150.58	33,061.96	1,054.58	0	0
5-11-2023	22,086.97	1,305.86	14,919.73	5,181.30	37,006.70	5,748.16	0	0
6-11-2023	26,138.95	1,389.47	5,684.82	1,054.37	31,823.77	934.95	0	0
7-11-2023	11,391.23	566.34	7,408.87	515.13	18,800.11	833.69	0	0
Total	150,849.55	2,187.05	-4,506.31	7,276.29	146,343.25	7,489.00	-	-

Table D-10: Additional metrics for the high wind scenario (Activation managed and not managed).

Date	Total AM	Total AM Std	Total ANM	Total ANM Std
1-11-2023	0	0	0	0
2-11-2023	0	0	0	0
3-11-2023	0	0	0	0
4-11-2023	4.67	4.12	0	0
5-11-2023	1	0	0	0
6-11-2023	1	0	0	0
7-11-2023	1	0	0	0
Total	6.67	4.12	0	0

D-2-3 SP week results: random draws

5-act scen Random (8 draws)

Table D-11: Performance metrics for the scenario *5-act Random Medium (8 draws)* (Revenue and Violations).

Date	FSR Mean	FSR Std	SSR Mean	SSR Std	Total Revenue Mean	Total Revenue Std	Violations Mean	Violations Std
1-11-2023	24,131.80	842.01	30,226.37	9,524.21	54,358.18	9,501.44	4.94	2.67
2-11-2023	32,434.97	808.99	21,972.61	5,765.49	54,407.57	5,477.22	3.67	1.71
3-11-2023	16,949.68	770.75	10,051.57	1,146.47	27,001.25	607.78	3.61	0.85
4-11-2023	28,564.06	859.63	17,549.63	3,520.63	46,113.69	3,255.19	7.44	1.54
5-11-2023	27,097.73	596.97	24,294.39	6,270.77	51,392.11	5,938.43	6.11	1.68
6-11-2023	28,361.02	886.44	10,972.71	1,018.97	39,333.73	1,022.86	3.11	1.02
7-11-2023	12,705.95	676.61	9,771.91	678.21	22,477.86	454.31	0.11	0.32
Total	170,245.21	2,023.33	124,839.19	14,497.54	295,084.40	14,006.80	29.00	2.33

Table D-12: Additional metrics for the scenario *5-act Random Medium (8 draws)* (Activation managed and not managed).

Date	Total AM	Total AM Std	Total ANM	Total ANM Std
1-11-2023	6.11	1.32	2.89	1.32
2-11-2023	3.56	0.92	1.44	0.92
3-11-2023	2.28	0.46	1.72	0.46
4-11-2023	4.83	0.92	4.17	0.92
5-11-2023	4.06	1.11	3.94	1.11
6-11-2023	4.44	0.86	1.56	0.86
7-11-2023	5.06	1.89	0.11	0.32
Total	30.33	3.01	15.83	1.65

5 Random Act (15 draws)

Table D-13: Performance metrics for the scenario *5 Random Act (15 draws)* (Revenue and Violations).

Date	FSR Mean	FSR Std	SSR Mean	SSR Std	Total Revenue Mean	Total Revenue Std	Violations Mean	Violations Std
1-11-2023	24,061.25	1,147.55	19,179.02	5,608.27	43,240.27	5,360.39	1.90	2.23
2-11-2023	32,130.38	659.47	9,450.40	3,259.20	41,580.77	3,447.48	1.10	1.91
3-11-2023	17,287.60	658.49	7,351.75	1,138.59	24,639.35	596.53	2.20	0.92
4-11-2023	28,495.13	739.63	12,306.49	2,322.16	40,801.63	1,601.37	5.50	0.97
5-11-2023	26,563.59	700.42	18,512.62	5,213.08	45,076.20	5,100.79	4.40	2.32
6-11-2023	28,129.02	505.41	8,234.08	433.64	36,363.10	634.31	0.20	0.42
7-11-2023	13,417.03	1,087.13	8,933.96	622.03	22,350.98	508.30	-	-
Total	170,083.99	1,667.52	83,968.32	11,607.74	254,052.31	10,985.52	15.30	4.35

Table D-14: Additional metrics for the scenario *5 Random Act (15 draws)* (Activation managed and not managed and Computation Time).

Date	Total AM	Total AM Std	Total ANM	Total ANM Std	Comp Time Mean	Comp Time Std
1-11-2023	5.90	3.31	1.30	1.34	735.60	15.36
2-11-2023	4.30	1.06	0.70	1.06	747.04	6.91
3-11-2023	2.60	0.52	1.40	0.52	879.29	81.70
4-11-2023	5.90	0.88	3.10	0.88	743.74	7.61
5-11-2023	4.50	1.90	2.70	1.42	744.73	13.06
6-11-2023	5.40	1.58	0.10	0.32	731.44	7.93
7-11-2023	1.00	-	-	-	750.91	10.41
Total	29.60	5.19	9.30	1.95	5,332.76	79.22

SP: 10 Random Act High

Data for scenario programming using 10 different scenarios with 15 random draws for up and down combined.

Table D-15: Performance metrics for the scenario *10 Random Act High*.

Date	FSR (Mean)	FSR (Std)	SSR (Mean)	SSR (Std)	Total Revenue (Mean)	Total Revenue (Std)
1-11-2023	22,998.24	1,222.03	15,146.28	3,105.83	38,144.53	2,680.50
2-11-2023	32,047.60	455.28	8,196.46	630.06	40,244.06	230.43
3-11-2023	16,526.59	472.41	6,208.85	802.82	22,735.45	672.62
4-11-2023	28,439.19	463.58	11,249.89	2,235.92	39,689.08	2,285.74
5-11-2023	25,979.08	822.96	12,074.54	4,570.36	38,053.62	3,826.10
6-11-2023	27,991.50	607.85	8,333.99	502.47	36,325.48	356.10
7-11-2023	13,274.12	934.57	8,854.05	609.20	22,128.17	422.03
Total	167,256.32	1,900.36	70,064.06	6,038.09	237,320.38	4,860.32

Table D-16: Additional metrics for the scenario *10 Random Act High*.

Date	Violations (Mean)	Violations (Std)	Total AM	Total AM (Std)	Total ANM	Total ANM (Std)	Comp Time (Mean)	Comp Time (Std)
1-11-2023	0.63	0.74	5.00	4.17	0.63	0.74	1,398.12	125.34
2-11-2023	0.50	0.53	4.50	0.53	0.50	0.53	1,412.41	20.11
3-11-2023	-	-	4.00	-	-	-	1,694.86	282.31
4-11-2023	3.63	0.92	6.63	0.52	2.38	0.52	1,394.41	13.30
5-11-2023	0.75	0.89	6.25	2.66	0.75	0.89	1,379.64	14.19
6-11-2023	-	-	6.00	-	-	-	1,367.02	13.32
7-11-2023	-	-	1.00	-	-	-	1,452.76	54.53
Total	5.50	0.93	33.38	4.81	4.25	1.04	10,099.22	397.24

SP: no PI

Scenario programming for week 2023-11-01 till 2023-11-07. With no PI first the base cases:

Table D-17: Performance metrics for the scenario *No PI base* (Revenue and Violations).

Date	FSR Mean	FSR Std	SSR Mean	SSR Std	Total Revenue Mean	Total Revenue Std	Violations Mean	Violations Std
1-11-2023	19,989.00	339.55	4,026.94	297.25	24,015.93	54.54	1.10	0.57
2-11-2023	31,110.35	299.05	2,234.79	41.23	33,345.14	260.70	8.00	2.49
3-11-2023	15,994.82	433.79	2,183.33	134.31	18,178.15	316.80	3.60	3.53
4-11-2023	27,478.81	144.90	5,705.40	204.90	33,184.21	70.31	-	-
5-11-2023	23,673.85	268.77	3,593.73	142.55	27,267.58	132.26	1.70	1.16
6-11-2023	26,843.69	385.88	6,400.71	80.56	33,244.40	317.96	0.40	0.52
7-11-2023	11,771.57	818.92	7,592.04	310.31	19,363.62	539.56	-	-
Total	156,862.09	892.71	31,736.94	474.44	188,599.03	740.65	14.80	5.41

Table D-18: Additional metrics for the scenario *No PI - 510 Runs* (Activation managed and not managed).

Date	Total AM	Total AM Std	Total ANM	Total ANM Std
1-11-2023	-	-	-	-
2-11-2023	-	-	-	-
3-11-2023	-	-	-	-
4-11-2023	9.00	-	-	-
5-11-2023	-	-	-	-
6-11-2023	1.00	-	-	-
7-11-2023	1.00	-	-	-
Total	11.00	-	-	-

Table D-19: Comparison of Models and Budgets

Model	Γ^W (Wind Budget)	$\Gamma^{A,\uparrow}$ (Activation Up)	$\Gamma^{A,\downarrow}$ (Activation Down)
Base	24	15	8
MA (Medium Activation)	24	8	4
MW (Mid Wind)	12	15	8
LA (Low Activation)	24	3	2

Table D-20: Comparison of RO models with key metrics.

Model	Total FSR	FSR Std	Total SSR	SSR Std	Total Revenue	Revenue Std	Violations	Violations Std
RO - base	126,299.97	4,243.02	111,566.18	16,923.83	237,866.15	12,931.24	2.50	0.52
RO - MA	126,113.57	6,262.85	121,257.13	20,501.33	247,370.70	14,298.14	3.00	1.41
RO - LA	134,315.84	1,033.96	154,996.57	3,231.92	289,312.42	2,197.96	16.50	6.36
RO - MW	126,283.08	5,795.52	106,831.63	18,352.23	233,114.71	12,559.23	2.33	0.58
RO (No Plmb) - base	129,748.05	2,938.44	81,175.09	8,120.40	210,923.15	5,397.12	2.17	0.41
RO (No Plmb) - MA	126,377.59	1,516.89	103,354.99	6,061.77	229,732.58	4,602.24	3.50	0.71
RO (No Plmb) - LA	136,137.44	926.95	130,054.32	3,823.81	266,191.75	2,938.96	24.50	3.57
RO (No Plmb) - MW	128,350.21	5,176.22	92,976.81	18,615.36	221,327.02	13,546.52	2.70	1.06

NO pi 10 random draws

Table D-21: Performance metrics for the scenario *NO pi 10 random scenarios 15 draws* (Revenue and Violations).

Date	FSR Mean	FSR Std	SSR Mean	SSR Std	Total Revenue Mean	Total Revenue Std	Violations Mean	Violations Std
1-11-2023	21,828.97	663.58	8,482.57	6,146.62	30,311.54	6,437.68	1.00	0.82
2-11-2023	31,865.21	361.00	7,168.52	103.72	39,033.73	376.38	7.75	2.36
3-11-2023	16,852.45	417.59	4,644.70	588.71	21,497.16	735.71	0.50	0.58
4-11-2023	28,106.92	144.23	8,470.30	3,512.32	36,577.22	3,603.16	4.75	1.50
5-11-2023	26,503.85	433.08	11,233.76	7,181.07	37,737.61	7,492.42	2.50	1.29
6-11-2023	27,891.05	496.62	6,638.24	617.05	34,529.30	972.15	-	-
7-11-2023	12,476.08	742.25	7,347.19	240.92	19,823.26	552.10	-	-
Total	165,524.53	1,960.88	53,985.29	10,225.22	219,509.81	10,689.44	16.50	4.12

Table D-22: Additional metrics for the scenario *NO pi 10random* (Activation managed and not managed).

Date	Total AM	Total AM Std	Total ANM	Total ANM Std
1-11-2023	4.25	4.92	0.25	0.50
2-11-2023	2.50	0.58	2.50	0.58
3-11-2023	4.00	-	-	-
4-11-2023	6.00	0.82	3.00	0.82
5-11-2023	5.00	3.46	1.00	1.15
6-11-2023	3.50	2.89	-	-
7-11-2023	1.00	-	-	-
Total	26.25	2.50	6.75	1.26

D-3 Robust optimization weekly results

D-3-1 Different budgets with passive imbalance option

Table D-23: First-stage and second-stage revenue metrics for Robust Optimization (HWA).

Date	FSR Mean	FSR Std	SSR Mean	SSR Std	Total Revenue Mean	Total Revenue Std
1-11-2023	16,742.28	627.76	28,844.55	4,030.70	45,586.84	3,402.94
2-11-2023	26,015.83	0.00	15,735.12	0.00	41,750.95	0.00
3-11-2023	5,537.59	252.63	17,071.25	574.09	22,608.83	351.08
4-11-2023	15,760.51	50.43	43,666.69	160.30	59,427.20	203.00
5-11-2023	18,865.13	696.86	24,129.57	3,099.93	42,994.69	2,452.44
6-11-2023	21,225.50	0.00	9,748.68	0.00	30,974.18	0.00
7-11-2023	7,142.26	0.81	11,481.54	9.56	18,623.80	8.75
Total	111,289.09	1,012.01	150,677.40	4,980.26	261,966.49	3,993.30

Table D-24: Additional metrics for Robust Optimization (HWA).

Date	Violations Mean	Violations Std	Total A_M	Total A_M Std	Total A_NM	Total A_NM Std	Comp Time Mean
1-11-2023	-	-	1.80	3.79	-	-	34.02
5.45							
2-11-2023	-	-	-	-	-	-	32.91
8.73							
3-11-2023	-	-	4.00	-	-	-	99.09
62.48							
4-11-2023	-	-	9.00	-	-	-	157.23
62.93							
5-11-2023	-	-	4.00	4.22	-	-	37.45
6.62							
6-11-2023	-	-	1.00	-	-	-	30.05
3.65							
7-11-2023	-	-	1.00	-	-	-	31.12
4.12							
Total	-	-	20.80	5.67	-	-	421.86
89.91							

Table D-25: First-stage and second-stage revenue metrics for Robust Optimization (MAHW).

Date	FSR Mean	FSR Std	SSR Mean	SSR Std	Total Revenue Mean	Total Revenue Std
1-11-2023	17,110.00	1.89	26,926.35	19.29	44,036.35	17.41
2-11-2023	26,015.83	0.00	15,944.24	71.52	41,960.07	71.52
3-11-2023	5,333.42	146.24	18,020.10	530.34	23,353.53	517.58
4-11-2023	16,226.05	409.20	41,709.16	1,682.17	57,935.21	1,280.91
5-11-2023	21,356.82	541.19	20,233.46	1,539.19	41,590.28	1,020.31
6-11-2023	22,312.65	536.16	9,831.96	658.42	32,144.60	122.99
7-11-2023	7,146.83	0.00	11,462.15	0.00	18,608.97	0.00
Total	115,501.59	890.94	144,127.42	2,405.21	259,629.02	1,684.82

Table D-26: Additional metrics for Robust Optimization (MAHW).

Date	Violations Mean	Violations Std	Total A_M	Total A_M Std	Total A_NM	Total A_NM Std	Comp Time Mean	Comp Time Std
1-11-2023	-	-	-	-	-	-	46.93	12.54
2-11-2023	-	-	-	-	-	-	35.60	8.67
3-11-2023	-	-	4.00	-	-	-	211.35	194.25
4-11-2023	-	-	9.00	-	-	-	62.20	15.09
5-11-2023	-	-	1.60	3.28	-	-	58.04	14.90
6-11-2023	-	-	1.60	1.47	-	-	43.31	17.12
7-11-2023	-	-	1.00	-	-	-	36.42	11.62
Total	-	-	17.20	3.78	-	-	493.85	208.42

Table D-27: First-stage and second-stage revenue metrics for Robust Optimization (LAHW).

Date	FSR Mean	FSR Std	SSR Mean	SSR Std	Total Revenue Mean	Total Revenue Std
1-11-2023	18,230.83	503.67	31,750.59	3,806.81	49,981.42	3,459.37
2-11-2023	24,531.59	420.99	16,969.56	2,730.79	41,501.14	2,635.64
3-11-2023	6,653.86	296.96	18,513.41	894.11	25,167.27	703.11
4-11-2023	16,588.58	23.51	40,256.39	66.59	56,844.97	51.97
5-11-2023	22,356.37	1,599.07	25,974.44	8,136.08	48,330.81	6,563.23
6-11-2023	22,154.65	366.01	10,523.39	818.10	32,678.04	455.90
7-11-2023	7,013.62	256.72	11,832.31	258.58	18,845.93	352.00
Total	117,529.49	1,556.45	155,820.09	10,436.77	273,349.58	8,928.12

Table D-28: Additional metrics for Robust Optimization (LAHW).

Date	Violations Mean	Violations Std	Total A_M	Total A_M Std	Total A_NM	Total A_NM Std	Comp Time Mean	Comp Time Std
1-11-2023	-	-	8.10	2.85	-	-	37.65	13.39
2-11-2023	-	-	5.00	-	-	-	40.88	10.68
3-11-2023	-	-	4.00	-	-	-	50.80	14.70
4-11-2023	-	-	9.00	-	-	-	34.94	9.43
5-11-2023	-	-	5.60	3.86	-	-	42.77	11.49
6-11-2023	-	-	3.80	1.93	-	-	41.91	12.07
7-11-2023	-	-	5.00	-	-	-	41.52	12.63
Total	-	-	40.50	5.40	-	-	290.47	53.22

Table D-29: First-stage and second-stage revenue metrics for Robust Optimization (MWMW).

Date	FSR Mean	FSR Std	SSR Mean	SSR Std	Total Revenue Mean	Total Revenue Std
1-11-2023	17,286.83	542.26	21,787.83	6,100.18	39,074.67	5,702.46
2-11-2023	25,308.24	710.67	14,869.62	2,691.16	40,177.85	3,035.24
3-11-2023	6,104.82	286.77	17,391.26	467.49	23,496.08	226.01
4-11-2023	16,640.83	491.24	40,655.48	1,912.53	57,296.31	1,456.44
5-11-2023	19,733.88	2,240.91	23,102.56	12,890.11	42,836.44	10,724.38
6-11-2023	22,841.79	115.50	9,622.54	170.93	32,464.34	157.04
7-11-2023	7,169.86	282.68	11,123.77	653.64	18,293.63	622.48
Total	115,086.20	2,656.20	138,553.10	15,929.10	253,639.30	13,599.40

Table D-30: Additional metrics for Robust Optimization (MWMW).

Date	Violations Mean	Violations Std	Total A_M	Total A_M Std	Total A_NM	Total A_NM Std	Comp Time Mean	Comp Time Std
1-11-2023	-	-	0.90	2.85	-	-	71.07	47.33
2-11-2023	-	-	3.00	2.58	-	-	312.31	251.02
3-11-2023	-	-	4.00	-	-	-	154.14	31.00
4-11-2023	-	-	9.00	-	-	-	146.63	40.61
5-11-2023	-	-	8.00	-	-	-	614.73	346.74
6-11-2023	-	-	1.00	-	-	-	117.92	78.17
7-11-2023	-	-	1.40	1.26	-	-	100.52	32.96
Total	-	-	27.30	4.60	-	-	1,517.32	385.94

Table D-31: First-stage and second-stage revenue metrics for Robust Optimization (LWLA).

Date	FSR Mean	FSR Std	SSR Mean	SSR Std	Total Revenue Mean	Total Revenue Std
1-11-2023	17,364.80	3,490.94	39,876.19	22,318.90	57,240.98	19,056.21
2-11-2023	25,306.00	315.32	13,565.99	1,403.77	38,871.99	1,682.90
3-11-2023	8,857.39	697.44	16,276.52	982.38	25,133.91	841.65
4-11-2023	17,774.85	73.01	38,323.02	483.13	56,097.87	466.91
5-11-2023	22,464.25	596.26	23,104.68	4,245.81	45,568.93	3,686.48
6-11-2023	22,424.67	338.18	10,810.66	496.59	33,235.33	256.76
7-11-2023	7,651.55	296.74	11,502.34	797.07	19,153.89	505.06
Total	121,843.49	3,297.97	153,459.40	24,136.68	275,302.90	21,037.75

Table D-32: Additional metrics for Robust Optimization (LWLA).

Date	Violations Mean	Violations Std	Total A_M	Total A_M Std	Total A_NM	Total A_NM Std	Comp Time Mean	Comp Time Std
1-11-2023	-	-	7.20	4.02	-	-	149.71	136.21
2-11-2023	-	-	5.00	-	-	-	58.43	27.66
3-11-2023	-	-	4.00	-	-	-	50.41	6.12
4-11-2023	-	-	9.00	-	-	-	43.64	5.34
5-11-2023	-	-	8.00	-	-	-	56.48	14.47
6-11-2023	-	-	5.00	-	-	-	90.60	33.74
7-11-2023	-	-	5.00	-	-	-	310.15	354.05
Total	-	-	43.20	4.02	-	-	759.42	394.37

D-3-2 Different budgets No passive imbalance

Table D-33: First-stage and second-stage revenue metrics for NO PI (RO Base).

Date	FSR Mean	FSR Std	SSR Mean	SSR Std	Total Revenue Mean	Total Revenue Std
1-11-2023	16,370.06	759.95	7,705.19	4,298.71	24,075.26	3,538.77
2-11-2023	26,015.83	7.08E-12	3,026.78	1.70E-12	29,042.61	8.71E-12
3-11-2023	5,572.35	206.81	14,702.89	202.18	20,275.23	7.13
4-11-2023	15,733.32	41.82	32,782.64	123.99	48,515.96	154.62
5-11-2023	19,258.65	552.90	5,458.73	2,565.61	24,717.38	2,015.40
6-11-2023	21,225.50	4.55E-05	6,070.17	49.88	27,295.67	49.88
7-11-2023	7,142.41	1.07	6,898.38	23.88	14,040.79	23.93
Total	111,318.12	856.13	76,644.78	4,613.68	187,962.90	3,789.99

Table D-34: Additional metrics for NO PI (RO Base).

Date	Violations Mean	Violations Std	Total A_M	Total A_M Std	Total A_NM	Total A_NM Std
1-11-2023	-	-	4.05	4.59	0	0
2-11-2023	-	-	0	0	0	0
3-11-2023	-	-	4.00	0.00	0	0
4-11-2023	-	-	9.00	0.00	0	0
5-11-2023	-	-	1.60	3.28	0	0
6-11-2023	-	-	1.00	0.00	0	0
7-11-2023	1.00	-	1.00	0.00	0	0
Total	1.00	-	20.65	5.08	0	0

Table D-35: First-stage and second-stage revenue metrics for NO PI (RO MAHW).

Date	FSR Mean	FSR Std	SSR Mean	SSR Std	Total Revenue Mean	Total Revenue Std
1-11-2023	17,110.00	1.89	3,824.40	34.72	20,934.39	33.76
2-11-2023	26,015.83	1.53E-11	3,026.78	3.83E-12	29,042.61	1.68E-11
3-11-2023	5,292.31	33.21	15,254.12	81.39	20,546.42	81.16
4-11-2023	16,251.86	368.57	30,541.60	1,701.69	46,793.46	1,335.92
5-11-2023	21,074.02	687.86	6,047.12	3,071.78	27,121.14	2,385.05
6-11-2023	22,386.55	448.10	6,075.29	825.46	28,461.84	377.39
7-11-2023	7,146.83	0.00	6,899.69	22.87	14,046.51	22.87
Total	115,277.39	875.14	71,668.99	3,436.76	186,946.37	2,600.20

Table D-36: Additional metrics for NO PI (RO MAHW).

Date	Violations Mean	Violations Std	Total A_M	Total A_M Std	Total A_NM	Total A_NM Std
1-11-2023	-	-	0	0	0	0
2-11-2023	-	-	0	0	0	0
3-11-2023	-	-	4.00	0.00	0	0
4-11-2023	-	-	9.00	0.00	0	0
5-11-2023	-	-	3.20	4.02	0	0
6-11-2023	-	-	1.40	1.23	0	0
7-11-2023	0.95	0.22	1.00	0.00	0	0
Total	0.95	0.22	18.60	4.28	0	0

Table D-37: First-stage and second-stage revenue metrics for NO PI (LAHW).

Date	FSR Mean	FSR Std	SSR Mean	SSR Std	Total Revenue Mean	Total Revenue Std
1-11-2023	18,283.16	516.65	12,890.06	7,693.20	31,173.23	7,472.33
2-11-2023	24,457.43	525.00	19,166.58	5,255.67	43,624.02	4,738.51
3-11-2023	6,647.01	338.99	15,646.23	392.10	22,293.24	144.36
4-11-2023	16,585.13	22.34	29,256.28	38.23	45,841.41	32.28
5-11-2023	21,636.82	2,329.01	12,468.94	10,767.39	34,105.76	8,441.92
6-11-2023	21,815.46	429.33	8,758.31	1,420.36	30,573.77	996.06
7-11-2023	7,139.22	223.16	9,791.51	598.05	16,930.73	459.49
Total	116,564.23	2,771.94	107,977.93	16,993.44	224,542.16	14,602.61

Table D-38: Additional metrics for NO PI (LAHW).

Date	Violations Mean	Violations Std	Total A_M	Total A_M Std	Total A_NM	Total A_NM Std
1-11-2023	-	-	6.75	3.99	0	0
2-11-2023	1.80	1.01	4.15	1.08	0.60	0.50
3-11-2023	-	-	4.00	0.00	0	0
4-11-2023	-	-	9.00	0.00	0	0
5-11-2023	-	-	5.60	3.76	0	0
6-11-2023	-	-	4.80	0.89	0	0
7-11-2023	0.05	0.22	5.00	0.00	0	0
Total	1.85	1.04	39.30	5.86	0.60	0.50

Table D-39: Additional metrics for NO PI (RO LWLA).

Date	Violations Mean	Violations Std	Total A_M	Total A_M Std	Total A_NM	Total A_NM Std
1-11-2023	0.95	1.19	8.60	0.75	0.40	0.75
2-11-2023	5.15	1.57	4.10	0.64	0.90	0.64
3-11-2023	5.80	1.74	2.90	0.45	1.10	0.45
4-11-2023	2.45	0.94	8.45	0.51	0.55	0.51
5-11-2023	1.70	0.66	7.40	0.50	0.60	0.50
6-11-2023	0.90	0.79	4.55	0.60	0.45	0.60
7-11-2023	2.00	1.95	4.40	0.60	0.60	0.60
Total	18.95	3.55	40.40	1.39	4.60	1.39

Table D-40: Additional metrics for NO PI (RO MWMW).

Date	Violations Mean	Violations Std	Total A_M	Total A_M Std	Total A_NM	Total A_NM Std
1-11-2023	-	-	-	-	-	-
2-11-2023	0.07	0.26	2.00	2.54	-	-
3-11-2023	0.07	0.26	3.93	0.26	0.07	0.26
4-11-2023	-	-	9.00	-	-	-
5-11-2023	0.13	0.35	7.47	2.07	-	-
6-11-2023	-	-	1.00	-	-	-
7-11-2023	0.13	0.35	1.53	1.41	-	-
Total	0.40	0.63	24.93	4.06	0.07	0.26

Table D-41: First-stage and second-stage revenue metrics for NO PI (RO LWLA).

Date	FSR Mean	FSR Std	SSR Mean	SSR Std	Total Revenue Mean	Total Revenue Std
1-11-2023	18,702.07	606.86	18,522.82	5,339.25	37,224.89	5,287.69
2-11-2023	24,008.74	546.63	22,526.45	3,696.01	46,535.18	3,231.19
3-11-2023	9,588.63	520.46	13,093.81	548.15	22,682.45	452.69
4-11-2023	18,479.50	647.92	27,696.14	1,690.07	46,175.65	1,092.31
5-11-2023	21,538.50	798.26	19,074.80	3,921.28	40,613.31	3,147.43
6-11-2023	21,437.18	400.13	10,866.24	821.73	32,303.42	511.72
7-11-2023	7,397.17	404.69	10,025.26	556.17	17,422.43	281.20
Total	121,151.79	1,623.47	121,805.53	9,423.90	242,957.33	8,283.21

Table D-42: Additional metrics for NO PI (RO LWLA).

Date	Violations Mean	Violations Std	Total A_M	Total A_M Std	Total A_NM	Total A_NM Std
1-11-2023	0.95	1.19	8.60	0.75	0.40	0.75
2-11-2023	5.15	1.57	4.10	0.64	0.90	0.64
3-11-2023	5.80	1.74	2.90	0.45	1.10	0.45
4-11-2023	2.45	0.94	8.45	0.51	0.55	0.51
5-11-2023	1.70	0.66	7.40	0.50	0.60	0.50
6-11-2023	0.90	0.79	4.55	0.60	0.45	0.60
7-11-2023	2.00	1.95	4.40	0.60	0.60	0.60
Total	18.95	3.55	40.40	1.39	4.60	1.39

Old values of RO using convex hull. Shows the lack of robustness.

Table D-43: Comparison of RO models with key metrics (totals), using only convex hull and old constraint

Model	Total FSR	FSR Std	Total SSR	SSR Std	Total Rev	Rev Std	Violations
RO - base	126,299.97	4,243.02	111,566.18	16,923.83	237,866.15	12,931.24	2.50 ± 0.52
RO - MA	126,113.57	6,262.85	121,257.13	20,501.33	247,370.70	14,298.14	3.00 ± 1.41
RO - LA	134,315.84	1,033.96	154,996.57	3,231.92	289,312.42	2,197.96	16.50 ± 6.36
RO - MW	126,283.08	5,795.52	106,831.63	18,352.23	233,114.71	12,559.23	2.33 ± 0.58
RO (No PImb) - base	129,748.05	2,938.44	81,175.09	8,120.40	210,923.15	5,397.12	2.17 ± 0.41
RO (No PImb) - MA	126,377.59	1,516.89	103,354.99	6,061.77	229,732.58	4,602.24	3.50 ± 0.71
RO (No PImb) - LA	136,137.44	926.95	130,054.32	3,823.81	266,191.75	2,938.96	24.50 ± 3.57
RO (No PImb) - MW	128,350.21	5,176.22	92,976.81	18,615.36	221,327.02	13,546.52	2.70 ± 1.06

Appendix E

Appendix: Frameworks enlarged

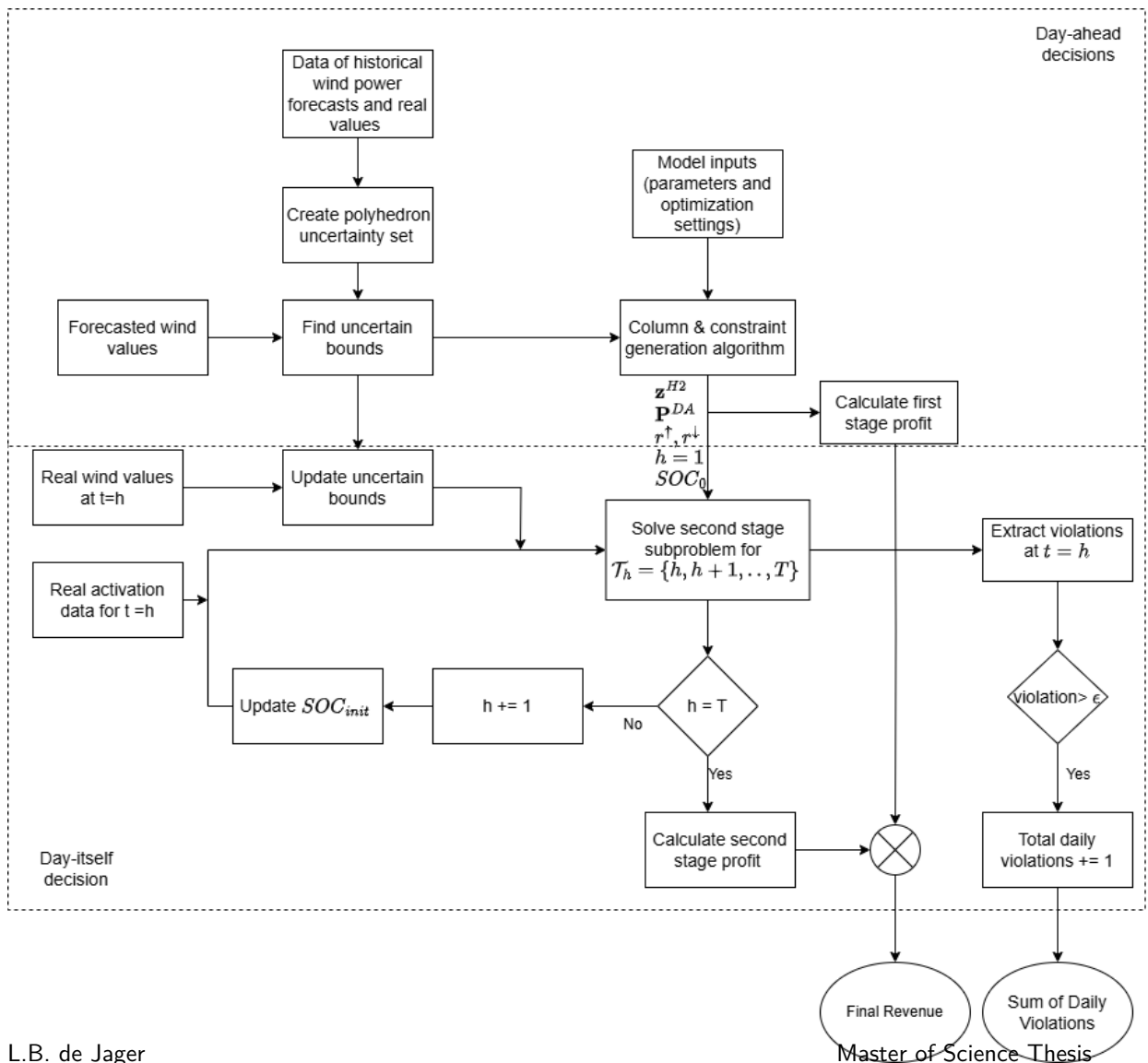
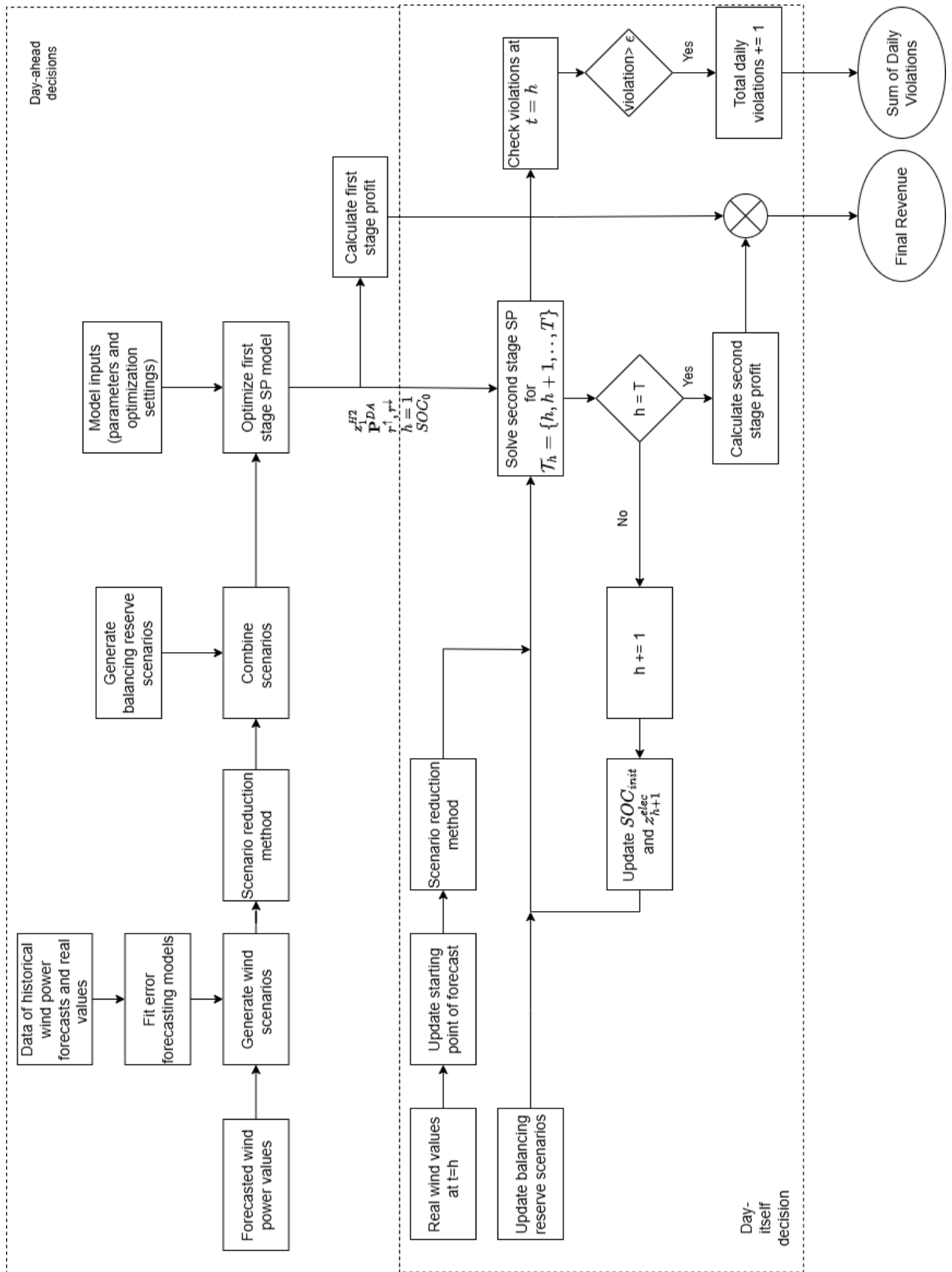


Figure E-1: Robust optimization framework



Appendix F

Appendix: stochastic full model

Here is the full model for the stochastic optimization for the first stage:

$$\max_{\omega \in \Omega} \sum_{\omega \in \Omega} \pi_{\omega} \left(\sum_{t \in \mathcal{T}} \left(P_t^{\text{DA},*} \Delta T \lambda_{t,\omega}^{\text{DA}} + r^{\uparrow} \lambda^{r\uparrow} + r^{\downarrow} \lambda^{r\downarrow} + Q_{t,\omega}^{\text{H2}} \lambda_t^{\text{H2}} - z_{t,\omega}^{\text{SU}} C^{\text{SU}} - \beta_t^{\downarrow} r^{\downarrow} \lambda_t^{r,\text{act},\downarrow} \right) \right) \quad (\text{F-1})$$

Subject to

Power Balancing Constraints:

$$P_t^{\text{DA}} = P_{t,\omega}^{\text{W}} - P_{t,\omega}^{\text{H2}} + P_{t,\omega}^{\text{bat}} - P_{t,\omega}^{\Delta}, \quad \forall t \in \mathcal{T}, \omega \in \Omega \quad (\text{F-2})$$

$$r^{\uparrow} = r_{t,\omega}^{\uparrow,\text{bat}} + r_{t,\omega}^{\uparrow,\text{H2}}, \quad \forall t \in \mathcal{T}, \omega \in \Omega \quad (\text{F-3})$$

$$r^{\downarrow} = r_{t,\omega}^{\downarrow,\text{bat}} + r_{t,\omega}^{\downarrow,\text{H2}}, \quad \forall t \in \mathcal{T}, \omega \in \Omega \quad (\text{F-4})$$

$$P_{t,\omega}^{\text{DA}} + P_{t,\omega}^{\Delta} + r_{t,\omega}^{\uparrow} \leq \overline{P}^{\text{net}}, \quad \forall t \in \mathcal{T}, \omega \in \Omega \quad (\text{F-5})$$

$$P_{t,\omega}^{\text{DA}} + P_{t,\omega}^{\Delta} - r_{t,\omega}^{\downarrow} \geq -\underline{P}^{\text{net}}, \quad \forall t \in \mathcal{T}, \omega \in \Omega \quad (\text{F-6})$$

State Constraints for the Electrolyzer:

$$z_{t,\omega}^{\text{su}} = 0, \text{ if } t = 0, \quad \forall \omega \in \Omega \quad (\text{F-7})$$

$$z_{t,\omega}^{\text{su}} \geq z_{t,\omega}^{\text{on}} - z_{t-1,\omega}^{\text{on}} - z_{t-1,\omega}^{\text{sb}}, \quad \forall t > 0, \omega \in \Omega \quad (\text{F-8})$$

$$z_{t-1,\omega}^{\text{off}} + z_{t,\omega}^{\text{sb}} \leq 1, \quad \forall t > 0, \omega \in \Omega \quad (\text{F-9})$$

$$z_{t,\omega}^{\text{on}} + z_{t,\omega}^{\text{off}} + z_{t,\omega}^{\text{sb}} = 1, \quad \forall t \in \mathcal{T}, \omega \in \Omega \quad (\text{F-10})$$

Electrolyzer Constraints:

$$Q_{t,\omega}^{\text{H2}} = \left(A(\hat{P}_{t,\omega}^{\text{H2}} - \beta_{t,\omega}^{\uparrow} r_{t,\omega}^{\uparrow,\text{H2}} + \beta_{t,\omega}^{\downarrow} r_{t,\omega}^{\downarrow,\text{H2}}) + B z_{t,\omega}^{\text{on}} \right) \Delta T, \quad \forall t \in \mathcal{T}, \omega \in \Omega \quad (\text{F-11})$$

$$\underline{P}^{\text{H2}} z_{t,\omega}^{\text{on}} \leq \hat{P}_{t,\omega}^{\text{H2}} \leq \overline{P}^{\text{H2}} z_{t,\omega}^{\text{on}}, \quad \forall t \in \mathcal{T}, \omega \in \Omega \quad (\text{F-12})$$

$$P_{t,\omega}^{\text{H2}} = \hat{P}_{t,\omega}^{\text{H2}} + P^{\text{sb}} z_{t,\omega}^{\text{sb}}, \quad \forall t \in \mathcal{T}, \omega \in \Omega \quad (\text{F-13})$$

$$\hat{P}_{t,\omega}^{H2} - r_{t,\omega}^{\uparrow,H2} \geq \underline{P}^{H2} z_{t,\omega}^{\text{on}}, \quad \forall t \in \mathcal{T}, \omega \in \Omega \quad (\text{F-14})$$

$$\hat{P}_{t,\omega}^{H2} + r_{t,\omega}^{\downarrow,H2} \leq \overline{P}^{H2} z_{t,\omega}^{\text{on}}, \quad \forall t \in \mathcal{T}, \omega \in \Omega \quad (\text{F-15})$$

Battery Constraints:

$$\text{SOC}_{t=1,\omega}^{\text{bat}} = \text{SOC}^{\text{init}} + \sum_{t \in \mathcal{T}} \frac{P_{t,\omega}^{\text{bat}} - \beta_{t,\omega}^{\uparrow} r_{t,\omega}^{\uparrow,\text{bat}} + \beta_{t,\omega}^{\downarrow} r_{t,\omega}^{\downarrow,\text{bat}}}{P_{\text{bat},\text{cap}}} \Delta T, \quad \forall \omega \in \Omega \quad (\text{F-16})$$

$$\text{SOC}_{t,\omega}^{\text{bat}} = \text{SOC}_{t-1,\omega}^{\text{bat}} + \frac{P_{t,\omega}^{\text{bat}} - \beta_{t,\omega}^{\uparrow} r_{t,\omega}^{\uparrow,\text{bat}} + \beta_{t,\omega}^{\downarrow} r_{t,\omega}^{\downarrow,\text{bat}}}{P_{\text{bat},\text{cap}}} \Delta T, \quad \forall t \in \mathcal{T} \setminus \{1\}, \omega \in \Omega \quad (\text{F-17})$$

$$\text{SOC}^{\text{init}} + \sum_{t \in \mathcal{T}} \frac{P_{t,\omega}^{\text{bat}} - \beta_{t,\omega}^{\uparrow} r_{t,\omega}^{\uparrow,\text{bat}} + \beta_{t,\omega}^{\downarrow} r_{t,\omega}^{\downarrow,\text{bat}}}{P_{\text{bat},\text{cap}}} \Delta T \leq \text{SOC}^{\text{final}}, \quad \forall \omega \in \Omega \quad (\text{F-18})$$

$$\underline{\text{SOC}} \leq \text{SOC}_{t,\omega}^{\text{bat}} \leq \overline{\text{SOC}}, \quad \forall t \in \mathcal{T}, \omega \in \Omega \quad (\text{F-19})$$

$$\text{SOC}_{t-1,\omega}^{\text{bat}} - \frac{(P_{t,\omega}^{\text{bat}} + r_{t,\omega}^{\uparrow,\text{bat}})}{P_{\text{bat},\text{cap}}} \Delta T \geq \text{SOC}_{t,\omega}^{\text{min}}, \quad \forall t \in \mathcal{T} \setminus \{1\}, \omega \in \Omega \quad (\text{F-20})$$

$$\text{SOC}^{\text{init}} - \frac{(P_{t=1,\omega}^{\text{bat}} + r_{t=1,\omega}^{\uparrow,\text{bat}})}{P_{\text{bat},\text{cap}}} \Delta T \geq \text{SOC}_{t,\omega}^{\text{min}}, \quad \forall \omega \in \Omega \quad (\text{F-21})$$

$$\text{SOC}_{t-1,\omega}^{\text{bat}} + \frac{(-P_{t,\omega}^{\text{bat}} + r_{t,\omega}^{\downarrow,\text{bat}})}{P_{\text{bat},\text{cap}}} \Delta T \leq \overline{\text{SOC}}, \quad \forall t \in \mathcal{T} \setminus \{1\}, \omega \in \Omega \quad (\text{F-22})$$

$$\text{SOC}^{\text{init}} + \frac{(-P_{t=1,\omega}^{\text{bat}} + r_{t=1,\omega}^{\downarrow,\text{bat}})}{P_{\text{bat},\text{cap}}} \Delta T \leq \overline{\text{SOC}}, \quad \forall \omega \in \Omega \quad (\text{F-23})$$

$$-\overline{P}^{\text{bat, ch}} \leq P_{t,\omega}^{\text{bat}} \leq \overline{P}^{\text{bat, dis}}, \quad \forall t \in \mathcal{T}, \omega \in \Omega \quad (\text{F-24})$$

$$P_{t,\omega}^{\text{bat}} + r_{t,\omega}^{\downarrow,\text{bat}} \leq \overline{P}^{\text{bat, dis}}, \quad \forall t \in \mathcal{T}, \omega \in \Omega \quad (\text{F-25})$$

$$-P_{t,\omega}^{\text{bat}} + r_{t,\omega}^{\uparrow,\text{bat}} \leq \overline{P}^{\text{bat, ch}}, \quad \forall t \in \mathcal{T}, \omega \in \Omega \quad (\text{F-26})$$

$$(\text{F-27})$$

For the second stage:

$$\max \sum_{\omega \in \Omega} \pi_{\omega} \left(\sum_{t \in \mathcal{T}} \left(Q_{t,\omega}^{H2} \lambda_t^{H2} - z_{t,\omega}^{SU} C^{SU} + P_{t,\omega}^{\Delta+} \lambda_t^{\Delta \text{ up}} - P_{t,\omega}^{\Delta-} \lambda_t^{\Delta \text{ down}} \right. \right. \\ \left. \left. + \beta_t^{\uparrow} r_t^{\uparrow, \text{act}, \uparrow} - \beta_t^{\downarrow} r_t^{\downarrow, \text{act}, \downarrow} \right) \right) \quad (\text{F-28})$$

Subject to

Power Balancing Constraints:

$$P_t^{\text{DA},*} = P_{t,\omega}^{\text{W}} - P_{t,\omega}^{\text{H2}} + P_{t,\omega}^{\text{bat}} - P_{t,\omega}^{\Delta}, \quad \forall t \in \mathcal{T}, \omega \in \Omega \quad (\text{F-29})$$

$$r_t^{\uparrow,*} = r_{t,\omega}^{\uparrow,\text{bat}} + r_{t,\omega}^{\uparrow,\text{H2}}, \quad \forall t \in \mathcal{T}, \omega \in \Omega \quad (\text{F-30})$$

$$r_t^{\downarrow,*} = r_{t,\omega}^{\downarrow,\text{bat}} + r_{t,\omega}^{\downarrow,\text{H2}}, \quad \forall t \in \mathcal{T}, \omega \in \Omega \quad (\text{F-31})$$

$$P_{t,\omega}^{\text{DA}} + P_{t,\omega}^{\Delta} + r_{t,\omega}^{\uparrow} \leq \overline{P}^{\text{net}}, \quad \forall t \in \mathcal{T}, \omega \in \Omega \quad (\text{F-32})$$

$$P_{t,\omega}^{\text{DA}} + P_{t,\omega}^{\Delta} - r_{t,\omega}^{\downarrow} \geq -\underline{P}^{\text{net}}, \quad \forall t \in \mathcal{T}, \omega \in \Omega \quad (\text{F-33})$$

State Constraints for the Electrolyzer:

$$z_{t,\omega}^{\text{su}} = 0, \text{ if } t = 0, \quad \forall \omega \in \Omega \quad (\text{F-34})$$

$$z_{t,\omega}^{\text{su}} \geq z_{t,\omega}^{\text{on}} - z_{t-1,\omega}^{\text{on}} - z_{t-1,\omega}^{\text{sb}}, \quad \forall t > 0, \omega \in \Omega \quad (\text{F-35})$$

$$z_{t-1,\omega}^{\text{off}} + z_{t,\omega}^{\text{sb}} \leq 1, \quad \forall t > 0, \omega \in \Omega \quad (\text{F-36})$$

$$z_{t,\omega}^{\text{on}} + z_{t,\omega}^{\text{off}} + z_{t,\omega}^{\text{sb}} = 1, \quad \forall t \in \mathcal{T}, \omega \in \Omega \quad (\text{F-37})$$

Electrolyzer Constraints:

$$Q_{t,\omega}^{\text{H2}} = \left(A(\hat{P}_{t,\omega}^{\text{H2}} - \beta_{t,\omega}^{\uparrow} r_{t,\omega}^{\uparrow,\text{H2}} + \beta_{t,\omega}^{\downarrow} r_{t,\omega}^{\downarrow,\text{H2}}) + Bz_{t,\omega}^{\text{on}} \right) \Delta T, \quad \forall t \in \mathcal{T}, \omega \in \Omega \quad (\text{F-38})$$

$$\underline{P}^{\text{H2}} z_{t,\omega}^{\text{on}} \leq \hat{P}_{t,\omega}^{\text{H2}} \leq \overline{P}^{\text{H2}} z_{t,\omega}^{\text{on}}, \quad \forall t \in \mathcal{T}, \omega \in \Omega \quad (\text{F-39})$$

$$P_{t,\omega}^{\text{H2}} = \hat{P}_{t,\omega}^{\text{H2}} + P^{\text{sb}} z_{t,\omega}^{\text{sb}}, \quad \forall t \in \mathcal{T}, \omega \in \Omega \quad (\text{F-40})$$

$$\hat{P}_{t,\omega}^{\text{H2}} - r_{t,\omega}^{\uparrow,\text{H2}} \geq \underline{P}^{\text{H2}} z_{t,\omega}^{\text{on}}, \quad \forall t \in \mathcal{T}, \omega \in \Omega \quad (\text{F-41})$$

$$\hat{P}_{t,\omega}^{\text{H2}} + r_{t,\omega}^{\downarrow,\text{H2}} \leq \overline{P}^{\text{H2}} z_{t,\omega}^{\text{on}}, \quad \forall t \in \mathcal{T}, \omega \in \Omega \quad (\text{F-42})$$

Battery Constraints:

$$\text{SOC}_{t=1,\omega}^{\text{bat}} = \text{SOC}^{\text{init}} + \sum_{t \in \mathcal{T}} \frac{P_{t,\omega}^{\text{bat}} - \beta_{t,\omega}^{\uparrow} r_{t,\omega}^{\uparrow,\text{bat}} + \beta_{t,\omega}^{\downarrow} r_{t,\omega}^{\downarrow,\text{bat}}}{P^{\text{bat,cap}}} \Delta T, \quad \forall \omega \in \Omega \quad (\text{F-43})$$

$$\text{SOC}_{t,\omega}^{\text{bat}} = \text{SOC}_{t-1,\omega}^{\text{bat}} + \frac{P_{t,\omega}^{\text{bat}} - \beta_{t,\omega}^{\uparrow} r_{t,\omega}^{\uparrow,\text{bat}} + \beta_{t,\omega}^{\downarrow} r_{t,\omega}^{\downarrow,\text{bat}}}{P^{\text{bat,cap}}} \Delta T, \quad \forall t \in \mathcal{T} \setminus \{1\}, \omega \in \Omega \quad (\text{F-44})$$

$$\text{SOC}^{\text{init}} + \sum_{t \in \mathcal{T}} \frac{P_{t,\omega}^{\text{bat}} - \beta_{t,\omega}^{\uparrow} r_{t,\omega}^{\uparrow,\text{bat}} + \beta_{t,\omega}^{\downarrow} r_{t,\omega}^{\downarrow,\text{bat}}}{P^{\text{bat,cap}}} \Delta T \leq \text{SOC}^{\text{final}}, \quad \forall \omega \in \Omega \quad (\text{F-45})$$

$$\underline{\text{SOC}} \leq \text{SOC}_{t,\omega}^{\text{bat}} \leq \overline{\text{SOC}}, \quad \forall t \in \mathcal{T}, \omega \in \Omega \quad (\text{F-46})$$

$$\text{SOC}_{t-1,\omega}^{\text{bat}} - \frac{(P_{t,\omega}^{\text{bat}} + r_{t,\omega}^{\uparrow,\text{bat}})}{P^{\text{bat,cap}}} \Delta T \geq \text{SOC}_{t,\omega}^{\text{min}}, \quad \forall t \in \mathcal{T} \setminus \{1\}, \omega \in \Omega \quad (\text{F-47})$$

$$\text{SOC}^{\text{init}} - \frac{(P_{t=1,\omega}^{\text{bat}} + r_{t=1,\omega}^{\uparrow,\text{bat}})}{P^{\text{bat,cap}}} \Delta T \geq \text{SOC}_{t,\omega}^{\text{min}}, \quad \forall \omega \in \Omega \quad (\text{F-48})$$

$$\text{SOC}_{t-1,\omega}^{\text{bat}} + \frac{(-P_{t,\omega}^{\text{bat}} + r_{t,\omega}^{\downarrow,\text{bat}})}{P^{\text{bat,cap}}} \Delta T \leq \overline{\text{SOC}}, \quad \forall t \in \mathcal{T} \setminus \{1\}, \omega \in \Omega \quad (\text{F-49})$$

$$\text{SOC}^{\text{init}} + \frac{(-P_{t=1,\omega}^{\text{bat}} + r_{t=1,\omega}^{\downarrow,\text{bat}})}{P^{\text{bat,cap}}} \Delta T \leq \overline{\text{SOC}}, \quad \forall \omega \in \Omega \quad (\text{F-50})$$

$$-\overline{P}^{\text{bat,ch}} \leq P_{t,\omega}^{\text{bat}} \leq \overline{P}^{\text{bat,dis}}, \quad \forall t \in \mathcal{T}, \omega \in \Omega \quad (\text{F-51})$$

$$P_{t,\omega}^{\text{bat}} + r_{t,\omega}^{\downarrow,\text{bat}} \leq \overline{P}^{\text{bat,dis}}, \quad \forall t \in \mathcal{T}, \omega \in \Omega \quad (\text{F-52})$$

$$-P_{t,\omega}^{\text{bat}} + r_{t,\omega}^{\uparrow,\text{bat}} \leq \overline{P}^{\text{bat,ch}}, \quad \forall t \in \mathcal{T}, \omega \in \Omega \quad (\text{F-53})$$

Imbalance Constraints:

$$P_{t,\omega}^{\Delta} = P_{t,\omega}^{\Delta+} - P_{t,\omega}^{\Delta-}, \quad \forall t \in \mathcal{T}, \omega \in \Omega \quad (\text{F-54})$$

$$P_{t,\omega}^{\Delta+} \geq P_{t,\omega}^{\Delta}, \quad \forall t \in \mathcal{T}, \omega \in \Omega \quad (\text{F-55})$$

$$P_{t,\omega}^{\Delta-} \geq -P_{t,\omega}^{\Delta}, \quad \forall t \in \mathcal{T}, \omega \in \Omega \quad (\text{F-56})$$

$$P_{t,\omega}^{\Delta+} \leq M \cdot u_{t,\omega}^{\text{imb}}, \quad \forall t \in \mathcal{T}, \omega \in \Omega \quad (\text{F-57})$$

$$P_{t,\omega}^{\Delta^-} \leq M \cdot (1 - u_{t,\omega}^{imb}), \quad \forall t \in \mathcal{T}, \omega \in \Omega \quad (\text{F-58})$$

It should be noted that the non-anticipatory constraints are not fully shown here as the constraints of the second-stage variables are fixed across all scenarios while in the other time-step they are dependent on the uncertainty set.

Bibliography

- [1] P. d. Lange, “Record op energiemarkt: Prijs elektriciteit dit jaar al 426 uur onder nul,” *De Volkskrant.*, Oct. 2024. [Online]. Available: <https://www.volkskrant.nl/economie/record-op-energiemarkt-prijs-elektriciteit-dit-jaar-al-426-uur-onder-nul~bdbaf2d9>.
- [2] I. Marouani, T. Guesmi, B. M. Alshammari, *et al.*, “Integration of Renewable-Energy-Based Green Hydrogen into the Energy Future,” *Processes*, vol. 11, no. 9, p. 2685, Sep. 2023. [Online]. Available: <https://www.mdpi.com/2227-9717/11/9/2685> [Accessed: Dec. 12, 2024].
- [3] M. T. Baumhof, E. Raheli, A. G. Johnsen, and J. Kazempour, “Optimization of Hybrid Power Plants: When Is a Detailed Electrolyzer Model Necessary?” In *2023 IEEE Belgrade PowerTech*, IEEE, Jun. 2023, pp. 1–10.
- [4] M. Saretta, E. Raheli, and J. Kazempour, “Electrolyzer Scheduling for Nordic FCR Services,” *arXiv preprint arXiv:2306.10962*, Sep. 2023.
- [5] L. A. Roald, D. Pozo, A. Papavasiliou, D. K. Molzahn, J. Kazempour, and A. Conejo, “Power systems optimization under uncertainty: A review of methods and applications,” *Electric Power Systems Research*, vol. 214, p. 108725, Jan. 2023.
- [6] A. J. Conejo, M. Carrión, and J. M. Morales, *Decision Making Under Uncertainty in Electricity Markets* (International Series in Operations Research & Management Science). Boston, MA: Springer US, 2010, vol. 153.
- [7] X. A. Sun and A. J. Conejo, *Robust Optimization in Electric Energy Systems* (International Series in Operations Research & Management Science). Cham, Switzerland: Springer International Publishing, 2021, vol. 313.
- [8] P. Mohajerin Esfahani and D. Kuhn, “Data-driven distributionally robust optimization using the Wasserstein metric: Performance guarantees and tractable reformulations,” *Mathematical Programming*, vol. 171, no. 1-2, pp. 115–166, Sep. 2018.
- [9] Y. Zheng, J. Wang, S. You, X. Li, H. W. Bindner, and M. Münster, “Data-driven scheme for optimal day-ahead operation of a wind/hydrogen system under multiple uncertainties,” *Applied Energy*, vol. 329, p. 120201, Jan. 2023.

- [10] A. Baringo, L. Baringo, and J. M. Arroyo, “Day-Ahead Self-Scheduling of a Virtual Power Plant in Energy and Reserve Electricity Markets Under Uncertainty,” *IEEE Transactions on Power Systems*, vol. 34, no. 3, pp. 1881–1894, May 2019.
- [11] Y. Zhang, F. Liu, Z. Wang, Y. Su, W. Wang, and S. Feng, *Robust Scheduling of Virtual Power Plant under Exogenous and Endogenous Uncertainties*, Feb. 2021. [Online]. Available: <http://arxiv.org/abs/2101.10800> [Accessed: Dec. 21, 2024].
- [12] M. Houwing, N. Cassamo, and E. Wiggelinkhuizen, “Energy management system for combined renewable generation, storage and conversion (EMERGE model): Renewable Hybrid Power Plant Optimization,” 2022.
- [13] TenneT, *aFRR manual for BSPs en.pdf*, Aug. 2023. [Online]. Available: <https://tennet-drupal.s3.eu-central-1.amazonaws.com/default/2023-08/aFRR%20manual%20for%20BSPs%20en.pdf> [Accessed: Feb. 1, 2024].
- [14] TenneT, *Onbalansprijsystematiek*, Mar. 2022. [Online]. Available: <https://tennet-drupal.s3.eu-central-1.amazonaws.com/default/2022-06/Onbalansprijsystematiek.pdf>.
- [15] K. Pandžić, I. Pavić, I. Androćec, and H. Pandžić, “Optimal Battery Storage Participation in European Energy and Reserves Markets,” *Energies*, vol. 13, no. 24, p. 6629, Dec. 2020. [Online]. Available: <https://www.mdpi.com/1996-1073/13/24/6629> [Accessed: Jun. 12, 2024].
- [16] A. G. Johnsen, L. Mitridati, D. Zarrilli, and J. Kazempour, “The Value of Ancillary Services for Electrolyzers,” *arXiv preprint Electrolyzer Scheduling for NordiarXiv:2310.04321*, Oct. 2023.
- [17] J. Lago, G. Marcjasz, B. De Schutter, and R. Weron, “Forecasting day-ahead electricity prices: A review of state-of-the-art algorithms, best practices and an open-access benchmark,” *Applied Energy*, vol. 293, p. 116 983, Jul. 2021.
- [18] I. Abdelmottaleb, A. Esmat, S. Tijm, and M. Gibescu, “Deep Learning-Based Imbalance Market Price Range Predictions in the Day-Ahead Horizon,” in *2023 IEEE Belgrade PowerTech*, Belgrade, Serbia: IEEE, Jun. 2023, pp. 1–8. [Online]. Available: <https://ieeexplore.ieee.org/document/10202684/> [Accessed: Dec. 15, 2024].
- [19] L. Molin, “Predicting Electricity Imbalance Prices,” Ph.D. dissertation, Tilburg University, 2023.
- [20] R. Tyrrell Rockafellar and S. Uryasev, “Conditional Value-at-Risk for General Loss Distributions,” *Journal of banking & finance*, vol. 26, no. 7, pp. 1443–1471, 2002.
- [21] C. Z. Mooney, *Monte Carlo Simulation*. SAGE, Apr. 1997.
- [22] J. Dupacová, N. Gröwe-Kushka, and W. Römisch, “Scenario reduction in stochastic programming,” *Mathematical Programming*, vol. 95, no. 3, pp. 493–511, Mar. 2003.
- [23] J. Morales, S. Pineda, A. Conejo, and M. Carrion, “Scenario Reduction for Futures Market Trading in Electricity Markets,” *IEEE Transactions on Power Systems*, vol. 24, no. 2, pp. 878–888, May 2009.
- [24] H. Heitsch and W. Römisch, “Scenario reduction algorithms in stochastic programming,” *Computational Optimization and Applications*, vol. 24, no. 2/3, pp. 187–206, 2003. [Online]. Available: <http://link.springer.com/10.1023/A:1021805924152> [Accessed: Nov. 23, 2023].

- [25] D. Bertsimas, D. B. Brown, and C. Caramanis, *Theory and Applications of Robust Optimization*, Oct. 2010. [Online]. Available: <http://arxiv.org/abs/1010.5445> [Accessed: Oct. 25, 2023].
- [26] M. Kazemi, H. Zareipour, N. Amjady, W. D. Rosehart, and M. Ehsan, “Operation Scheduling of Battery Storage Systems in Joint Energy and Ancillary Services Markets,” *IEEE Transactions on Sustainable Energy*, vol. 8, no. 4, pp. 1726–1735, Oct. 2017. [Online]. Available: <http://ieeexplore.ieee.org/document/7932132/> [Accessed: Jun. 12, 2024].
- [27] P. Pinson, “Estimation of the uncertainty in wind power forecasting,” Engineering Sciences, École Nationale Supérieure des Mines de Paris, 2006.
- [28] B. Zeng and L. Zhao, “Solving two-stage robust optimization problems using a column-and-constraint generation method,” *Operations Research Letters*, vol. 41, no. 5, pp. 457–461, Sep. 2013.
- [29] C. Gessel, *Vattenfall’s largest hybrid energy park is taking shape in the Netherlands*. [Online]. Available: <https://group.vattenfall.com/press-and-media/newsroom/2020/vattenfalls-largest-hybrid-energy-park-is-taking-shape-in-the-netherlands#:~:text=In%20the%20Netherlands%20Vattenfall%20is,turbines%2C%20solar%20panels%20and%20batteries.&text=In%20the%20south%2Dwest%20of,its%20largest%20hybrid%20energy%20park.> [Accessed: Oct. 10, 2024].
- [30] M. Sánchez, E. Amores, L. Rodríguez, and C. Clemente-Jul, “Semi-empirical model and experimental validation for the performance evaluation of a 15 kW alkaline water electrolyzer,” *International Journal of Hydrogen Energy*, vol. 43, no. 45, pp. 20 332–20 345, Nov. 2018. [Online]. Available: <https://linkinghub.elsevier.com/retrieve/pii/S0360319918328751> [Accessed: Dec. 19, 2024].
- [31] E.-E. ENTSO-E, *Transparency Platform*, 2017. [Online]. Available: <https://transparency.entsoe.eu>.
- [32] L. Zhao and B. Zeng, “An Exact Algorithm for Two-stage Robust Optimization with Mixed Integer Recourse Problems,”
- [33] R. Zhu, K. Das, O. Lindberg, P. E. Sørensen, and A. D. Hansen, *Robust Optimal Offering and Operation Framework for Hybrid Power Plants in Voluntary Balancing Markets with Decision Dependent Uncertainties*, Aug. 2023. [Online]. Available: <https://www.techrxiv.org/doi/full/10.36227/techrxiv.23899470.v1> [Accessed: Dec. 4, 2024].
- [34] L. Baringo, M. Freire, R. García-Bertrand, and M. Rahimiyan, “Offering strategy of a price-maker virtual power plant in energy and reserve markets,” *Sustainable Energy, Grids and Networks*, vol. 28, p. 100 558, Dec. 2021. [Online]. Available: <https://linkinghub.elsevier.com/retrieve/pii/S2352467721001296> [Accessed: Oct. 19, 2023].
- [35] J. Wang, J. Xu, J. Wang, *et al.*, “Two-stage distributionally robust offering and pricing strategy for a price-maker virtual power plant,” *Applied Energy*, vol. 363, p. 123 005, Jun. 2024. [Online]. Available: <https://linkinghub.elsevier.com/retrieve/pii/S030626192400388X> [Accessed: Dec. 21, 2024].

Glossary

List of Acronyms

HPP	hybrid power plant
VPP	virtual power plant
aFRR	automatic Frequency Restoration Reserve
ISP	Imbalance Settlement Period
SOC	state-of-charge
BSP	balance service provider
ARO	adaptive robust optimization
SP	stochastic programming
CCGA	column and constraint generation algorithm
DF	deterministic forecast
PI	perfect information
MILP	mixed-integer linear program
FSR	first-stage revenue
SSR	second-stage revenue

List of Symbols

β_t^\downarrow	Fraction of aFRR down reserve activated at time t
β_t^\uparrow	Fraction of aFRR up reserve activated at time t
ΔT	Time step duration (hours)
Γ^W	Uncertainty budget for wind scenarios
$\Gamma^{A,\downarrow}$	Uncertainty budget for aFRR down activations
$\Gamma^{A,\uparrow}$	Uncertainty budget for aFRR up activations

$\lambda_t^{\Delta\downarrow}$	Imbalance price for downward correction at time t (€/MWh)
$\lambda_t^{\Delta\uparrow}$	Imbalance price for upward correction at time t (€/MWh)
λ_t^{DA}	Day-ahead market price at time t (€/MWh)
$\lambda_t^{\text{r,act}\downarrow}$	Activation price for aFRR down at time t (€/MWh)
$\lambda_t^{\text{r,act}\uparrow}$	Activation price for aFRR up at time t (€/MWh)
$P_t^{\Delta+}$	Positive power imbalance at time t (MW)
$P_t^{\Delta-}$	Negative power imbalance at time t (MW)
P_t^{Δ}	Power imbalance at time t (MW)
P_t^{bat}	Battery power at time t (MW)
P_t^{DA}	Net power injected into the grid at time t (MW)
$P^{\text{H2, sb}}$	Standby power consumption of the electrolyzer (MW)
P^{H2}	Power used by the electrolyzer (MW)
P_t^{W}	Wind power at time t (MW)
Q_t^{H2}	Hydrogen production at time t (kg)
r^{\downarrow}	aFRR down reserve capacity (MW)
r^{\uparrow}	aFRR up reserve capacity (MW)
$\text{SOC}^{\text{final}}$	Final state of charge of the battery (-)
SOC^{init}	Initial state of charge of the battery (-)
SOC_{bat}	State of charge of the battery (-)
z_t^{off}	Binary variable indicating whether the electrolyzer is off at time t
z_t^{on}	Binary variable indicating whether the electrolyzer is on at time t
z_t^{sb}	Binary variable indicating whether the electrolyzer is in standby mode at time t